ANOMALOUS MECHANICAL BEHAVIOR OF ALUMINO-SILICATE REFRACTORIES AT ELEVATED TEMPERATURES

A THESIS

Presented to

The Faculty of the Division

of Graduate Studies

By

James Bennett

In Partial Fulfillment

of the Requirements for the Degree

Master of Science in Ceramic Engineering

Georgia Institute of Technology

December, 1975

ANOMALOUS MECHANICAL BEHAVIOR OF ALUMINO-SILICATE REFRACTORIES AT ELEVATED TEMPERATURES

Approved:

James F. Benzel, Chairman

Alan T. Chapman

Joe K. Cochran, Jr.

Date approved by Chairman: 1 Dec 75

ACKNOWLEDGMENTS

I wish to thank Dr. J. F. Benzel, Dr. A. T. Chapman, and Dr. J. K. Cochran for their patience and advice on this research project. Special thanks go to Dr. Cochran for his endless help with both the x-ray and linear thermal expansion results, and to Dr. Benzel for his help throughout the whole project. I would also like to express my thanks to the Refractories Institute which gave financial support to this study. This thesis was more to me than just another obstacle to overcome in obtaining a Masters degree. My deepest thanks go to my wife, Eileen, who let the writing of this thesis interfere with the first months of our marriage. May she forgive me.

TABLE OF CONTENTS

LIST OF TABLES

LIST OF FIGURES

SUMMARY

Hot modulus of rupture, quantitative x-ray phase analysis, and thermal expansion data were investigated to determine which of two theories explained the strength increase of alumino-silicate refractories at elevated temperatures. Stress relief and crystal precipitation are the basis of the disputed theories. Alumina-silica compositions containing 63 and 90 percent alumina were tested. Modulus of rupture values were measured up to 2800°F. Maximum strength was found at 1800° and 2000°F. X-ray phase analysis showed no significant phase deviations with temperature in the area of strength increases. Thermal expansion curves indicated a relationship between maximum strength at high temperatures and thermal expansion slope changes. Results indicated that differential thermal expansion and stress relief were responsible for the observed strength increases.

CHAPTER I

INTRODUCTION

Alumino-silicate refractories show an anomalous strength increase between 1700 and 2100°F. Since the discovery of the anomalous strength increase, numerous theories have been forwarded as to the probable cause. Two theories, crystal precipitation and relief of differential thermal expansion stresses by glass relaxation, have been supported by Russell Smith [1] and Frank Duncan [2]. The experimental procedures leading to their proposals were not similar, making comparison impossible. The purpose of this study is to resolve the differences between the two theories: crystal precipitation and stress relief as the cause of the anomalous strength increase. X-ray phase analysis and thermal expansion will be compared with hot modulus of rupture data.

CHAPTER II

REVIEW OF THE LITERATURE

Alumino-silicate refractories have been the subject of extensive research due to their unusual strength behavior at high temperatures. Hot load deformation run by Bodin [3] early in the 1920's showed alumino-silicate refractories exhibiting a maximum in crushing strength at about 1000°C. Further rise in temperature caused these values to fall rapidly. Crushing strengths as high as four times the room temperature values were reported.

Some other early reports mentioning the high-temperature, high strength characteristics of alumino-silicates were published by Heindl and Pindergast [4], Hirsch [5], Roberts and Cobb [6], and Hunt and Bradley [7]. Heindl and Pindergast tested the modulus of elasticity and the modulus of rupture of several sagger clays. Of the 17 clays tested, 15 were found to have a modulus of rupture that stayed the same or increased slightly at high temperatures. Only two clays had a sharp decrease in modulus of rupture at high temperatures. Heindl and Pindergast concluded that a positive relationship existed between transverse strength and modulus of elasticity. Strength rose when elasticity did. They noticed that plastic deformation took place in the samples

at about 950°C. Samples became deformed above this temperature.

Hirsch [5] investigated the compressive strength of refractory materials as a function of temperature. He found that strengths tended to peak at about 1000°C by as much as five times strength values recorded at room temperature.

Roberts and Cobb [6] studied the torsion behavior of refractory materials up to 1050°C. Resistance to torsion stress was found to attain a maximum value between 750 to 900°C. They stated that the development of an increased resistance to shearing stresses as the temperature was raised was characteristic in the materials examined containing free silica in a crystalline condition, and the magnitude of the change depended on the amount of crystallizing silica present. Roberts and Cobb considered the maximum strength to mark the beginning of plastic flow in the alumino-silicates.

Hunt and Bradley [7] described equipment and test procedures for running a standardized modulus of rupture and crushing strength. Test brick included alumino-silicate refractories. It was noted that modulus of rupture values became somewhat higher in the temperature range of 1800 to 2000°F. Above 2000°F, modulus of rupture and crushing samples became bent or compressed, which indicated the plastic flow mentioned by Roberts and Cobb.

Several theories have been proposed in an attempt to explain the anamolous strength increase at high temperatures

of alumino-silicate refractories. Many of the theories given as probable causes fall under the headings of:

1. Glass Softening
2. Capillary Suction
3. Differential Thermal Expansion
4. Crystal Precipitation

Several of the theories make use of more than one effect. Two theories, differential thermal expansion with stress relief and crystal precipitation, are the subjects of this investigation.

1. Glass Softening

Proposed theories of strength increases due to the presence of a glass phase have been made by Wiechula and Roberts [8]; Padgett [9]; Padgett, Cox, and Clements [10]; Folk and Bohling [11]; and Rigby [12]. Wiechula and Roberts investigated a large range of commercial alumino-silicate refractories. Alumina content of the five brick compositions varied from 30 to 80 percent. They examined torsion, modulus of rigidity, shear, and flow rates up to 1400°C. Their results indicated that rigidity increased with temperature increases. The more siliceous material present, the larger the increase. In the region where plasticity developed (700 to 800°C) and rigidity began to decrease (700°C), strength increases were observed. The transition from a rigid to a plastic sample occurred from 700 to 800°C

regardless of composition. Wiechula and Roberts concluded that the same euctectic composition must be present in all the bricks. A considerable amount of highly viscous liquid is formed at temperatures well below those predicted by the phase diagram. They concluded that the glassy phase consisted predominantly of alkali and silica. The glassy phase was responsible for the onset of flow in refractories and the corresponding loss in strength.

Padgett [9] reasoned that the high temperature mechanical behavior of refractories could be attributed to the behavior of the continuous phase. In the case of glass bonded refractories, he found a time-temperature dependence for load deformation.

In another publication Padgett, Cox, and Clements [10] made a study of high-alumina refractories. Examining deformation data, they concluded that there is elastic fracture at room temperature, a yield point at higher temperatures, and viscous movement at still higher temperatures. This softening behavior is characteristic of a glass bond and results in a weakening of the sample.

Folk and Bohling [11] had data supporting the idea that the larger the glass content present in an alumino-silicate refractory, the higher would be its hot modulus of rupture. They investigated alumino-silica firebrick with alumina content varying from 45 to 95 percent. They concluded that the high temperature strength of alumino-

silicate refractories is influenced by its firing temperature as well as composition. Both of these affect the glass content.

In a study discussing the origin of strength in ceramic materials, Rigby [12] included alumino-silicates. Rigby noted that the glass matrix associated with fireclay refractories possessed a higher viscosity than would a glass free from crystalline phases. Drawing an analogy with clay slips, he used orientation of the random network to explain strength increases.

2. Capillary Suction

The effect noted by Rigby [12] of a glassy phase increasing in viscosity when a crystalline material was dispersed within could have been due to capillary suction. Houseman [13]; Allison, Brock, and White [14]; and Houseman and White [15] concluded that there is evidence to support strength increases due to capillary suction occurring in refractories at high temperatures. This theory is similar to the glass relaxation proposal in that it requires a softening of the glass present before it becomes a mechanism of strength increase.

Houseman [13] investigated hot compressive strength of silica and sillimanite refractories in his studies. Once a certain temperature was reached (1100°C for his silica samples and a much lower temperature for the sillimanite bricks), hot strength rose rapidly. Houseman believed a

continuous film of liquid developed over grain surfaces in this temperature range. Subsequently, a "cementing together" of the grains occurred and strength rapidly increased. Further heating produced decreases in strength due to a lower liquid viscosity. Cooling the samples produced strength increases due to solidification of the liquid bond. Strength drops on continued cooling due to strains set up in the sample and possible cracking.

Allison, Brock, and White [14] agreed with Houseman that cohesion between the crystalline phases was the cause of strength increases. They used compressive strength, tensile strength, and cohesion data to support their hypothesis. Their final results indicated that some solid-to-liquid bonding probably occurs between particles as well as continuous film capillary forces. Continuous films form lenses of liquid which tend to draw particles together by capillary forces. Allison, Brock, and White pointed out this case did not ideally exist in alumino-silicates. Instead the liquid phase tends to coalesce to form globules within a solid matrix. Strength is affected very little by capillary forces when these glowules form. Instead liquid bonding gives a strength increase. Relations between the flow properties of commercial refractories at high temperatures and those of liquid bonded aggregates were given as evidence that many refractories behave as liquid bonded aggregates.

Houseman and White found [15] in their study of bond

strength that the crushing strength of alumino-silicate refractories was a maximum in the region of 1000 to 1080°C. They concluded that the strength increase was due to the presence of low melting liquids. On cooling from high temperatures, progressive stiffening of the bond occurs. Strength falls off due to the formation of microcracks created by a difference in thermal expansion between the crystalline matrix and the glass.

3. Differential Thermal Expansion

Crystals with a different thermal expansion than the glass matrix in which they are cooling causes stresses to set up in the system. Mattygsovsky-Zsolnay [16] gave much insight into the influence of particle size on the room temperature strength of porcelain bodies. He found that crystalline materials having a higher expansion than the matrix can favorably prestress it, causing increases in room temperature strength. A certain optimum size of quartz grains best withstood the stresses. Cracks that form due to differences in thermal expansion can cause the matrix to weaken due to Griffith's flaws. Particles larger than this optimum size cause strength decreases. Smaller particles do not create enough stress for sizable strength increases.

Richard Fulrath [17] showed how stresses develop in model systems. His studies were of crystals and glass fabricated by hot pressing. Examples of how the matrix

appears for samples in which the glass has a higher expansion than the crystal and for the reverse case are given in Figure 1. When the glass has the higher thermal expansion coefficient (Figure 1-a), cooling introduces tensile forces normal to the crystal glass interface. At crystal-crystal contacts a compressive stress is developed. Shear forces tangential to the surface places the glass in tension. When the crystal has the higher expansion (Figure 1-b), the force normal to the surface places the interface in compression. The tangential force places the glass in compression and the crystal in tension. The crystal-crystal contacts are also in tension. Fulrath does point out that crystals are not always spherical as in his ideal system, and that packing may not follow as anticipated.

Expansion differences such as those described by Fulrath have been used as an explanation of strength increases in alumino-silicate refractories. Thermal expansion, thermal expansion and stress relief, and crack rehealing caused by differential thermal expansion all involve differential thermal expansion. Expansion differences set up stresses in the crystal-glass interface and have been proposed as possible mechanisms for strength increases.

Thermal Expansion

Bressman [18]; Das and Roberts [19]; Davis and Rigby [20]; Chaklader and Roberts [21]; and Palfreyman [22] proposed that differences in thermal expansion are responsible

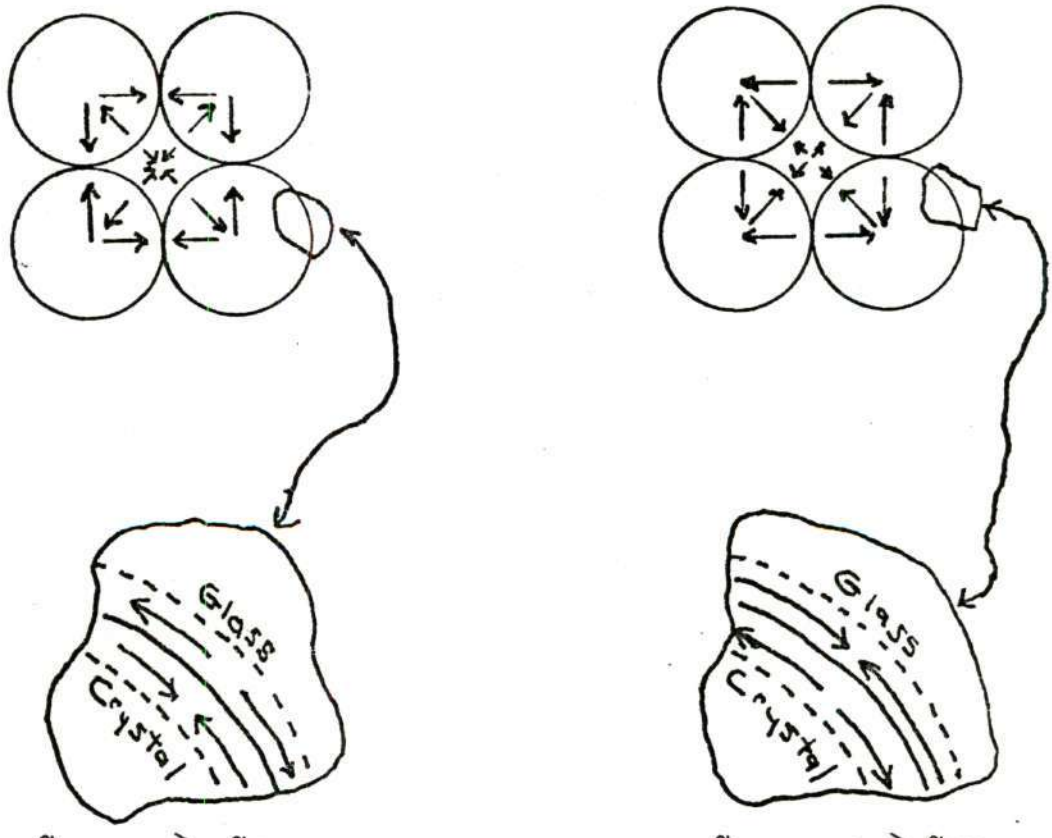

$\alpha_{Glass} > \alpha_{Crystal}$ a.

$\alpha_{Crystal} > \alpha_{Glass}$ b.

Stress on Crystal

	a	b
Normal to Crystal-Crystal Interface	Compression	Tension
Normal to Crystal-Glass Interface	Tension	Compression
Tangential to Crystal-Glass Interface	Compression	Tension

Figure 1. Stress in a Crystal-Glass Model System with Open Cubic Packing of Spherical Crystal Particles

for strength increases in refractories. Bressman used sillimanite refractories and investigated tensile strength, stress-to-rupture characteristics, and modulus of elasticity. He concluded that tensile strength increased to a maximum value at 1800°F. Phase changes such as the volume increase in cristobalite from 392 to 500°F and the healing by expansion of small cracks and stresses in the particles would cause the strength to increase.

Das and Roberts [19] studied commercial silica refractories by torsion measurements. They concluded that modulus of rigidity increases between 225°C to 1200°C were due to two factors: the differential expansion between crystals and matrix, and an inherent property of silica minerals. Rigidity decreases from 1200 to 1600°C were not explained.

Davis and Rigby [20] investigated commercial firebrick with alumina content varying from 24 to 72 percent. They concluded that differential thermal expansion was the main cause of the rise in the modulus of elasticity. A discontinuous clay matrix and grog grains departing from the ideal spherical shape discussed earlier in Figure 1 gives a "wedging" or "jamming" action of the particles. This "wedging" or "jamming" action results in modulus increases. Measurements were not made to show behavior above 1000°C, and thus no high temperature behavior was proposed.

Davis and Rigby [23] later continued their studies of

high temperature strength increases using chromite-magnesite refractories. They determined that differential thermal expansion played a major role in strength increases. Two effects were noted as possible causes of the strength increases: crystalline expansion into voids present due to differential thermal expansion and interlocking of the different grains expanding against each other. On cooling from peak strength temperatures, decreases in modulus of rupture from peak values at high temperatures occurred. The modulus decreases were attributed to a breakdown of the crystalline bond. Stresses from differential thermal expansion and jamming in the voids created by crystalline cooling cause a charge in low temperature strengths on thermal cycling.

In their studies of silica refractories, Chaklader and Roberts [21] supported the theory of Davis and Rigby that stresses due to differential thermal expansions cause strength increases. Figure 2 shows the case where the crystal has a greater expansion than the matrix. The crystal tends to break away from the matrix on cooling (Figure 2-a) and rejoin on heating (Figure 2-b). Further heating is likely to cause stresses in the sample (see Figure 2-c). Compressive stresses occur in the crystal and tensile stresses occur in the matrix. Crystals need not be round or surrounded by glass as in Figures 2 a-c. Condition a in Figure 2 with an irregular shaped particle might exist. Differential expansion

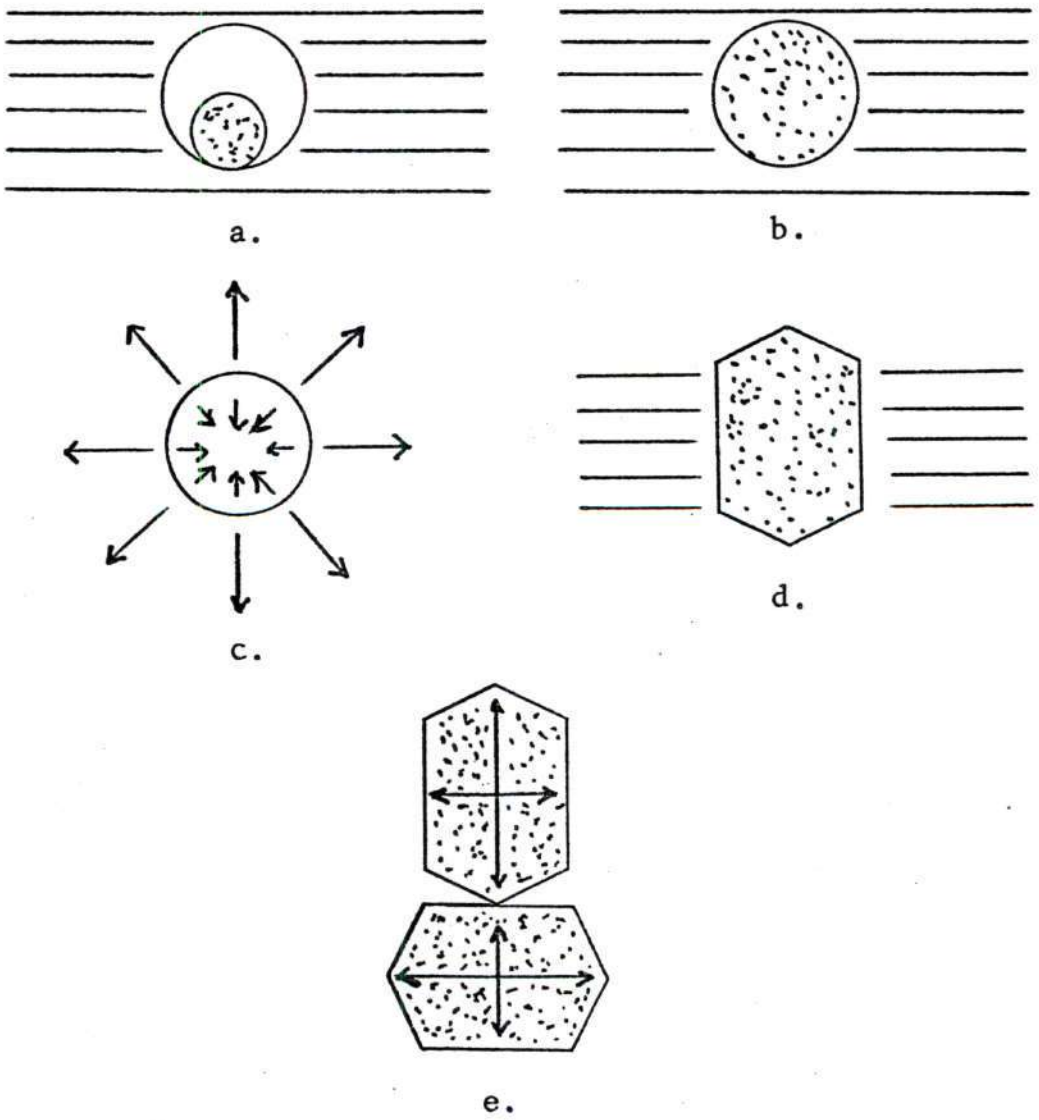

a = Crystal-Glass (Room Temperature)
b = Crystal-Glass (High Temperature)
c = Stresses on Cooling
d = Irregular Particle in Void
e = Anisotropic Expansion

Figure 2. Expansion Behavior of a Crystal in a Glass Matrix (Crystal has high expansion)

stress in Figure 2-a could be greatly reduced from Case c in Figure 2 due to stress relief by crystal movement on the axis. Chaklader and Roberts noted that above 600°C expansion differences between cristobalite and glass become very small. Adjacent crystals could have expansive stresses due to anisotropy on heating.

Palfreyman [22] made high-alumina refractory samples and investigated hot modulus of rupture from room temperature to 1400°C. Different raw materials were investigated to see their effect on hot modulus of rupture. The increases in hot strength were noted, their peaks occurring between 1000 and 1100°C. Results indicated that the grog, in addition to the binder, plays an important part with respect to strength. Different grogs such as fused versus tabular alumina, gave different strength curves. This effect was also noted in chromite-magnesite refractories by Davis and Rigby [23] With tabular alumina, mullite formed between the grog grains without bonding to them. The grog grains come apart on cooling from initial firings. As a result, the structure is discontinuous. The broken structure accounts for the lower cold strength, which increases as temperature is raised due to the rejoining of grains. Tightening of the structure is the result of the different expansions of the alumina and mullite. A lowering of strength could take place as the bonds become disrupted at high temperatures. This loss of strength is caused by microcracking from thermal stresses.

This would cause a strength peak. Above 1200°C, liquid phase formation by Na_2O impurities gives continued loss in strength.

Thermal Expansion and Stress Relief

The combination of thermal expansion and stress relief has been proposed to explain first the rise, then the loss in strength of alumino-silicates. This theory is one of the stronger ones, which evidence supports. A study by the Joint Refractories Research Committee [24] used alumino-silicates with an alumina content of 85 percent. The brick showed a maximum modulus of rupture at about 1000°C. The gain in strength was thought to be due to differential thermal expansion. They concluded that the strength reduction at higher temperatures due to the softening of the glassy phase bond.

Miller and Davis [25] in their modulus of rupture studies of alumino-silicate refractories tested commercially fabricated bricks ranging from conventional silica to 99 percent alumina. They found that the strength peak was most pronounced for refractories containing both crystalline and glassy phases. Gains in strength with increasing temperature were caused by changes in stresses resulting from dissimilar phases possessing different thermal expansion. Above 2000°F, strength loss was cuased to softening of the glass.

Duncan in his thesis at Ohio State University [2]

studied the elastic deformation and hot modulus of rupture of alumino-silicate bodies at high temperatures. Different loading rates were investigated for compositions ranging from 65 to 81 percent alumina. Stress-strain curves were drawn for each loading rate. His conclusions were that the bodies he studied were viscous in nature. Strength increases at high temperatures were the result of stress relief. Particle movement at higher temperatures caused the observed lowering of strength.

Padgett and Clements [26] studied the stress-strain and modulus of elasticity behavior of alumino-silicate bricks at high temperatures. Mullite particles were used with different bonding matrices of alumina, glass, and mullite. When the body behaved as a one-phase material (all mullite), a drop in the modulus of elasticity occurred with increasing temperature. A rise in the value for two-phase material occurred. Larger modulus of rupture increases were also reported for the two-phase materials versus the one-phase. Again, as noted by earlier investigators, strength dropped above 1000°C for all samples due to a softening of the glass. Differential thermal expansion and stress relief between the bond and the mullite affected strength.

Couch and Jolliffe [27] studied the stress rate and modulus of rupture of an 85 percent alumina refractory and a mullite refractory. Closely examining the fracture

surfaces at the high temperatures (1400°C) and comprising them with room temperature samples, the conclusion was reached that failure was due to plastic deformation and movement at the grain boundaries. They felt that the rise in fracture stress was produced by expansion differences between mullite, alumina, and the glassy phase. Their proposal of differential thermal expansion and stress relief thus adhered to the principles of several other researchers. Above 1000°C the strength falls off rapidly due to stress relief. Cooling the matrix below 1000°C increases strains imposed locally due to different thermal expansion. Thus, the external stress required to bring the internal stresses up to critical level for crack propogation is smaller at lower temperatures. The expansion of alumino-silicate glass is typically 4.5×10^{-6}/°C while that of mullite is about 5.6×10^{-6}/°C. Relaxation of the glass leads to a blunting of the crack tip and reduction of stresses. Thus, the stress required to initiate failure increases even more.

Alexanderson [28] related density, thermal shock resistance, and hot modulus of rupture in an attempt to find lightweight high-strength, high-alumina refractories. Alumina content varied between 90 to 99 percent. His data showed the same behavior of stress relief occurring in the matrix, then a rapid drop in strength due to softening of the glass.

Tripp [29] studied hot modulus of rupture behavior of alumino-silicate refractories with 50 to 90 percent alumina.

He concluded that the peak strength reflects the temperature where glass bond present enters an annealing range. Stresses due to different thermal expansion are relieved. Continued heating above where the strength peak occurs causes a softening of the glass and fracture occurs by deformation.

In contrast to the theories of differential thermal expansion as the cause of strength increases, Roberts [30] presented a different theory. He felt the differential expansion resulted in reduction of voidage to give an increased area or volume to resist the applied stress. Thus, strength increases are simply the reversal of physical changes that occur on cooling. The crystals tend to separate from the liquid once the latter has become rigid due to thermal expansion. Reheating causes the grains to gradually reoccupy the voids. When the crystals regain complete contact with the matrix, no further strength increase occurs. This is also the point where the matrix softens, giving a pronounced drop in strength. Roberts discounted the mechanism of internal stresses set up by the difference of expansion between two phases. "Stress might well arise in this way at innumerable localized points, but at each point the stress would have a definite and probably different direction, giving statistical equality between positive and negative stresses in the mass as a whole and thus an overall resultant of zero."

Rigby [31] enlarged upon the causes of the strength

increases mentioned earlier in basic brick to include all refractories where expansion mismatches occurred. He worked with bauxite refractories of about 85 percent alumina. His proposal was similar to Robert's void occupation. On reheating a brick, however, Rigby feels that little, if any, strength increase occurs until the cracks begin to close. Strength begins to increase once contact is established. Up to 850°C Rigby found no increase in modulus of rupture. Glass remote from crystal boundaries softens first above 850°C, then strength rises due to crack closure and healing of cracks. Bonds are then formed between particles. Strength drops when viscosity becomes too low (about 1100°C) and allows movement of particles occurs.

4. Crystal Precipitation

The possibility of phase precipitation being the cause of the strength increase in the mullite glass system was presented by Studt and Fulrath [32]. This phase was cristobalite and was suspected of helping bond glass and mullite. As temperatures rose to the strength peak, internal stresses due to large amounts of cristobalite formation outweighed the increased interfacial bonding, and strength began to decrease.

Viscosity changes due to cristobalite formation at high temperatures was proposed as the cause of peak strength in work by Chaklader and Roberts [33]. Their investigations

of silica refractories showed viscosity increases with cristobalite precipitation in the temperature range where strength peaked. They also found that room temperature modulus of rigidity values fell off greatly when cristobalite voids formed at room temperature.

Smith [1] studied bodies of 63 and 90 percent alumina. Smith noted that the modulus of rupture of a mullite firebrick showed a 54 percent strength increase at 2000°F. Cristobalite content increased seven percent, and glass decreased seven to nine percent. Mechanisms of the strength increase noted here were an increase in viscosity due to the presence of cristobalite crystals in the phase, the formation of cristobalite link between mullite and alumina, a decrease in bond thickness, and the reduction in the quantity of glass present.

5. Summary of Leading Theories

The strengthening mechanism in alumino-silicate refractories has several possible causes. One of the more recent theories was supported by Duncan at Ohio State University. As mentioned earlier, he felt that stresses set up by differential thermal expansion and the relief of these stresses at high temperatures by glass relaxation caused the observed strength increases. In contrast, Smith showed by x-ray phase identification that the non-crystalline portion of a mullite firebrick devitrified into a significant amount

of cristobalite in the same temperature range where an increase in the modulus of rupture occurred. Smith felt, as stated under an earlier theory, that the increase in cristobalite, cristobalite linking between mullite grains, and the decrease in glass content were the major causes of strength increase. The purpose of this work is to analyze and resolve possible differences in the strengthening mechanisms reported by Smith and Duncan. The two investigations could have the same results; yet, because Duncan did not use x-ray phase identifications, comparison of the two works is impossible.

CHAPTER III

PROCEDURE

Seven alumino-silicate compositions of 63 and 90 percent alumina were investigated. Two of the compositions were similar to those used by Smith [1] and Duncan [2]. Modulus of rupture at elevated temperatures and its peak strength were related to crystalline phase changes and thermal expansion behavior. Crystalline behavior was analyzed by the x-ray internal standard procedure. Thermal expansion measurements were used to analyze stress relief in the samples.

Sample Preparation

The calculated oxide formula of the seven compositions investigated are listed in Table 1. Mixes I-IV are of a high mullite composition, and mixes V-VII are of a high alumina composition. Mix I is a body similar to that studied by Smith, and mix III is similar to that studied by Duncan. Grain sizing and raw material sources are the differences between mixes I-IV. Mix II is a fine grained body of mix I. Mix IV is a fine grained body of Duncan's mix III using the same raw material sources as Smith. Mix VI is a coarse grained 90 percent alumina composition and is a fine grained body of mix V. Mix VII is the same as mix VI

Table 1. Oxide Formula for Mixes I-VII

Mix No.	Mix Characteristic	Chemical Composition of the Fired Body (wt.%)							
		S_iO_2	Al_2O_3	TiO_2	Fe_2O_3	C_8O	MgO	Na_2O	K_2O
I	Smith's Mullite body, coarse grained	32.95	63.75	1.99	.89	.07	.00	.15	.13
II	Smith's Mullite body, fine grained	32.95	63.75	1.99	.89	.07	.00	.15	.13
III	Duncan's fine grained composition	33.43	62.41	2.17	.84	.30	.53	.05	.26
IV	Duncan's fine grained composition--same raw materials used by Smith	35.08	61.41	1.99	.99	.13	.08	.13	.17
V	High Alumina, coarse grained (SiO_2 source-Quartz)	9.97	89.71	.02	.02	.02	.01	.07	
VI	High Alumina, fine grained (SiO_2 source-Quartz)	9.97	89.71	.02	.02	.02	.01	.07	
VII	High Alumina, fine grained (same as 6) except only source of SiO_2 was Kaolin	10.18	89.01	.28	.08	.11	.17	.06	.10

except kaolin is the raw material source of silica instead of the flint.

The screen analyses of all mixes are given in Table 2, and are plotted in Figure 3. It should be noted that mixes I and V are coarse grained, while mixes II, III, IV, VI, and VII are fine grained. The fine mix compositions can be further subdivided into two groups having similar screen analysis, namely mixes II, III, and IV; and mixes VI and VII.

All samples compositions were weighed in 100-pound batches and were mixed in a Lancaster mixer for two minutes dry. After this, three pounds water and one pound of an organic binder, Additive A, were added to mixes I-IV; and 2.5 pounds water and 2.5 pounds Additive A were added to mixes V-VII. Each was then mixed for an additional 15 minutes. Mixes were allowed to age 48 hours at room temperature in plastic bags before pressing. This was done to attain even moisture distribution. Samples 1" x 1" x 6" were pressed, using a screw press, to a constant but unknown pressure.

The samples were allowed to air dry overnight, and then were further dried in a gas fired drier at 220°F for at least 24 hours. Samples were gas fired in two groups: compositions I-IV at 2450°F for eight hours and compositions V-VII at 2700°F for one hour. Density was determined by measuring sample dimensions to 0.01 inch and weighing samples to 0.01 pound.

Table 2. Particle Size Analysis for Mixes I-VII (Weight %)

Tyler Screen Sizes	Mix 1	Mix 2	Mix 3	Mix 4	Mix 5	Mix 6	Mix 7
-6 + 8					9.3		
-8 + 10	7.9				19.0		
-10 + 14	8.6				9.2		
-14 + 20	6.9				5.6		
-20 + 28	5.5				3.6		
-28 + 35	4.9				2.9		
-35 + 48	5.6				2.3		
-48 + 65	7.3				4.9		
-65 + 100	9.0	0.8	0.6	0.8	6.1	2.4	2.1
-100+ 150	5.1	0.3	0.2	0.3	2.6	23.3	20.4
-150+ 200	4.1	1.5	1.2	1.5	3.8	15.3	13.4
-200++325	5.6	8.9	8.3	8.9	4.2	16.4	13.7
-325	30.2	88.3	89.8	88.3	26.8	42.7	50.4
Total	100.7	99.8	100.1	99.8	100.3	100.1	100.0

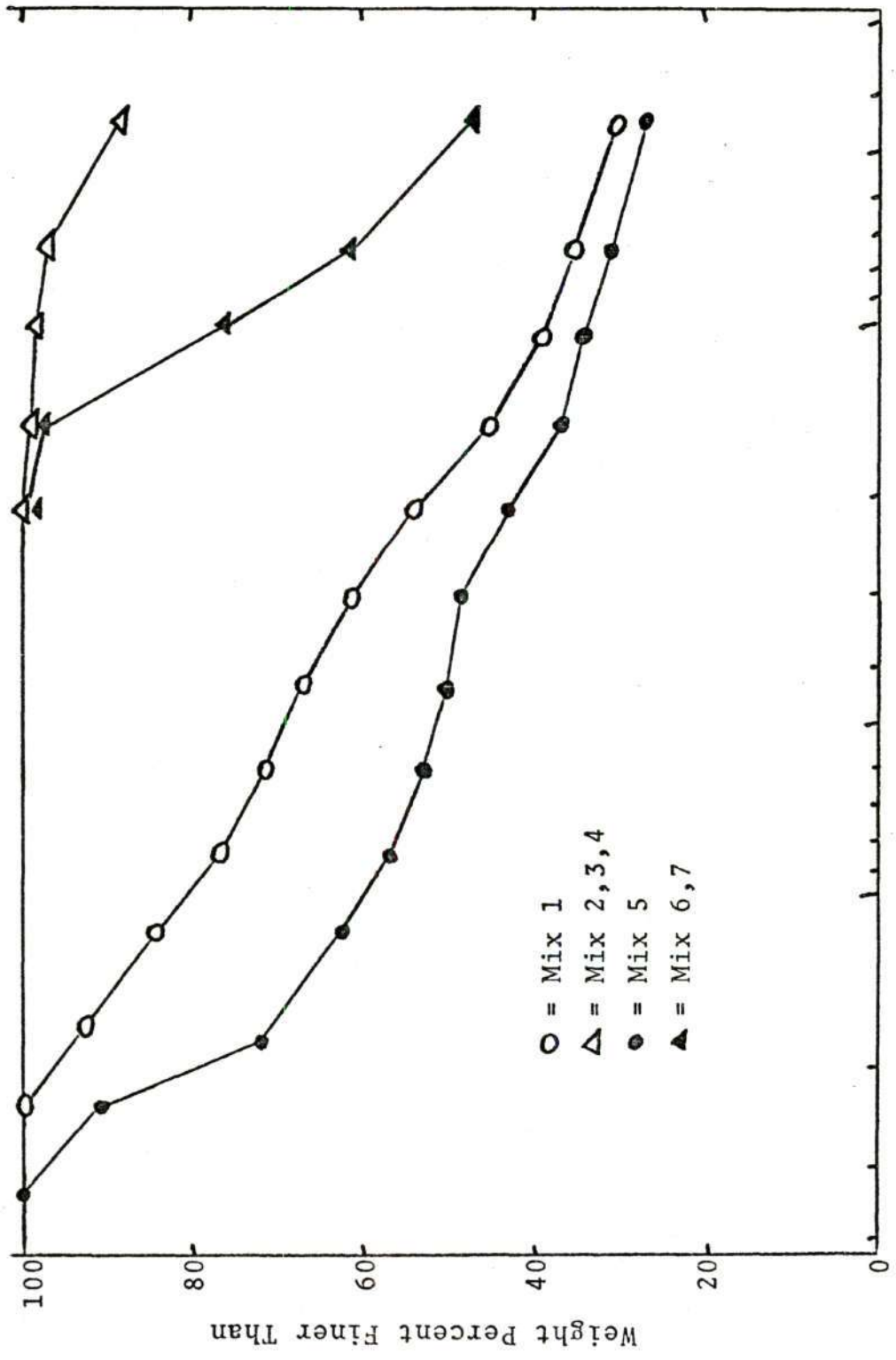

Figure 3. Log Plot of Size Fractions Present in Mixes I-VII

The following numbering system was used for all samples and will be used throughout the text: I-1. The first number (in Roman numerals) is the number of the mix and goes from I through VII. The second number refers to the particular sample of the mix being tested, goes from 1 through 40, and is explained in Appendix A.

Experimental Procedure

Hot Modulus of Rupture

Hot modulus of rupture data was measured on equipment similar to that described by Folk and Bohling [11]. The 1" x 1" x 6" samples were broken once every ten minutes. When the test temperature was changed, one hour was allowed to raise test temperature 200°F. Six test specimens were then broken allowing sufficient time for equilibrium to be established. Modulus of rupture was measured at the following temperatures:

Room Temperature	2200°F
1600°F	2400°F
1800°F	2600°F
2000°F	2800°F

The formula used to compute modulus of rupture (MOR) was:

$$MOR = 3/2 \frac{PL}{bd^2}$$

where

MOR = Modulus of rupture in psi

P = breaking load (pounds)

L = breaking span in inches (4 inches)

b = width of specimen in inches at fracture point

d = depth of specimen in inches at fracture point

X-Ray Phase Analysis

Phase Identification

The samples broken for the modulus of rupture determination were used for x-ray phase analysis. A cut 3/4" back from the broken face was made with a water-cooled diamond saw. This sample was used for x-ray examination. After allowing drying overnight in a gas drier, the samples were broken in a porcelain mortar and pestle until all the particles would fit into a tungsten carbide shatterbox. Samples were ground for ten minutes in the shatterbox. Wet screen analysis indicated less than two percent of +325 mesh particles.

X-ray diffractions analysis was performed with a Philips-Norelco diffractometer using nickel filtered Cu Kα radiation. X-ray counts were measured with a sintilitation detector and Ortec electronics. The x-ray beam geometry was defined by a 4° take-off angle, a 1° divergence slit, a 1° scatter slit, and a 0.003" receiving slit. Operating conditions were 45 KV, 25 ma. The following phases were identified in the samples by x-ray diffractions:

Quartz

Cristobalite

Mullite

Alumina

Internal Standard Technique

Quantitative phase analysis [34] was accomplished using the internal standard technique described by Klug and Alexander.

The internal standard technique involves scanning a characteristic diffraction peak of a crystalline phase to obtain the diffracted intensity. These intensities were measured by obtaining the number of counts in the peak. Comparison of these counts with the counts obtained for a known standard introduced into the material gives one an approximation of the amount of the phase present. The theoretical justification was explained by Klug and Alexander and is given the following equation:

$$X_j = K \frac{I_{ij}}{I_{ks}}$$

where

X_j = weight fraction of component j in a mixture

I_{ij} = intensity of line i of component j of a mixture (unknown)

I_{ks} = intensity of line k of component s of a mixture

K = constant

Thus, when the internal standard is added in a constant proportion X_s, the concentration of component j is a linear function of the intensity ratio: I_{ij}/I_{ks}. By the preparation of curves of known phase concentrations, an unknown concentration can be analyzed by comparison with these curves.

The intensity is obtained by scanning the diffraction peak characteristic of the crystalline material. This peak, for example the 110 peak of mullite centered at 16.42°2θ, is scanned from 16.00° to 17.00°2θ. The number of counts in the peak were determined. The background counts were subtracted from the total number of counts in the peak to determine net counts in the peak. The background was obtained by taking half the total scan time counting at the starting angle (16.00° in the above example), then counting at the finishing angle (17.00° in the above case) for an equal length of time. The total number of background counts was subtracted from the number of counts obtained from the angular scan (16.00° to 17.00°). This removes noise, giving one only the diffracted peak intensity.

To provide maximum accuracy of peak intensity measurements, angles must be chosen for minimal interference from the other crystalline phases present. The scanning angles chosen are listed in Table 3. The internal standard used was rutile (TiO_2) of a 2-5 μ particle size supplied by TAM. Approximately ten grams of sample was weighed to the nearest

Table 3. Internal Standard Scanning Conditions

Phase	Angle Scan (Degrees 2θ)		Peak Scan	Background Scan
	Start	Stop	Total time of scan (seconds)	1/2 time of scan (seconds)
Mullite	16.00°	17.00°	240	120
Quartz	20.50°	21.30°	192	96
Crist	21.20°	22.50°	312	156
Rutile	27.10°	28.00°	216	105
Al_2O_3	42.90°	44.00°	264	132

Scanning Conditions

Cu K_2 radiation with nickel filter

45 KV-25 ma

Scan rate 1/4°/minute

0.001 gram on a Mettler balance. Ten percent of the weight was added in rutile. The sample was then placed a second time in the shatterbox for two minutes. This was used to mix the components.

Sample preparation for x-ray analysis was performed by the back loading technique. The front of a sample holder that receives the diffracted beam was placed on a flat frosted glass slide. A second sample holder was placed on top of the first and powder was placed in both by tapping a spatula over the sample holder area until the cavity was filled. Excess powder was then scraped off, and the second holder removed. The flat blade of the spatula was used to press the powder into the back of the first sample holder. A random sample surface was obtained by pulling the frosted glass slide perpendicularly away from the holder (not sliding).

Standards to be used as a basis to compare with unknowns were prepared. Crystalline quartz, alumina, cristobalite, and mullite were obtained. In the case of mullite, the sample used was estimated to contain 10 percent glass and 90 percent mullite. Table 4 lists the compositions used to make calibration calibration curves. Once the ratio of the peak for a particular phase and the internal standard have been obtained, the amount of the phase present can be determined from the calibration curve.

The equations for the calibration curves were determined

Table 4. X-Ray Standards for Phase Identifications

Std. No.	Weight Percent				
	Quartz	Crist	Mullite	Alumina	Glass
1	0	25	45	25	5
2	0	10	72	10	8
3	10	10	27	50	3
4	25	25	22.5	25	2.5
5	5	0	4.5	90	0.5
6	5	5	4.5	85	0.5
7	10	5	13.5	70	5.5
8	0	30	63	0	7
9	15	15	63	0	7
10	5	10	13.5	70	1.5
11	10	10	63	10	7

by least squares regression analysis using a PDP-8/E computer. These equations along with their standard error of estimate and correlation coefficients are listed in Table 5. The raw data is included as Appendix B.

Standard sample 3 (see Appendix B) was x-rayed five times to determine the repeatability of the x-ray technique. The sample holder was repacked before each x-ray scan and the five scans were done on different days. The results obtained are given in Table 6.

Three samples were chosen for each composition from every grouping of a temperature at which hot MOR was determined. Each sample was x-rayed once and phase content of the three samples averaged together. The raw data is listed in Appendix B and the average values are presented in the Results and Discussion of Results Chapter.

An experiment to determine if specimen cooling rate affected the room temperature phase composition was performed since Smith had water quenched samples he used for phase analysis. Samples 1/2" x 1/2" x 1" were cut from specimen I-3. These were heated in an electric kiln at 250°F/hour to 1600°F. Samples were removed after a two-hour soak at the following temperature:

1600°F

1800°F

2000°F

2200°F

2400°F

Table 5. Phase Identification Equations

Mullite

$X = 63.36935\ (Y) + 1.499034$

Standard error of estimate = ±1.414163
Correlation Coefficient = 0.998440

Al_2O

$X = 28.77690\ (Y) + 5.653423$

Standard error of estimate = ±1.1722671
Correlation Coefficient = 0.999261

Quartz

$X = 35.352803\ (Y) + 1.186988$

Standard error of estimate = ±0.981896
Correlation Coefficient = 0.988711

Cristobalite

$X = 7.272886\ (Y) + 0.4531161$

Standard error of estimate = ±0.6490919
Correlation Coefficient = 0.997192

X = weight percent of component being examined

$$Y = \frac{\text{counts in peak of unknown}}{\text{counts in peak of rutile}}$$

Table 6. X-Ray Phase Analysis Reproducibility

Test No.	Weight Percent			
	Al_2O_3	Crist.	Quartz	Mullite
1	48.91	9.35	9.92	24.90
2	50.61	9.57	10.13	25.13
3	50.21	9.65	10.50	24.00
4	51.30	9.71	10.61	25.68
5	49.72	9.40	9.49	25.52
Average	50.15	9.54	10.13	25.05
Estimated Standard Deviation	0.90	0.16	0.45	0.66
High	50.61	9.71	10.61	25.68
Low	48.91	9.35	9.49	24.00

Test Sample = Std. 3

One sample was allowed to cool to room temperature in air, and the other sample was quenched in water. Each sample was ground in a mortar and pestle to pass 48 mesh. They were then individually ground in a Fisher automatic mortar and pestle for one hour. The rutile internal standard was added as described earlier. Mixing was accomplished by placing the powder in a small glass jar with two glass marbles and shaking for one hour in an automatic shaker. This data also appears in Appendix B.

Thermal Expansion

Thermal expansion was measured using an Orton Automatic Recording Dilatometer. Thermal expansion for all compositions was measured in the as-fired condition and after hot modulus of rupture determination at 2800°F. All of these specimens were cut from the "a" position, the length top, as shown in Figure 4. To determine the effect of sample orientation on thermal expansion, specimens were cut from sample numbers I-4 and II-37 in the a, b, c, and d positions explained in Figure 4. All samples were cut to approximately 1/4" by 1/4" by 1" with a water-cooled diamond saw. The one-inch dimension was ground on SiC paper to adjust length to 1±0.001 inch.

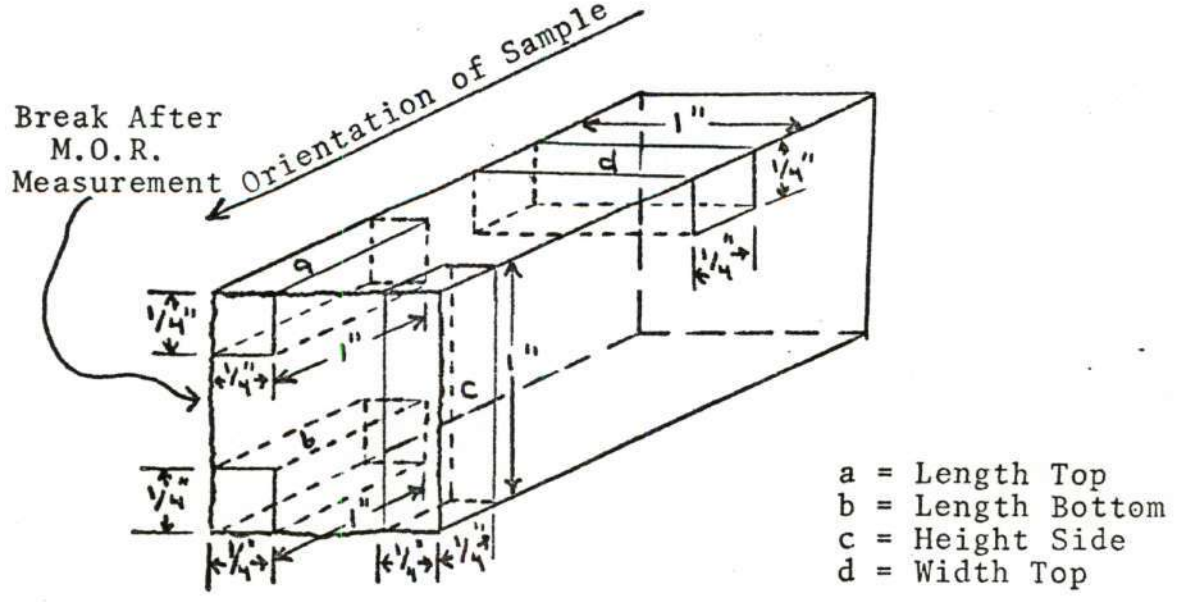

Figure 4. Thermal Expansion Sample Origin

CHAPTER IV

RESULTS AND DISCUSSION OF RESULTS

Density, modulus of rupture, phase behavior, and thermal expansion data were analyzed. The maximum strength between 1700 and 2100°F for the alumino-silicate compositions and its relationship to phases present and linear thermal expansion were examined for each mix. The two theories of crystal precipitation and stress relief by glass relaxation were investigated. Stresses relieved are those set up by differences in expansion between phases present and anisotropic expansion.

Sample Density

Variations in fired sample density occurred for both the mullite mixes I-IV and for the high-alumina mixes V-VII, Table 7. Raw materials and particle size were the causes of these density variations. The estimated standard deviations for density of each mix indicated that sample fabrication using the screw press gave uniform sample densities.

Modulus of Rupture

Modulus of rupture data reported in Table 8 is the average of five samples (for raw data see Appendix A). Plots of modulus of rupture versus temperature are shown in Figure

Table 7. Average Fired Density and Estimated Standard Deviation for Ten Specimens of Mixes I-VII

Mix Number	Density (lbs/ft^3)	Estimated Standard Deviation
I	143.5	1.20
II	109.8	1.28
III	135.9	1.08
IV	117.2	0.85
V	167.3	1.04
VI	146.0	1.55
VII	160.6	1.87

Table 8. Hot Modulus of Rupture Strengths* (psi)

Temperature	Mix I	Mix II	Mix III	Mix IV	Mix V	Mix VI	Mix VII
Room	761	555	1333	935	1514	1443	1328
1600°F	964	664	1653	1038	1744	1350	1304
1800°F	1167	896	1967	1083	2224	2241	1826
2000°F	1031	763	1789	1141	1536	1312	1498
2200°F	508	569	1307	866	788	789	1002
2400°F	401	349	771	530	863	536	536
2600°F	304	224	386	292	437	275	468
2800°F	229	194	238	244	461	949	334

*Each value represents an average of 5 samples

5 for mixes I-IV and Figure 6 for mixes V-VII.

It should be noted that every plot of hot modulus of rupture versus temperature has the characteristic rise in strength of alumino-silicate mixtures. These results are similar to those obtained by Russell Smith [1] and Frank Duncan [2], Figures 5, 6, and 7. The peak in strength occurred between 1800° and 2100°F. Notice that despite the chemical similarity of mixes I-IV, there is a large difference in the maximum strength observed in this high mullite series. Mix I, which had the largest grain size of these groups, shows a greater maximum strength than mixes II and IV, which were much finer in grain size. This was the reverse of the expected trend of smaller grain sizes giving greater strengths. Mix III, however, does appear to follow this expected trend. Its modulus of rupture values were larger than those for mix I, II, or IV. It had a grain sizing comparable to mixes II and IV.

Mix I had the highest density of these 4 mixes, followed by mix III (see Table 7). Mixes II and IV had the lowest densities. This agrees with the expectation that lower density specimens would have lower strength. When the densities are comparable (for example, mixes I and III), dramatic strength increases were observed when the particle size was decreased.

The same effect of the larger grain mixes having the greater strength was also noted in the high alumina mixes

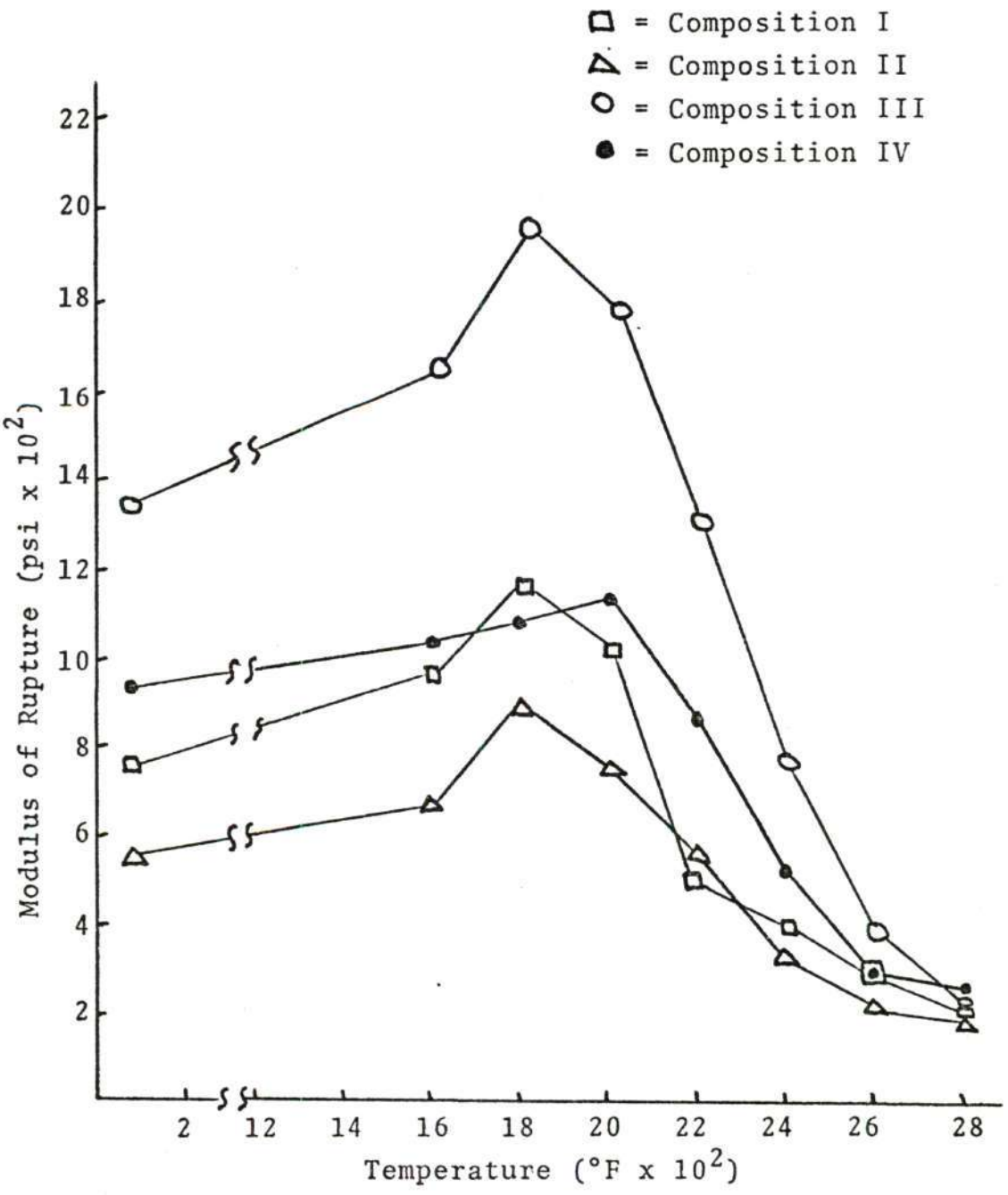

Figure 5. Hot Modulus of Rupture
Compositions I-IV

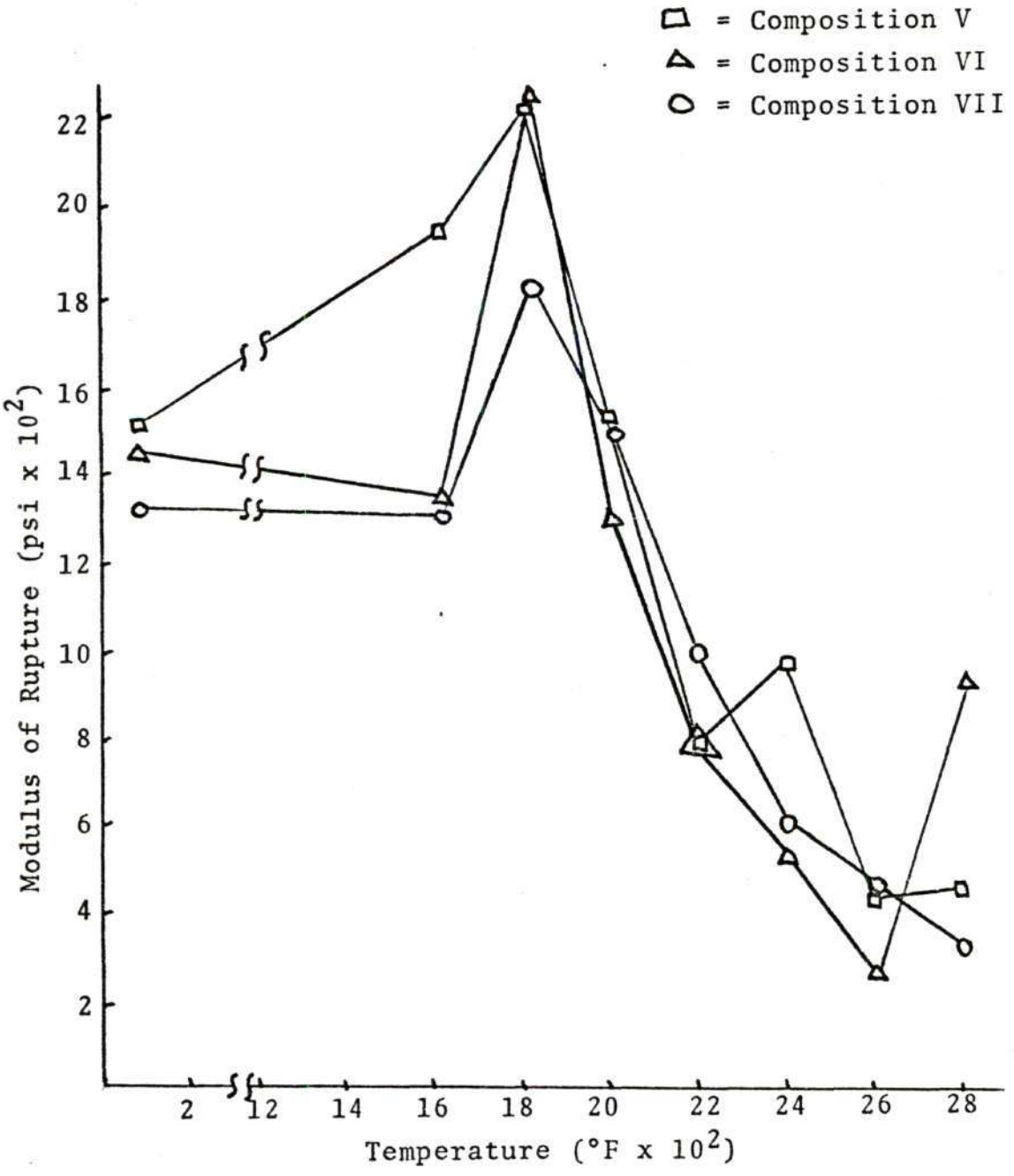

Figure 6. Hot Modulus of Rupture
Compositions V-VII

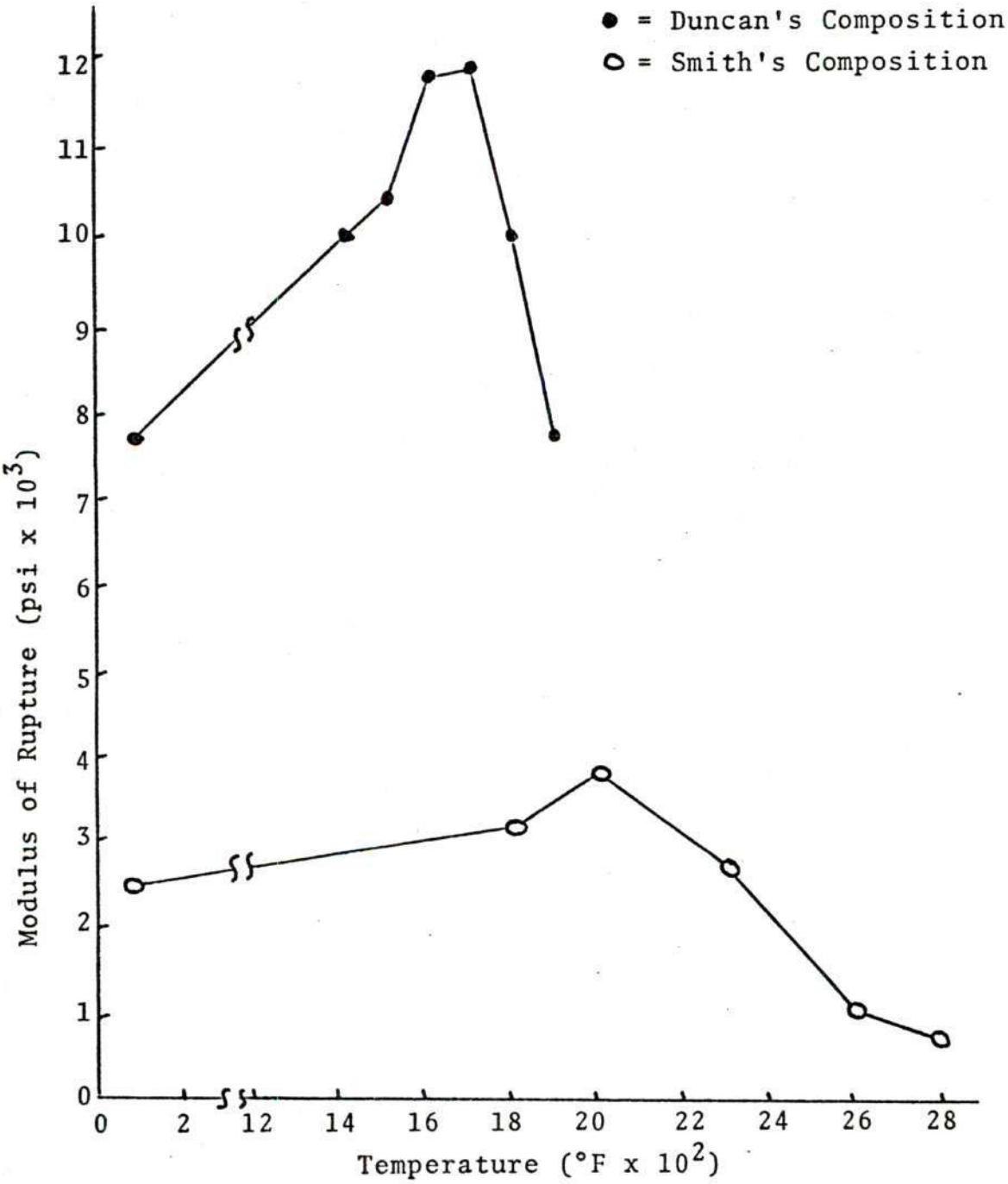

Figure 7. Hot Modulus of Rupture Strengths Obtained by Duncan and Smith

(V-VII). Strength differences were not as pronounced as those observed in the mullite mixes. Mix V had the largest particle size and showed the greatest strength. The fact that mix V also had the greatest fired density (Table 7) agrees with the above results. However, mix VII had a fired density similar to mix V and had a lower strength. This is probably due to the use of clay in mix VII as a source of SiO_2, which resulted in the formation of less glass as shown by x-ray analysis in the following section.

X-Ray Phase Analysis

Using the scan procedures outlined earlier, the amount of each phase present was estimated. X-ray data for individual samples is in Appendix B and summarized in Appendix C.

Rate of Quenching

The results obtained from the investigation into the difference between air and water quenched sampled are given in Table 9. No significant difference was detected in the phases present in the air and water quenched samples; thus present results are comparable.

Phase Analysis

The average phase composition for the seven mixes is summarized in Appendix C. The relative amount of glass present can be determined by subtracting the total crystalline phases from 100. One will notice that in the high-alumina

Table 9. The Effect of Quenching Rate on Phases Present

Quenching Temp.	Quenching Condition	Percent Mullite	Percent Quartz	Percent Crist	Percent Alumina	Glass
1600°F	Air	35.9	None	18.3	19.9	25.9
1600°F	Water	42.3	None	20.5	23.7	13.5
1800°F	Air	44.4	None	22.6	24.8	8.2
1800°F	Water	42.5	None	22.4	24.0	11.1
2000°F	Air	42.8	None	21.6	25.8	9.8
2000°F	Water	44.0	None	22.1	28.1	5.8
2200°F	Air	43.0	None	21.1	20.8	15.1
2200°F	Water	44.2	None	21.0	23.6	11.2
2400°F	Air	43.6	None	19.2	26.4	10.8
2400°F	Water	46.5	None	19.6	22.6	11.3

Test sample was I-3.

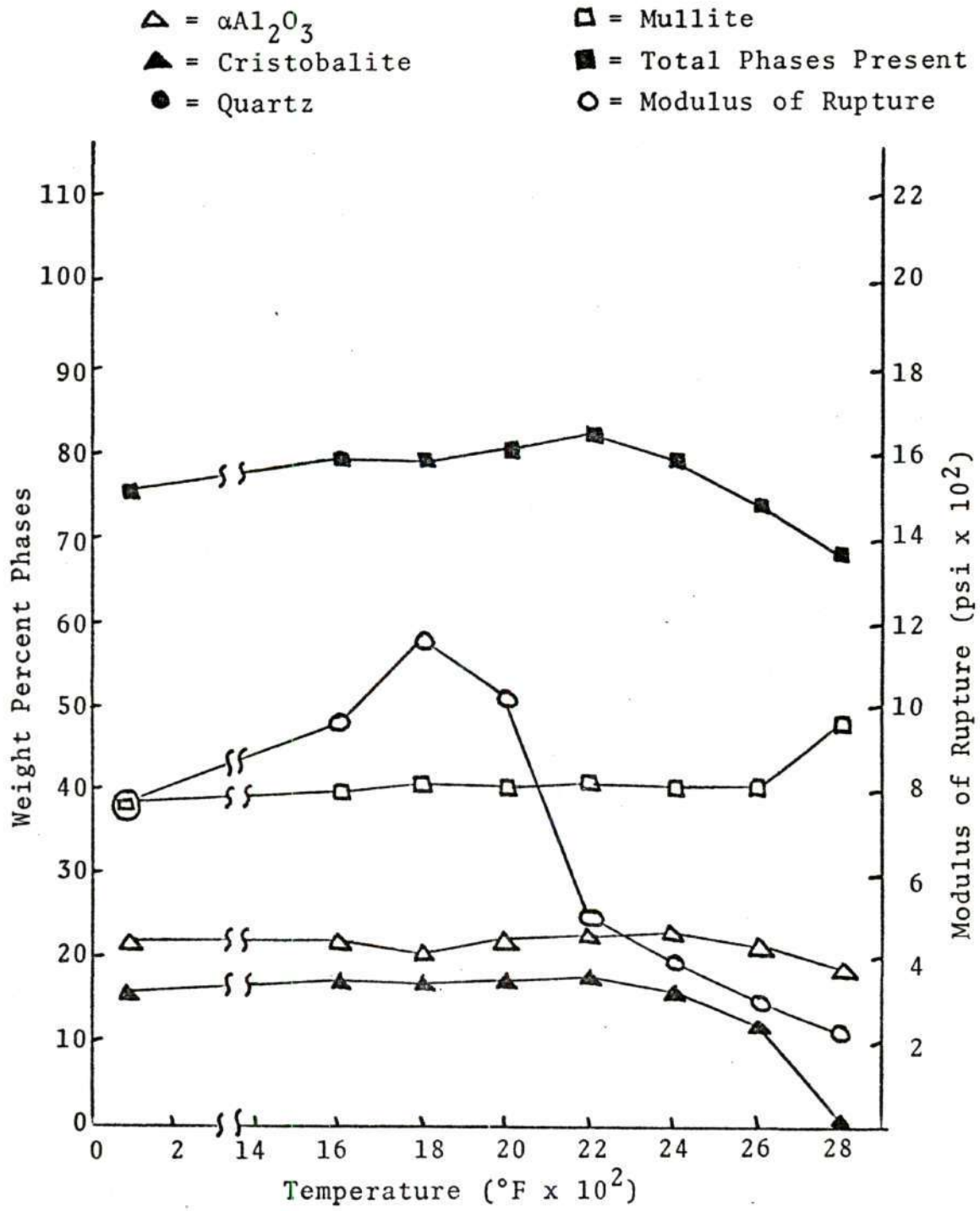

Figure 8. Phase and Strength Changes vs. Temperature Composition I

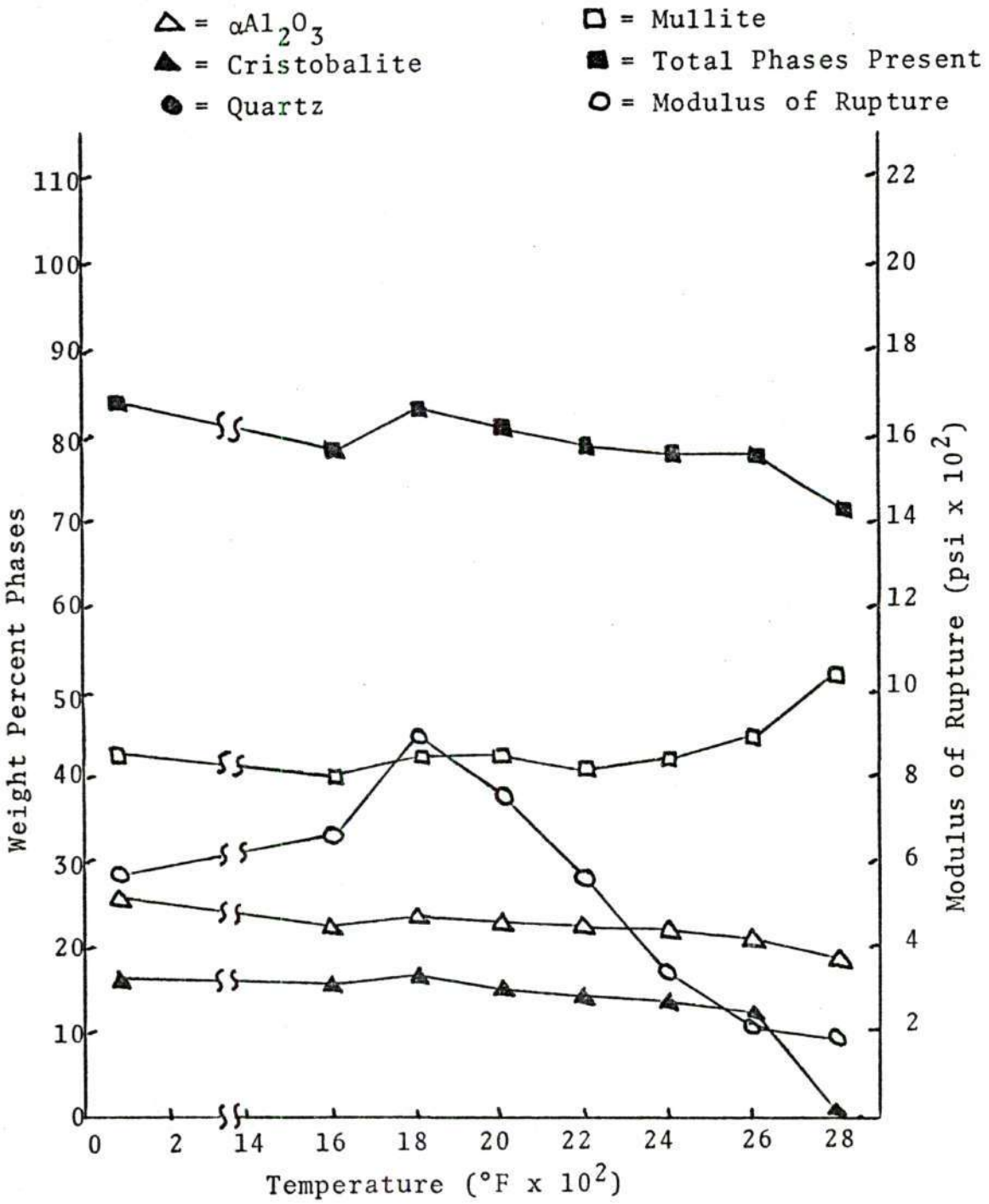

Figure 9. Phase and Strength Changes vs. Temperature Composition II

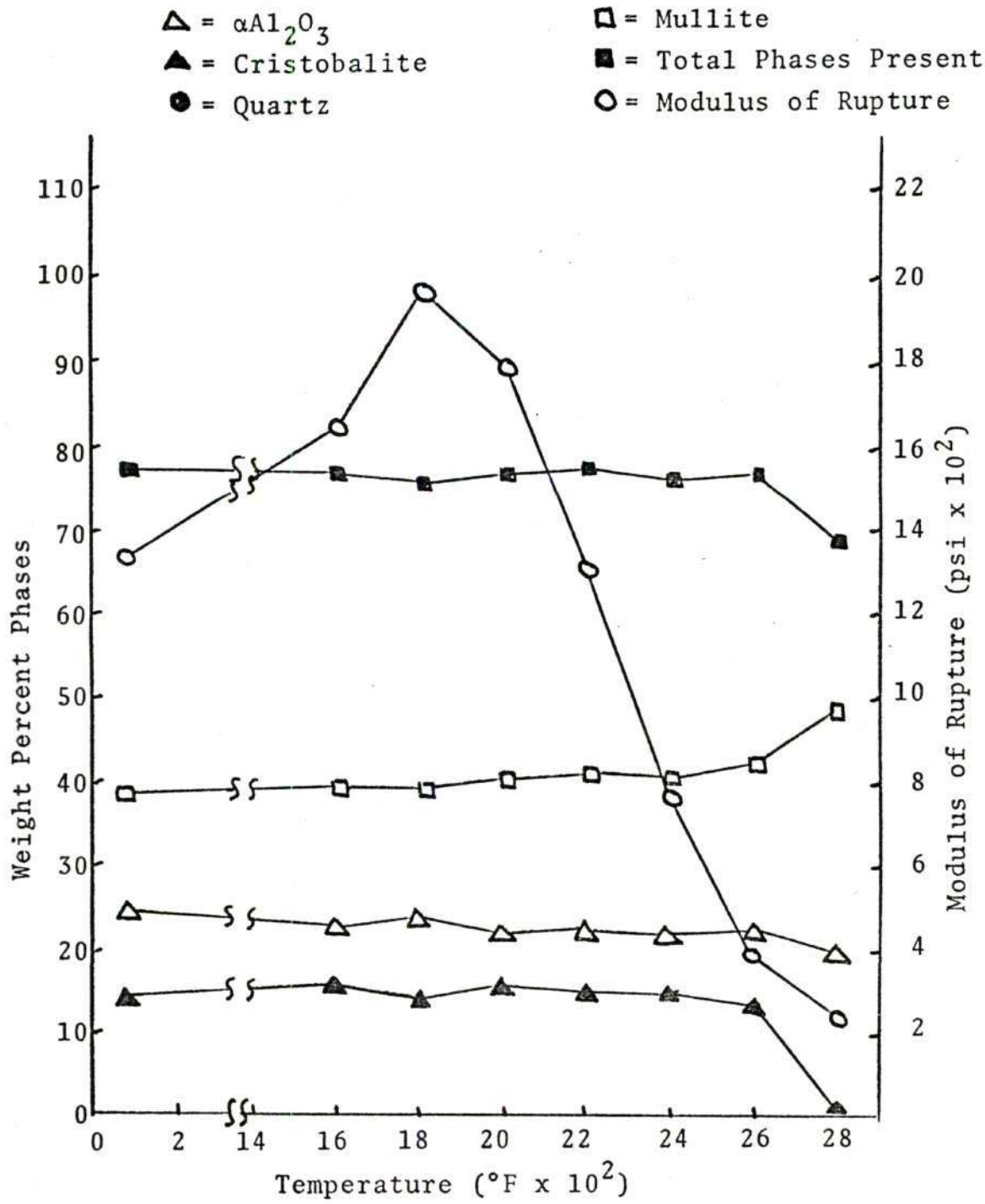

Figure 10. Phase and Strength Changes vs. Temperature Composition III

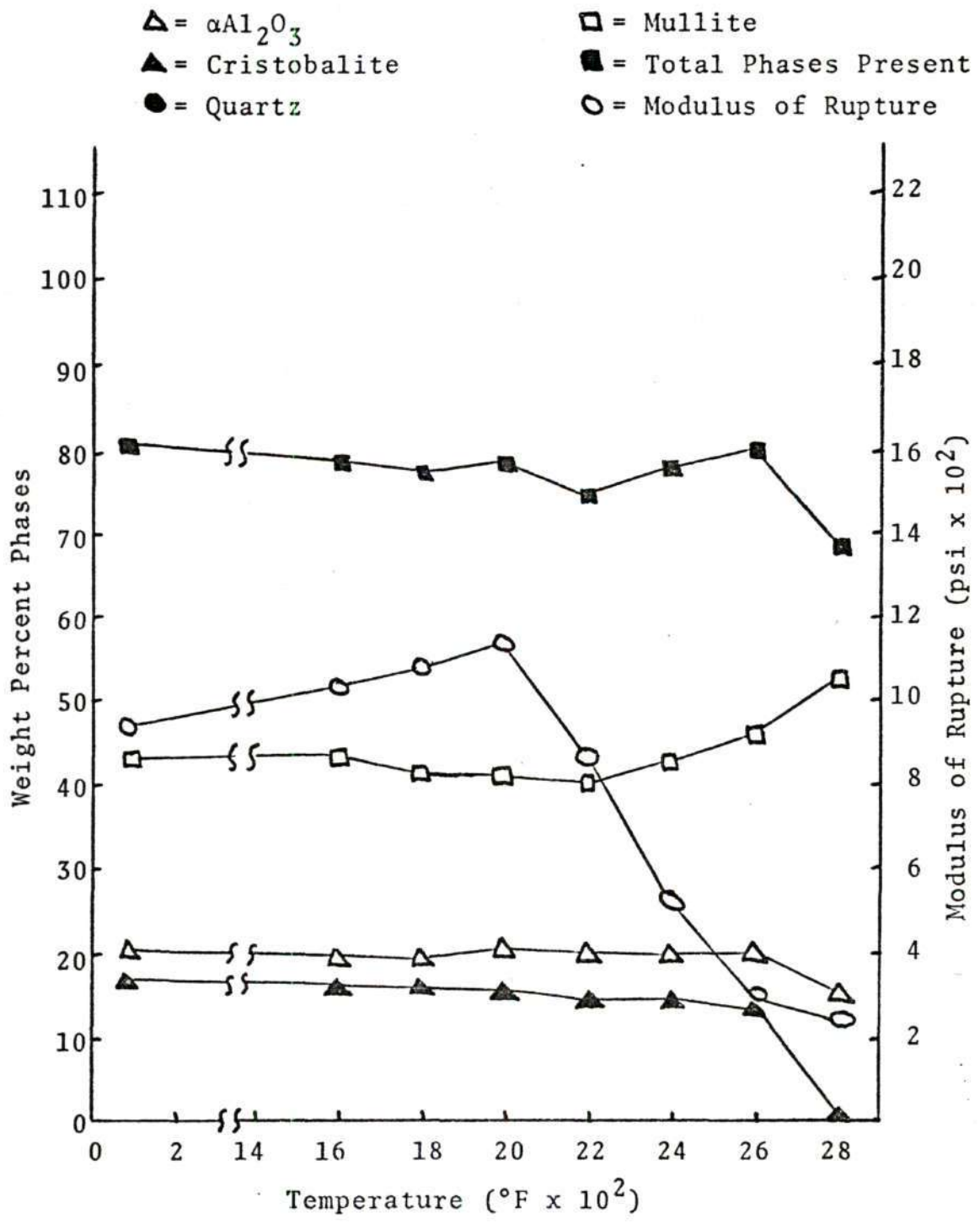

Figure 11. Phase and Strength Changes vs. Temperature Composition IV

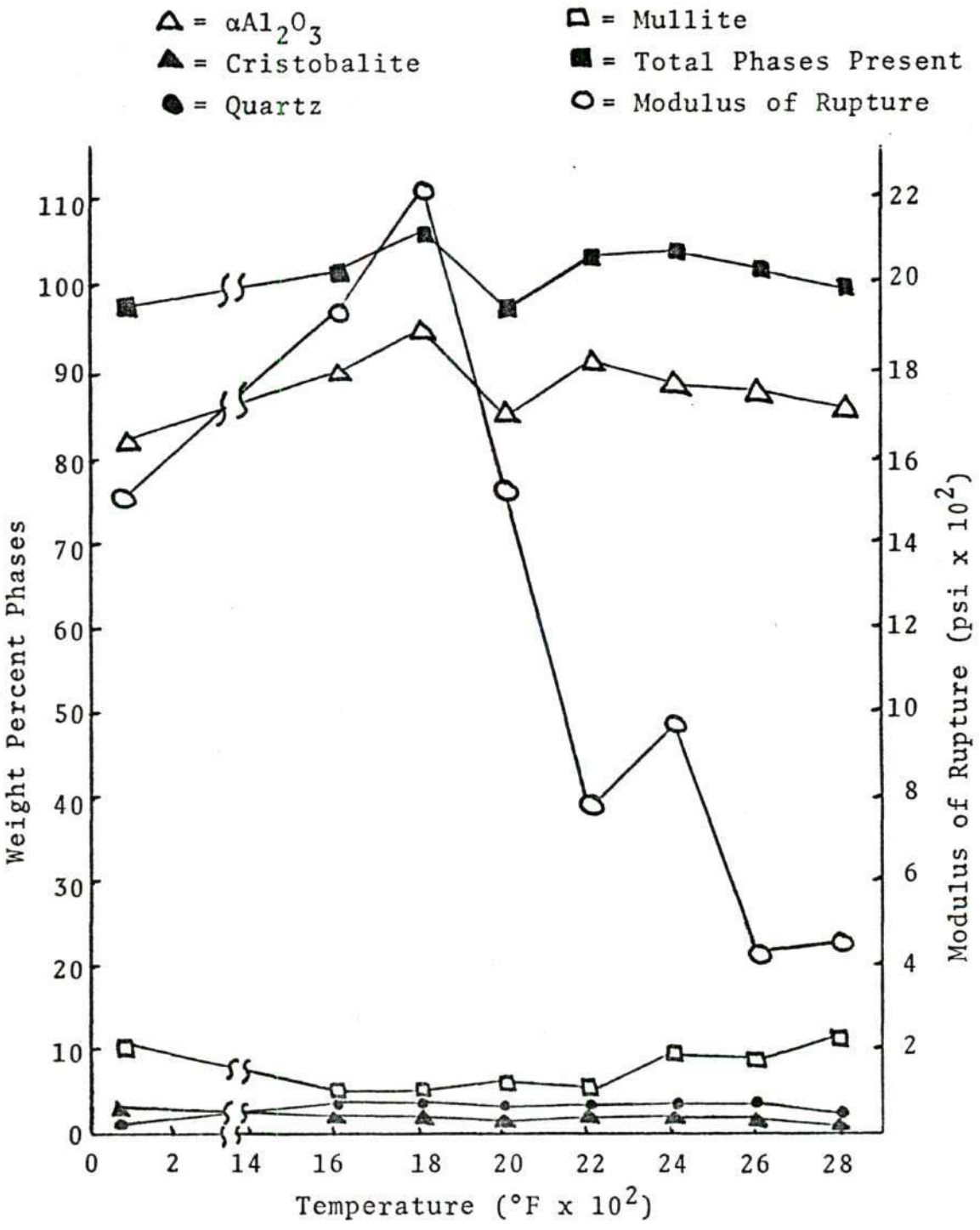

Figure 12. Phase and Strength Changes vs. Temperature Composition V

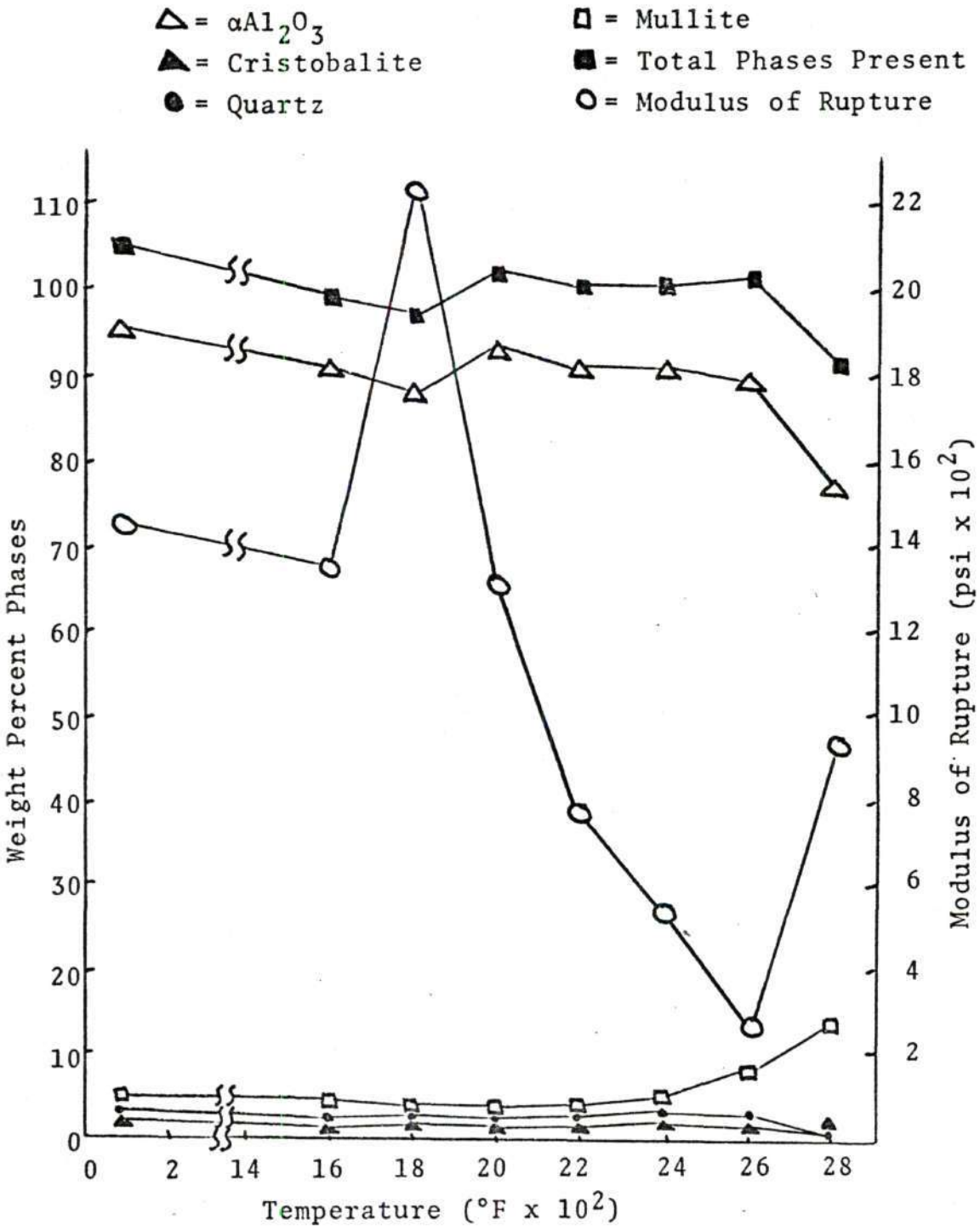

Figure 13. Phase and Strength Changes vs. Temperature Composition VI

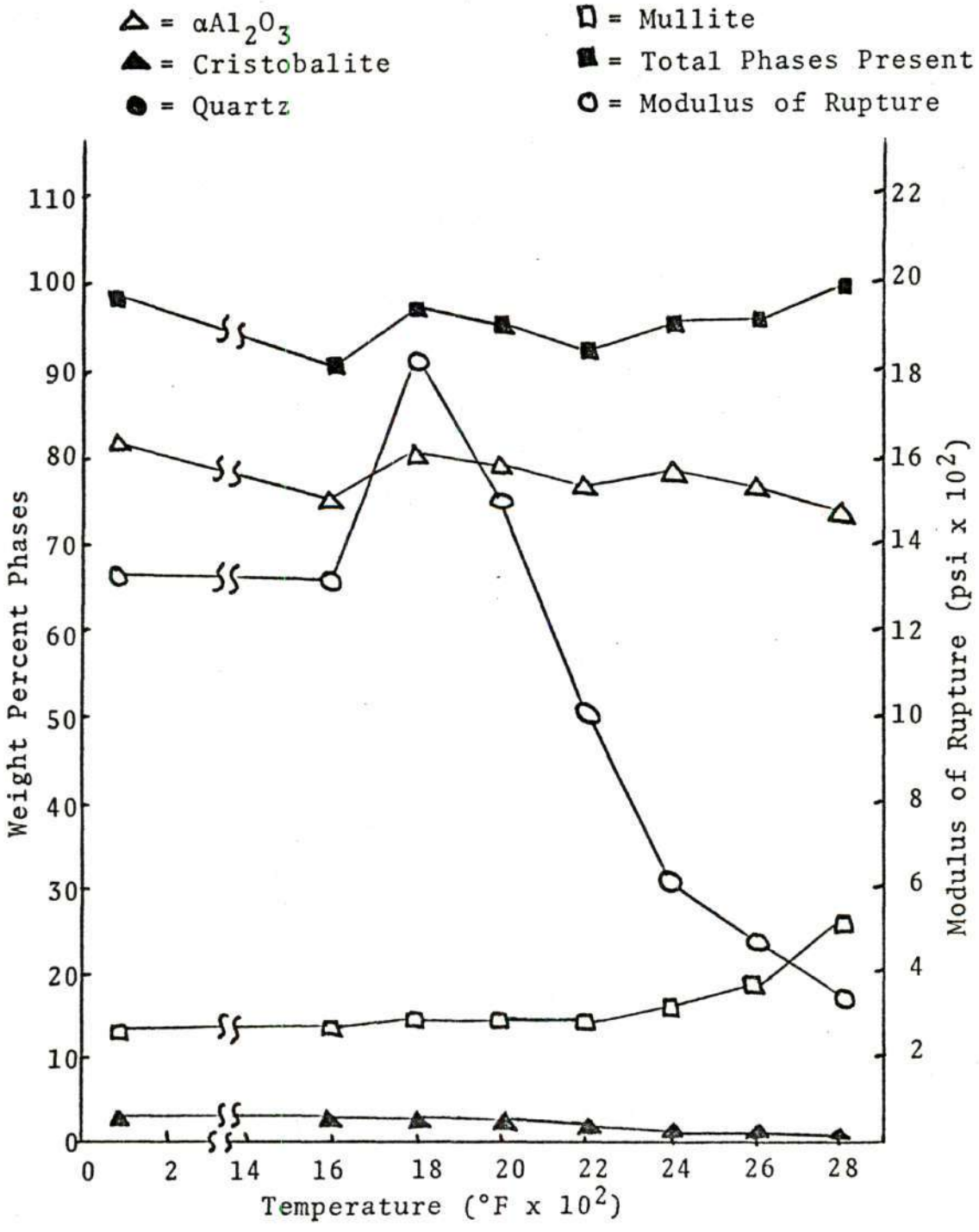

Figure 14. Phase and Strength Changes vs. Temperature Composition VII

compositions, total crystalline phases are often greater than 100 percent. This can be attributed to the accumulative errors for compositions having a large amount of crystalline material present. The variation of phases with temperature are plotted in Figures 8-14.

Compositions I-IV are similar in their relative phase content as would be expected due to their similar chemical composition. In mixes I-IV, alumina and cristobalite content remains essentially constant until approximately 2400°F, where they begin to decrease. The weight percent mullite stayed essentially constant to 2400°F, where it began to increase. It thus appears that Al_2O_3 and SiO_2 react, forming mullite above 2400°F. The large decrease in the amount of cristobalite indicates that besides reacting to form mullite, silica was also converted to form a glassy phase above this temperature. The total crystalline content thus gradually decreased at higher temperature as the glass content increased. This is due to two things: silica reacting at the higher temperatures to form mullite and glass and other crystalline phases reacting to form glass. No significant deviations of the strength peak with phase behavior was found.

The crystalline phase content of the high alumina mixes V-VII is shown in Figures 12, 13, and 14. Again, as noted for the mullite mixes, there was no significant relationship between the phase content and the hot modulus of rupture

below 2400°F. Cristobalite, quartz, and alumina decreased with temperature above 2400°F. In general, mullite and glass increased in this temperature range. Composition VII had no quartz present because clay was used as a source of SiO_2. The alumina and silica of the clay reacted to form mullite, cristobalite, and glass. Mullite content was higher in mix VII than in mixes V and VI while cristobalite, glass, and alumina were lower. The silica and alumina in clay is in a form that more readily reacts, forming mullite, versus free quartz and alumina, which relies on crystal-crystal contact or a glass solution. Strength is also much lower in composition VII, less glass was formed, and there is thus less glass bond. Consequently a lower strength results.

Phase Comparison

Smith's and Duncan's results for similar mullite compositions are shown in Figure 15. Modulus of rupture along with the cristobalite and glass content from Smith's work were plotted. Only modulus of rupture results from Duncan's investigation were plotted as no x-ray data were available. Results obtained from compositions similar to those used by Smith and Duncan are shown in Figures 8 and 10. Composition I is the same as that of the mullite brick used by Smith in his thesis, and composition III is the same as that used by Duncan.

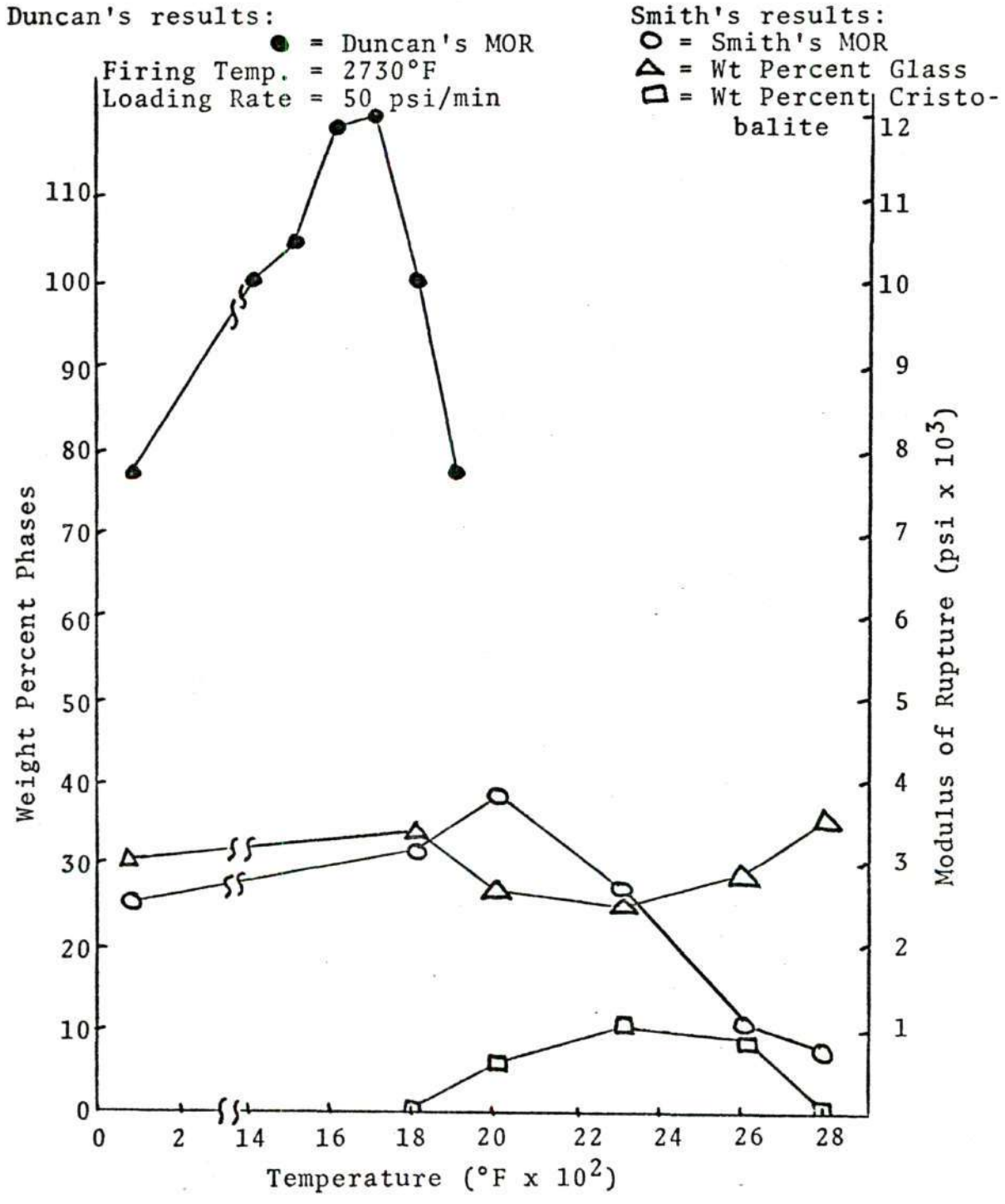

Figure 15. Results Obtained for Crystalline Analysis and Hot Modulus of Rupture by Smith and Duncan

Smith's data led him to conclude that a cristobalite increase and glass decrease were the causes of the hot modulus strength increase. There appears to be no significant differences in the phases content of Smith's samples and the present samples made of his and Duncan's compositions. Both mixes I and III had similar phase content; however, their similar chemical compositions cause this to be expected. All three works show the same hot modulus of rupture trend. It should be noted that Duncan's specimens were about five times stronger than those of the other two investigations. The temperature where maximum strength occurred depends on firing temperature, loading rate, sample density, and many other factors. Smith's results show a definite increase in the amount of cristobalite present, going from none detectable at 1800°F to a high of nearly 12 weight percent at 2300°F. This fact along with the decrease in glass content of 7.4 percent at 2300°F led Smith to conclude that the maximum in the modulus of rupture curve at about 2000°F was related to cristobalite precipitation from the glassy phase.

It appears that the current mullite compositions were fired to a temperature several hundred degrees Fahrenheit lower than Smith's. This assumption is based primarily on the fact that Smith's as fired composition did not contain a detectable amount of cristobalite (Table 10) and also that his samples contained more mullite. Since the phase content

Table 10. As Fired Phases Present in Smith's Composition

	Percent Alumina	Percent Mullite	Percent Quartz	Percent Crist	Total
Present Results	22.3	38.2	None	15.8	76.3
Smith's Results	16.6	50.7	None	None	67.3

of the current mullite specimens (fired to 2450°F) after being tested at 2800°F was similar to that of Smith's work, it appears that cristobalite and alumina reacted at the high test temperatures to form mullite and glass (see Figure 8).

Based on the fact that both Smith's work and the present investigation of high-mullite compositions showed that modulus of rupture values reach a maximum around 1800°F-2000°F and that no significant phase content changes were detected until testing temperature was around 2400°F, it appears that the cristobalite precipitation mechanism proposed by Smith is not the major cause of modulus of rupture strength increase. The behavior of the strength versus temperature curve may be influenced by cristobalite precipitation and glass decrease, but a different mechanism must cause the observed strength behavior.

No significant deviations of strength and phases were observed for the high-alumina experimental mixes up to 2400°F. Comparison of Figures 11-14 shows that the phase content remains constant in the area strength peaks (1800°F). Alumina content varied due to its high amount. Cristobalite increases and glass decreases may cause greater strength changes in the temperature range of 1800°F to 2100°F; however, mixes I-VII show no phase deviation.

Thermal Expansion

Since evidence by previous phase analysis indicated

that crystalline phase changes were not justified as the cause of the observed maximum strength, strength increases due to stress relief in the temperature region where viscous flow occurs were investigated by the use of thermal expansion. When a refractory composition containing glass cools, strains are set up in the materials as the glass reaches the point where it is perfectly elastic. These strains are set up by differential thermal expansion between the different phases and anisotropic expansion of the same phase. On reheating, these stresses can reach the zero strain point through relaxation of the glass. As the stresses are relieved, strength can increase, depending on the type stresses present. With further heating, the glass will reach its annealing temperature. Between this temperature and the yield point of the glass, glass can allow particle movement when a force is applied; and strength will drop. The thermal expansion curves in graphs 16-37 for mixes I-VII will be analyzed for this behavior.

Different thermal expansion sample orientations were tested due to expected differences in expansion behavior. Plastic flow would often create a bowed bar before the sample would break in hot air. It was felt that grain orientation or a difference in stresses may be set up in the sample. Figures 17-20 and 23-27 show the effect of different sample orientations shown in Figure 4 on thermal expansion. It appears that sample orientation has no effect on results.

There were no differences in the expansion characteristics whether the sample came from the top, bottom, or side of the broken bar.

The thermal expansion curves in Figures 16-37 show changes in linearity in the same temperature range that strength increases were observed. Although the exact temperature of change in slope is questionable, a change definitely occurred.

The change in linearity could be related to glass behavior. Figure 38 shows [35] the expansion behavior of a silicate glass. Stress relief occurs at low temperatures for a quenched glass and causes a dip in the glass expansion (curve a). The first dip is caused by the quenched glass relieving its stresses. It should be noted that a positive expansion occurred for both the quenched glass (a) and an annealed glass (b). The positive expansion is due to a reorientation of the glass structures while it becomes less dense. Further increases in its temperature cause the glass structure to become more fluid, causing the second dip.

Stress relief begins at some temperature, T_1, in Figure 38, called the strain point of the glass. As the temperature is raised, more stresses are relieved; and depending upon the magnitude of the stresses present, the dip shown in curve a may or may not be observed. As the temperature approaches T_2, the annealing temperature, thermal motion is sufficient to allow rearrangement of the glass

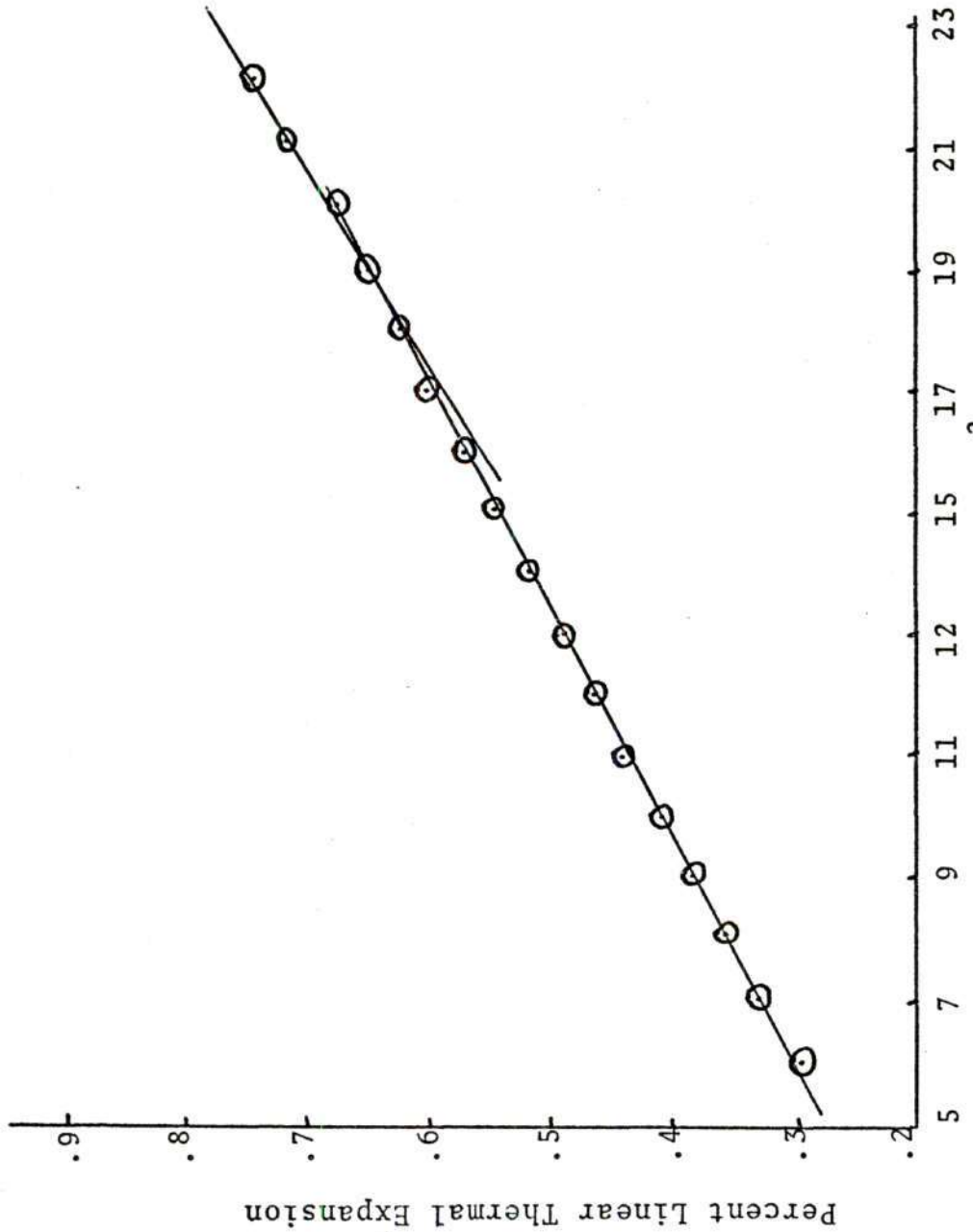

Figure 16. Linear Thermal Expansion Sample I-2

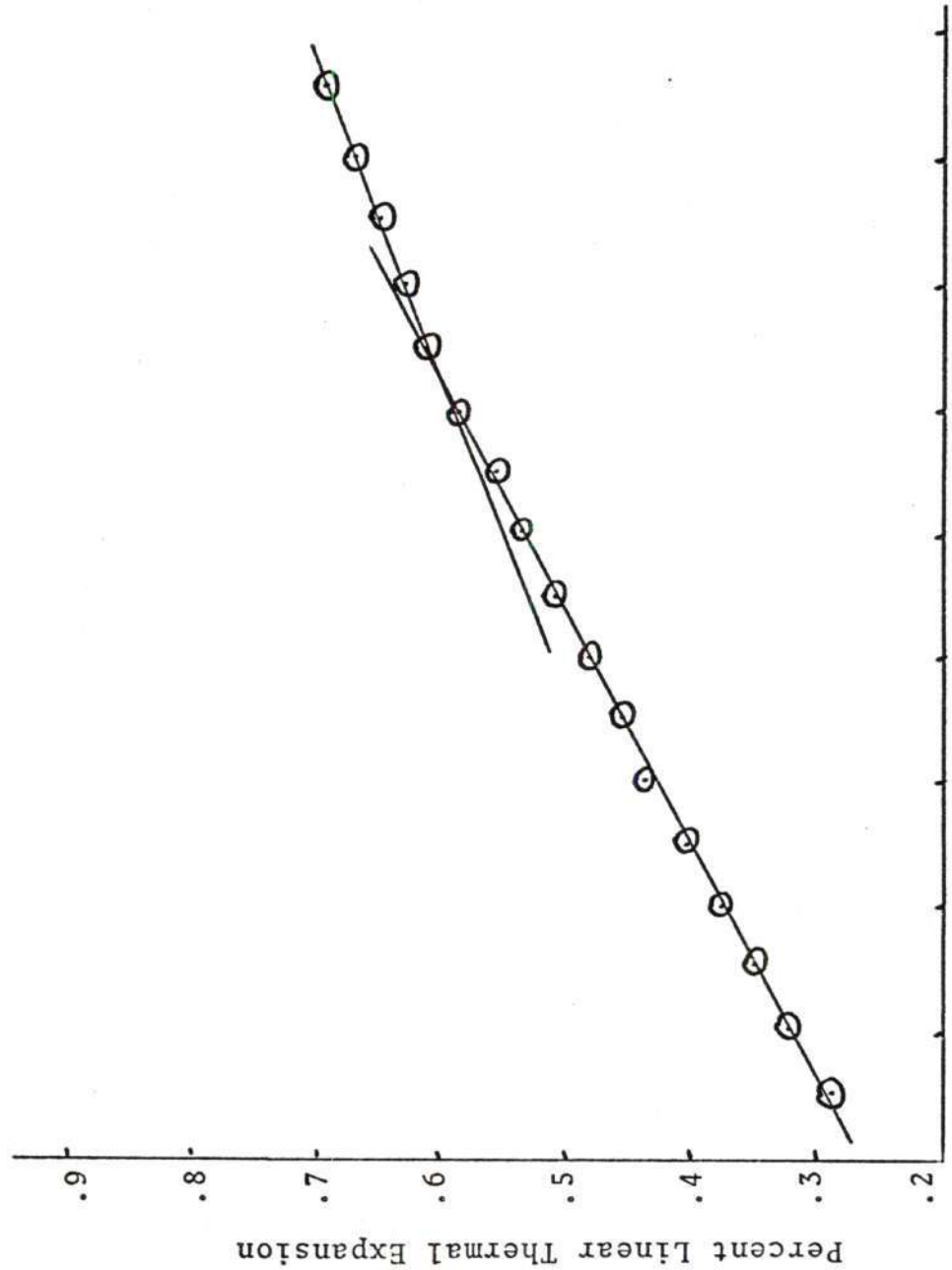

Figure 17. Linear Thermal Expansion Sample I-4
(Length Top)

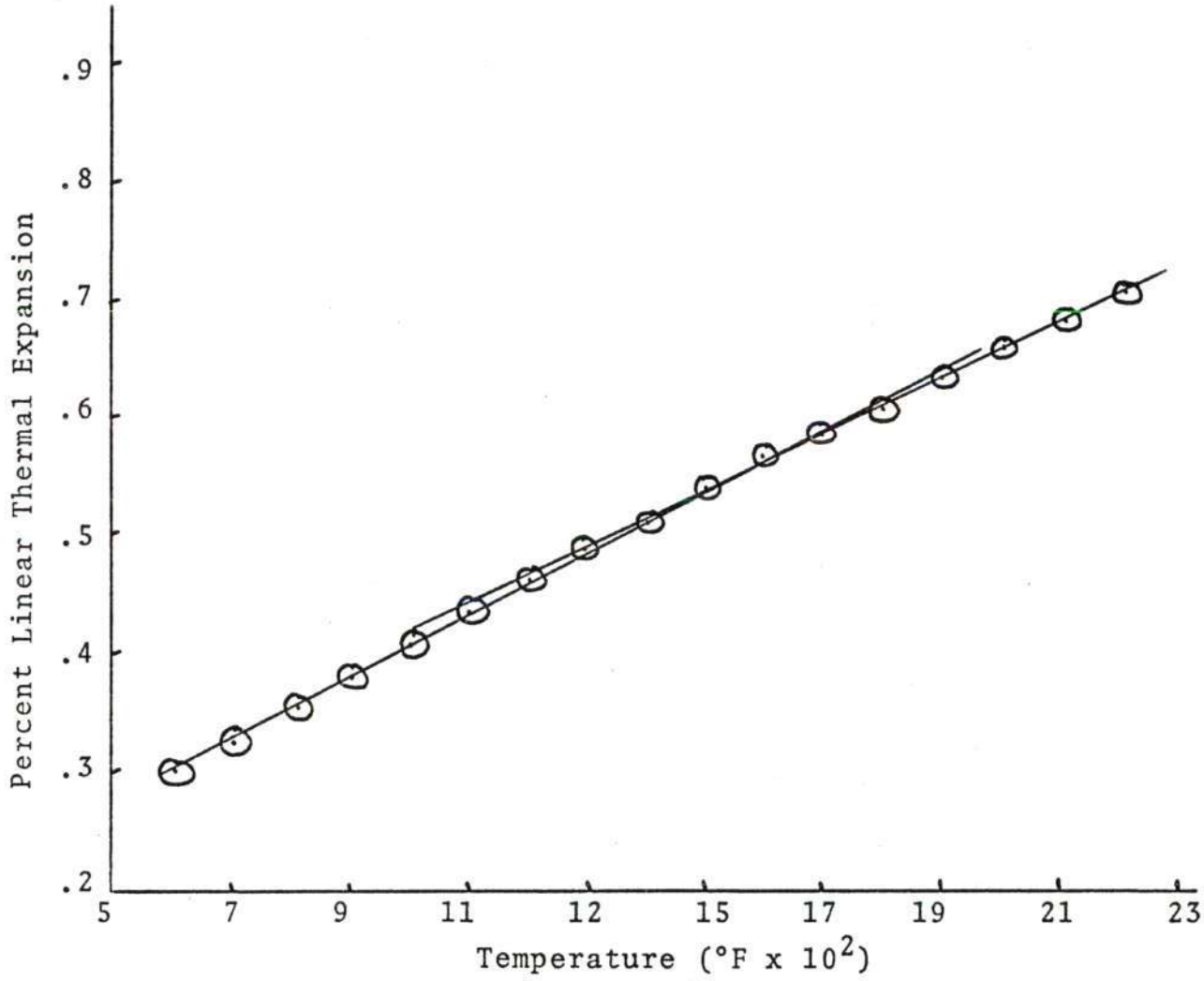

Figure 18. Linear Thermal Expansion Sample I-4 (Length Bottom)

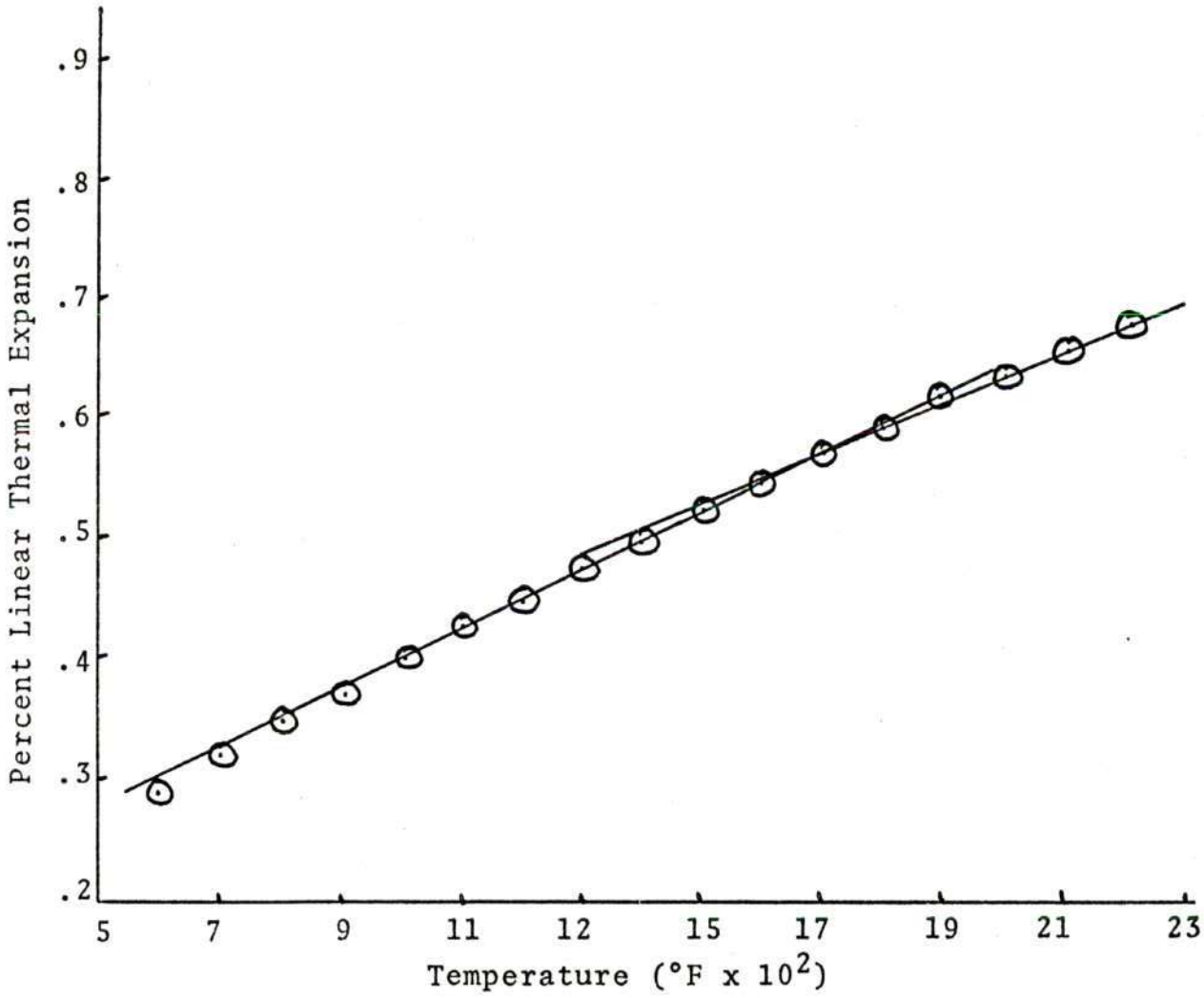

Figure 19. Linear Thermal Expansion Sample I-4 (Height Side)

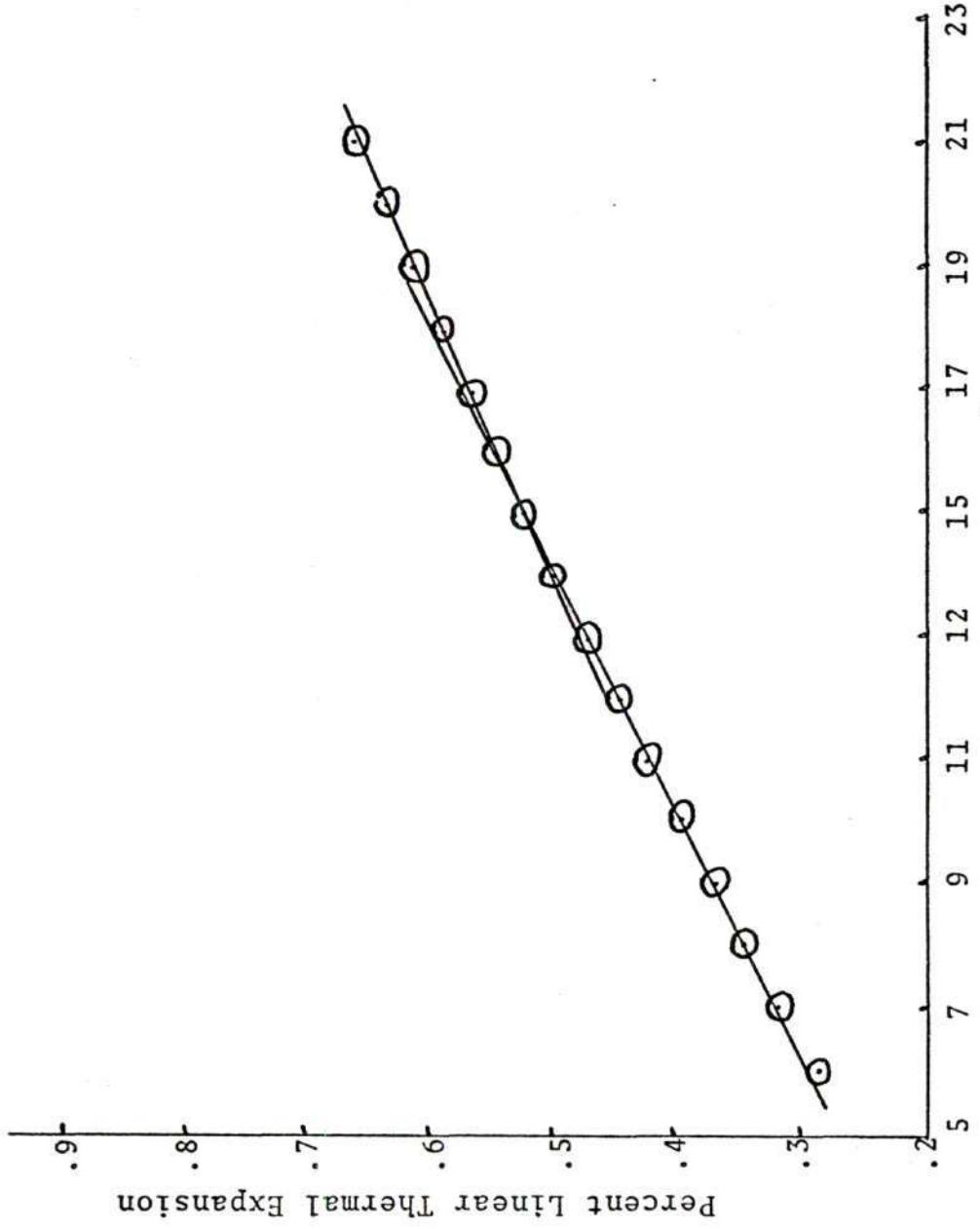

Figure 20. Linear Thermal Expansion Sample I-4 (Width Top)

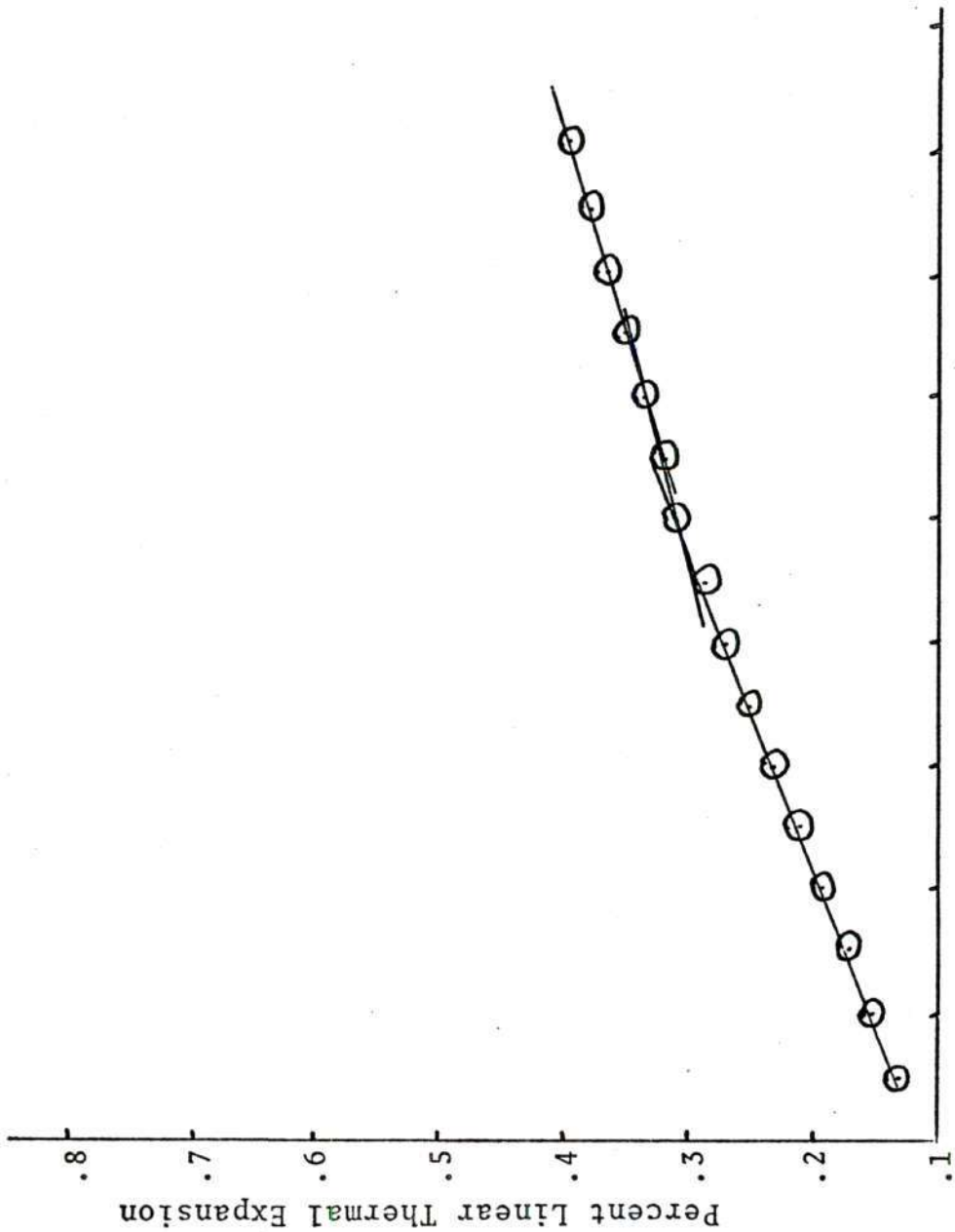

Figure 21. Linear Thermal Expansion Sample I-38

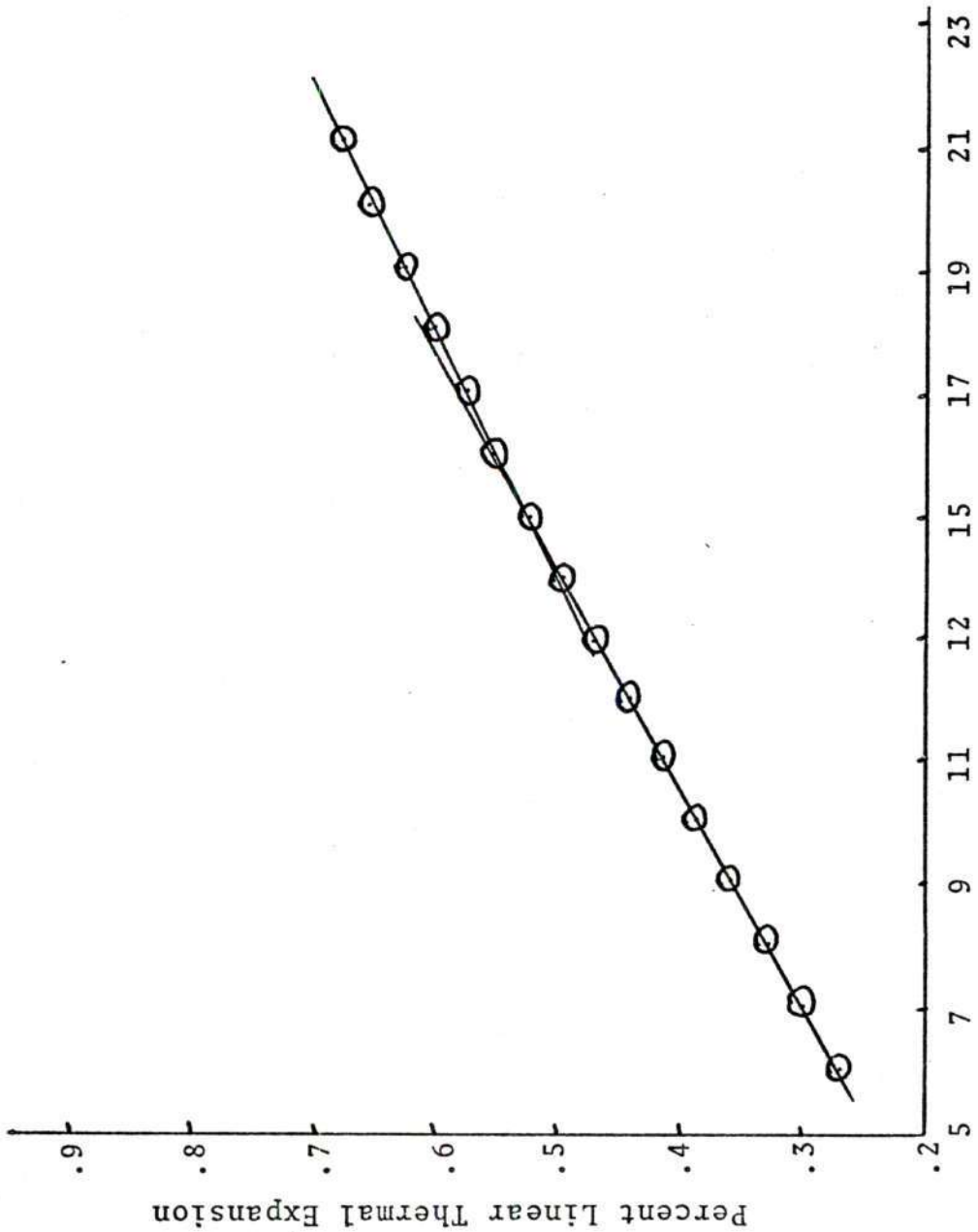

Figure 22. Linear Thermal Expansion Sample II-3

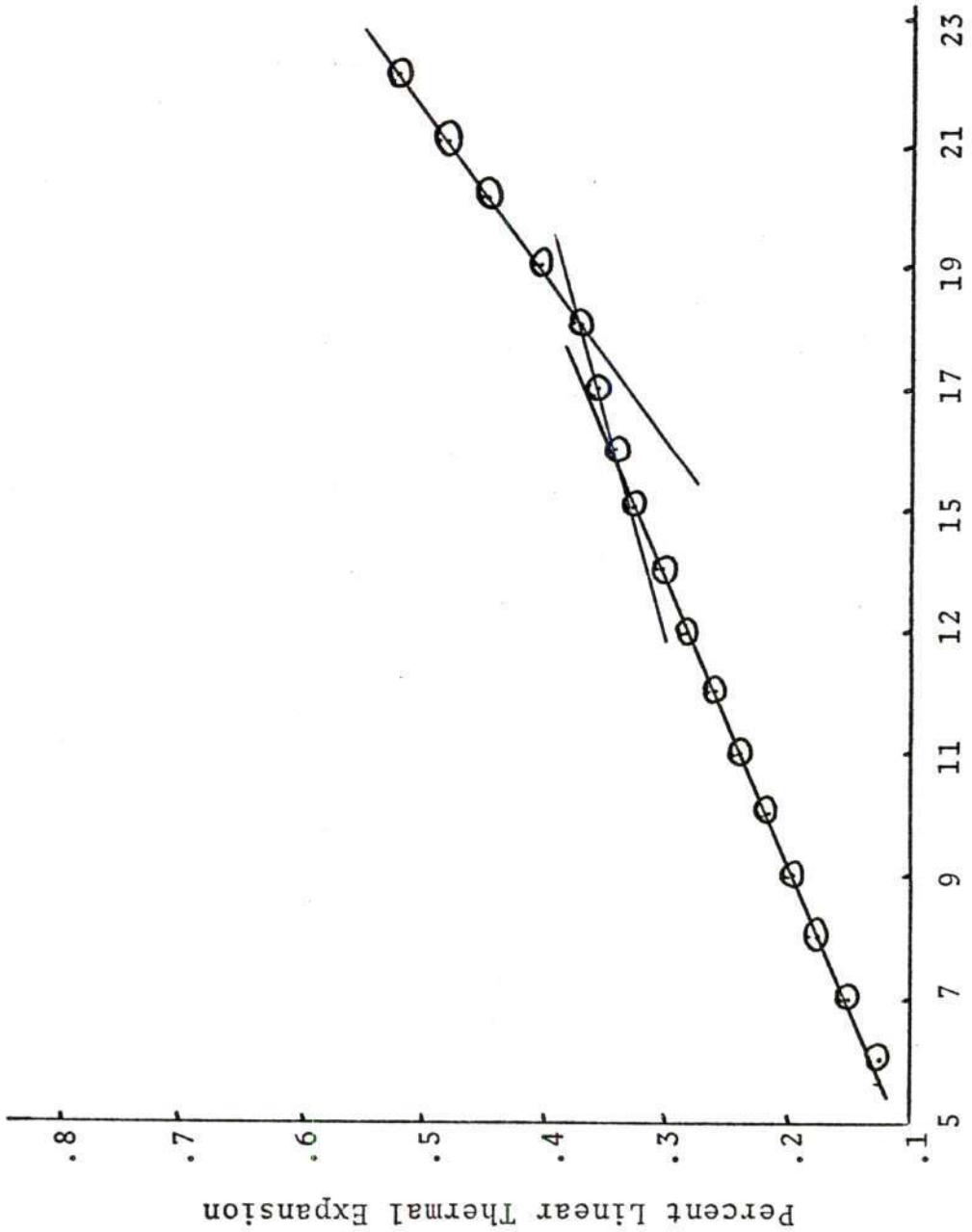

Figure 23. Linear Thermal Expansion Sample II-37 (Length Top)

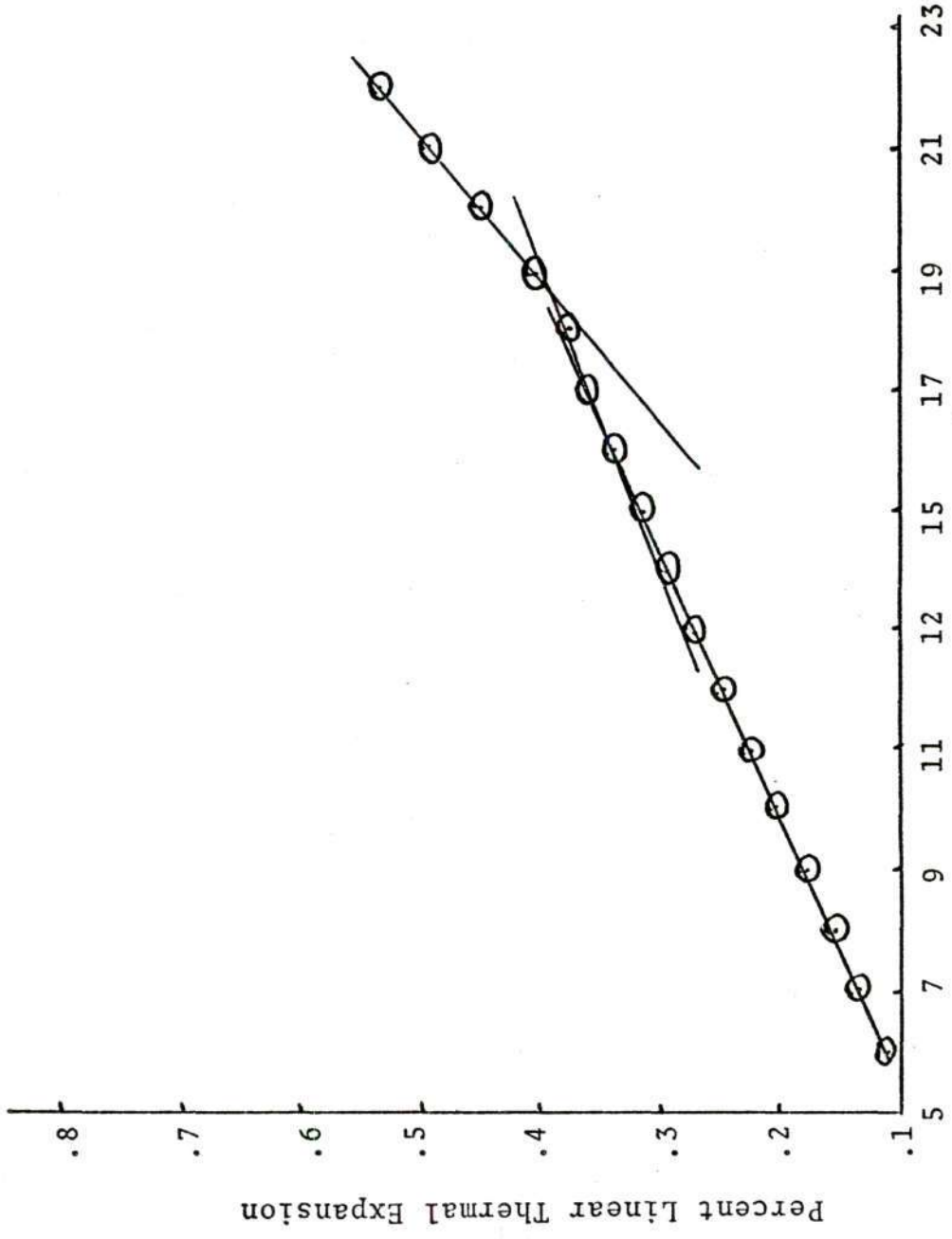

Figure 24. Linear Thermal Expansion Sample II-37 (Length Top)

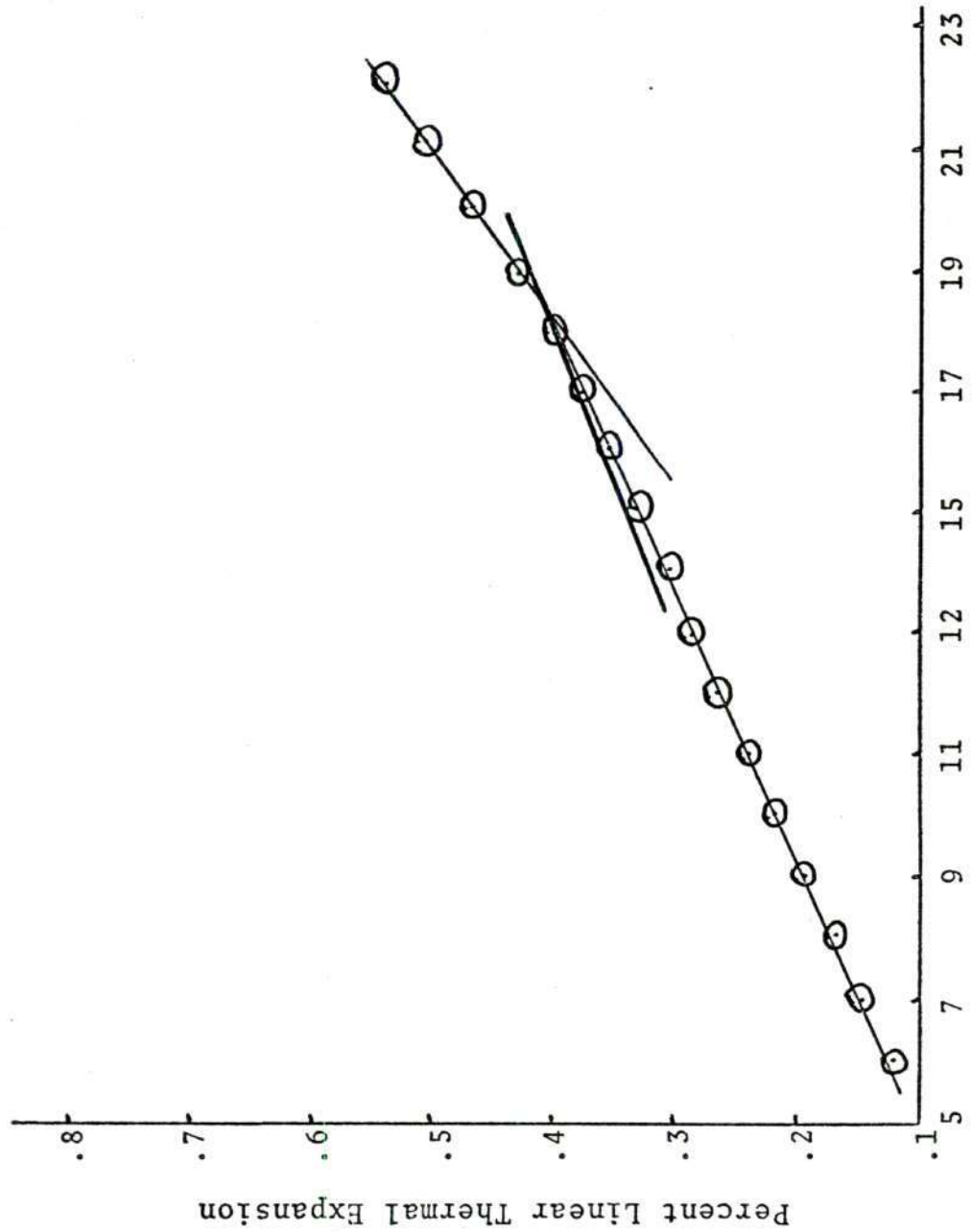

Figure 25. Linear Thermal Expansion Sample II-37 (Length Bottom)

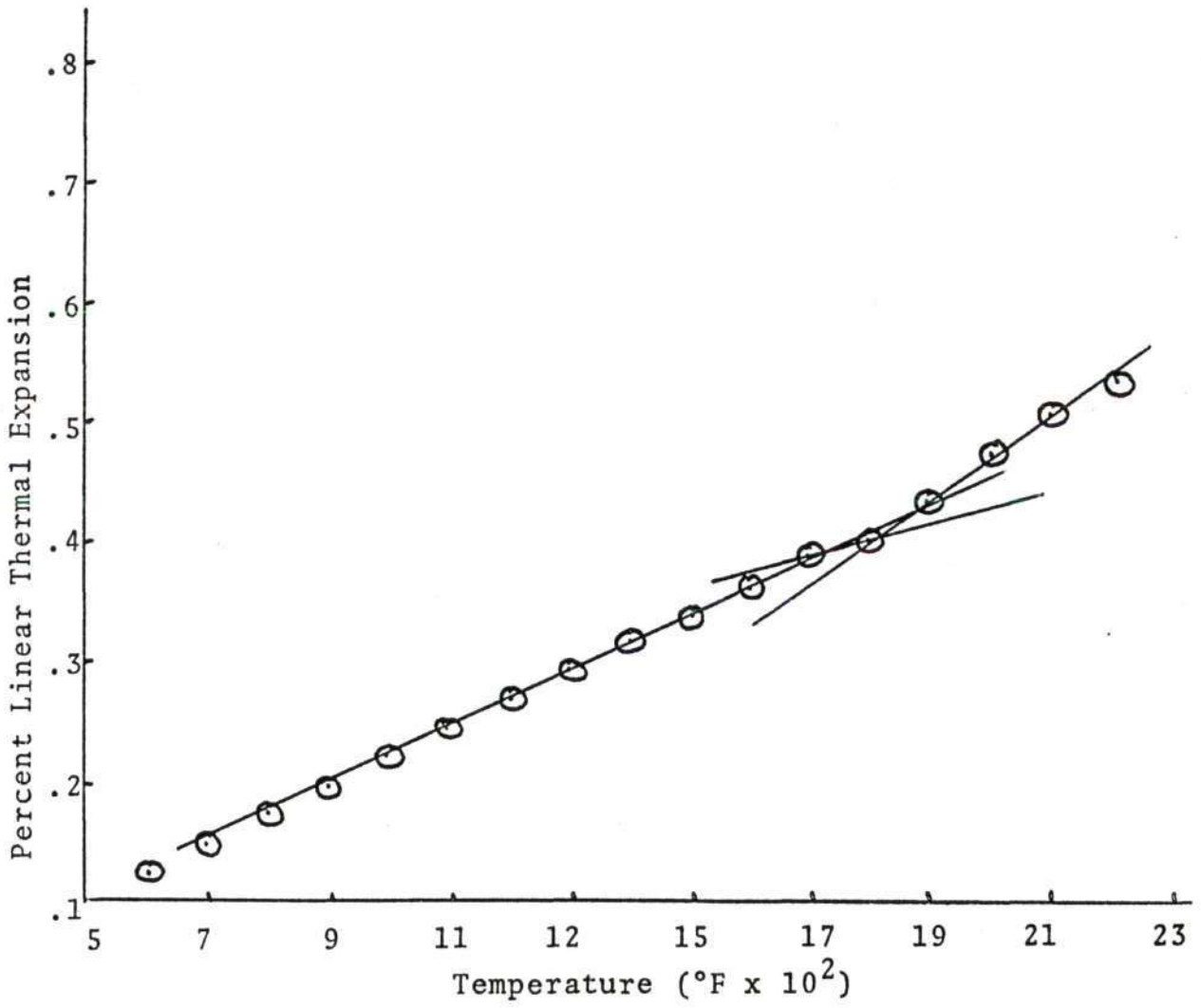

Figure 26. Linear Thermal Expansion Sample II-37 (Height Side)

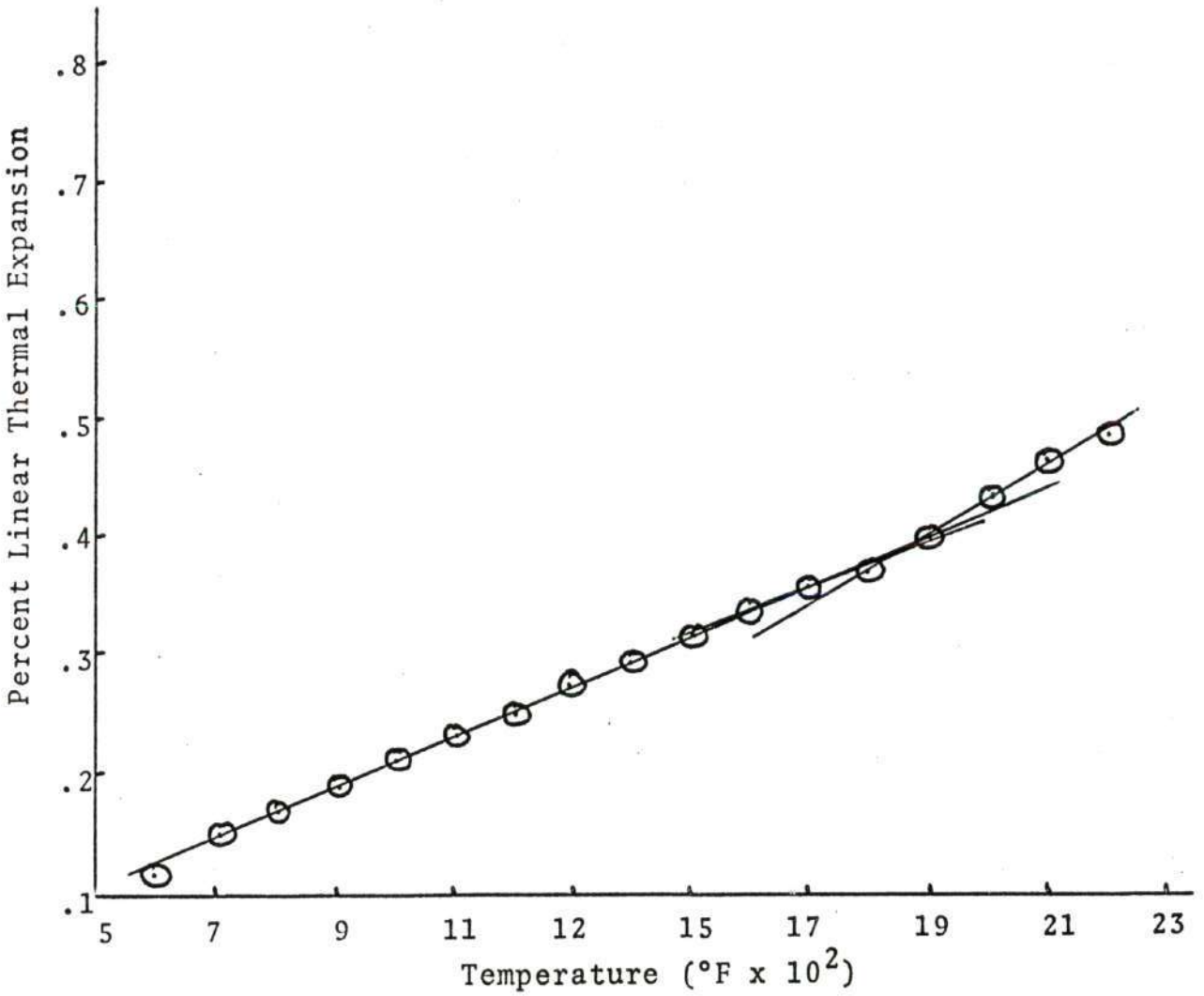

Figure 27. Linear Thermal Expansion Sample II-37 (Width Top)

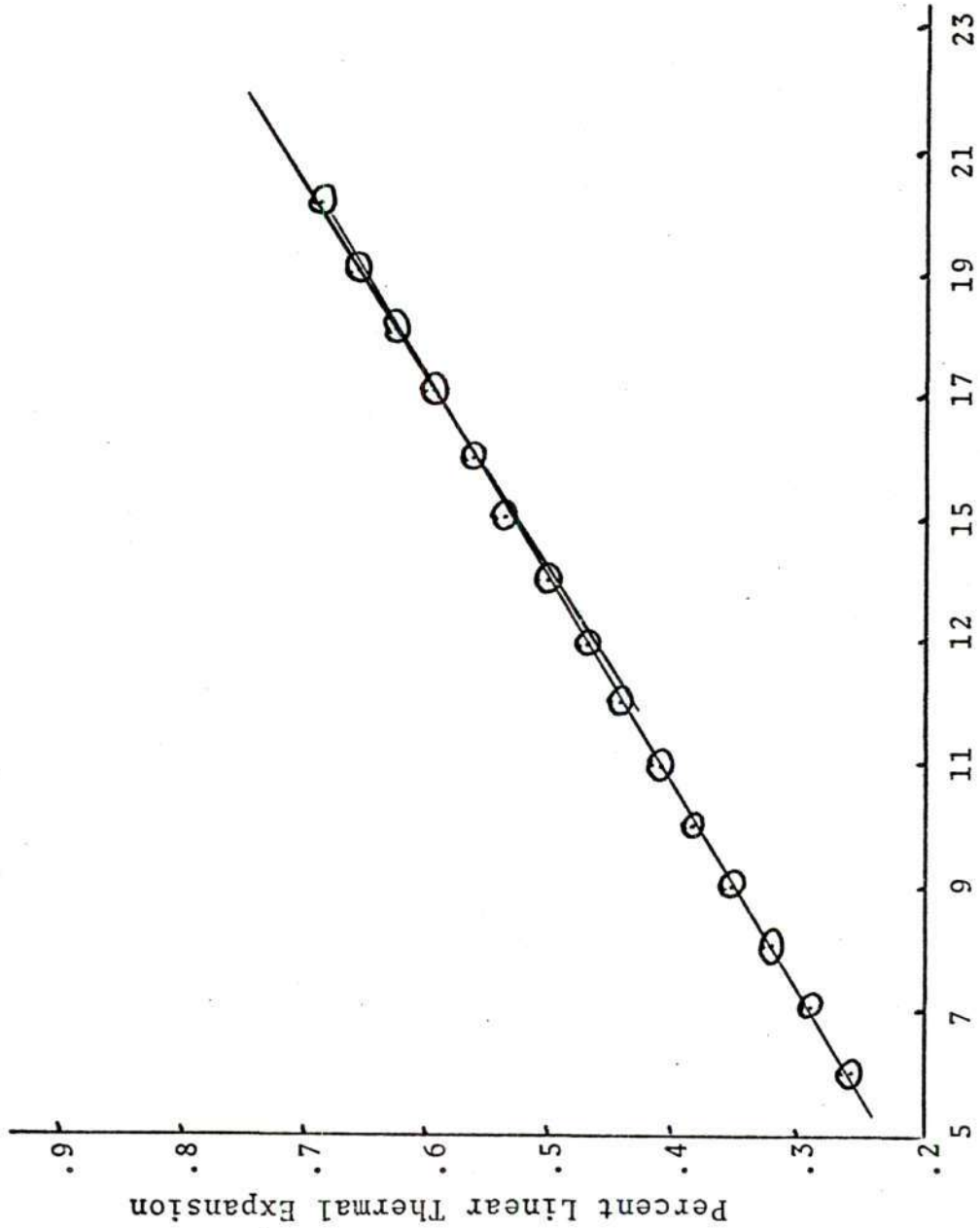

Figure 28. Linear Thermal Expansion Sample III-3

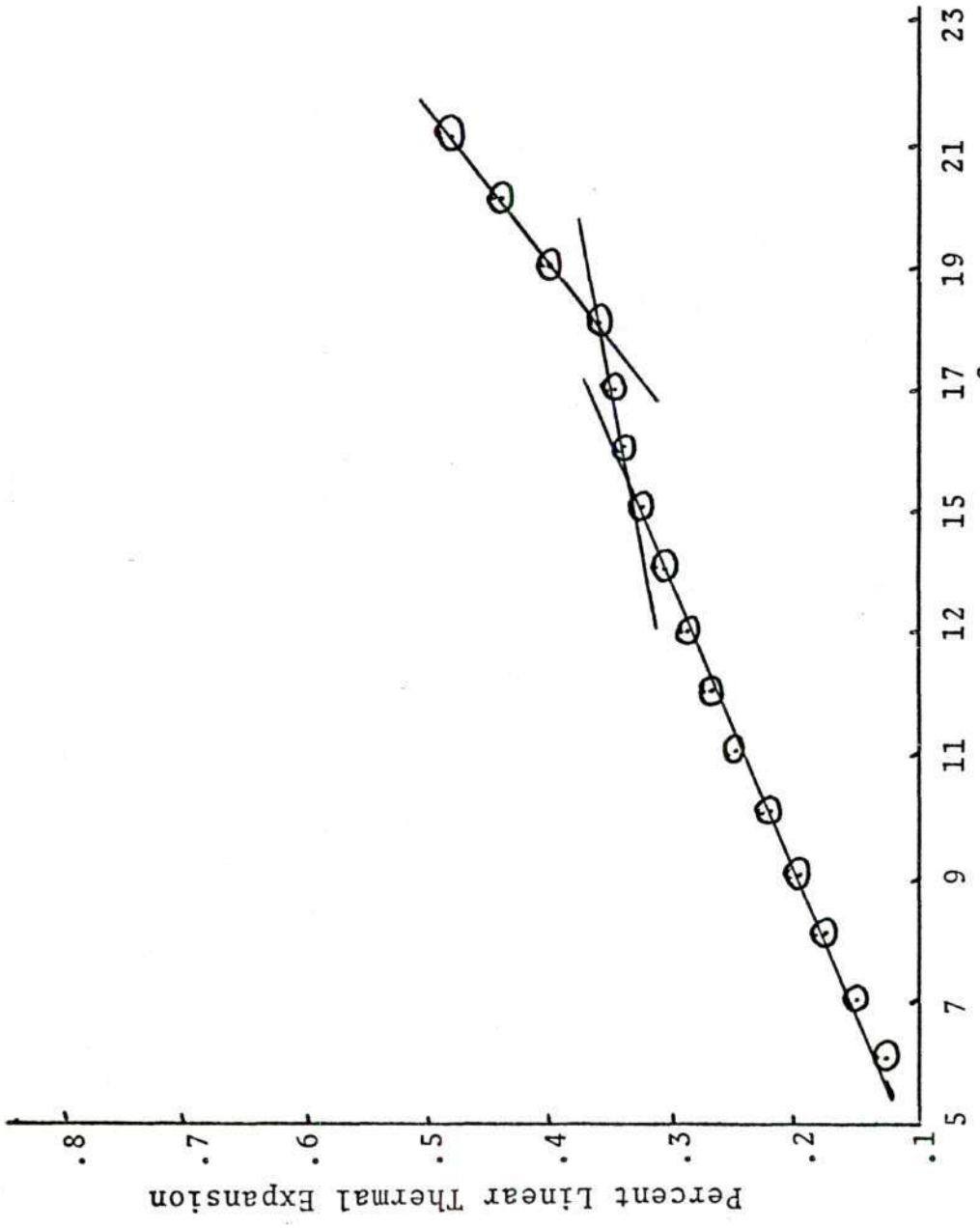

Figure 29. Linear Thermal Expansion Sample III-38

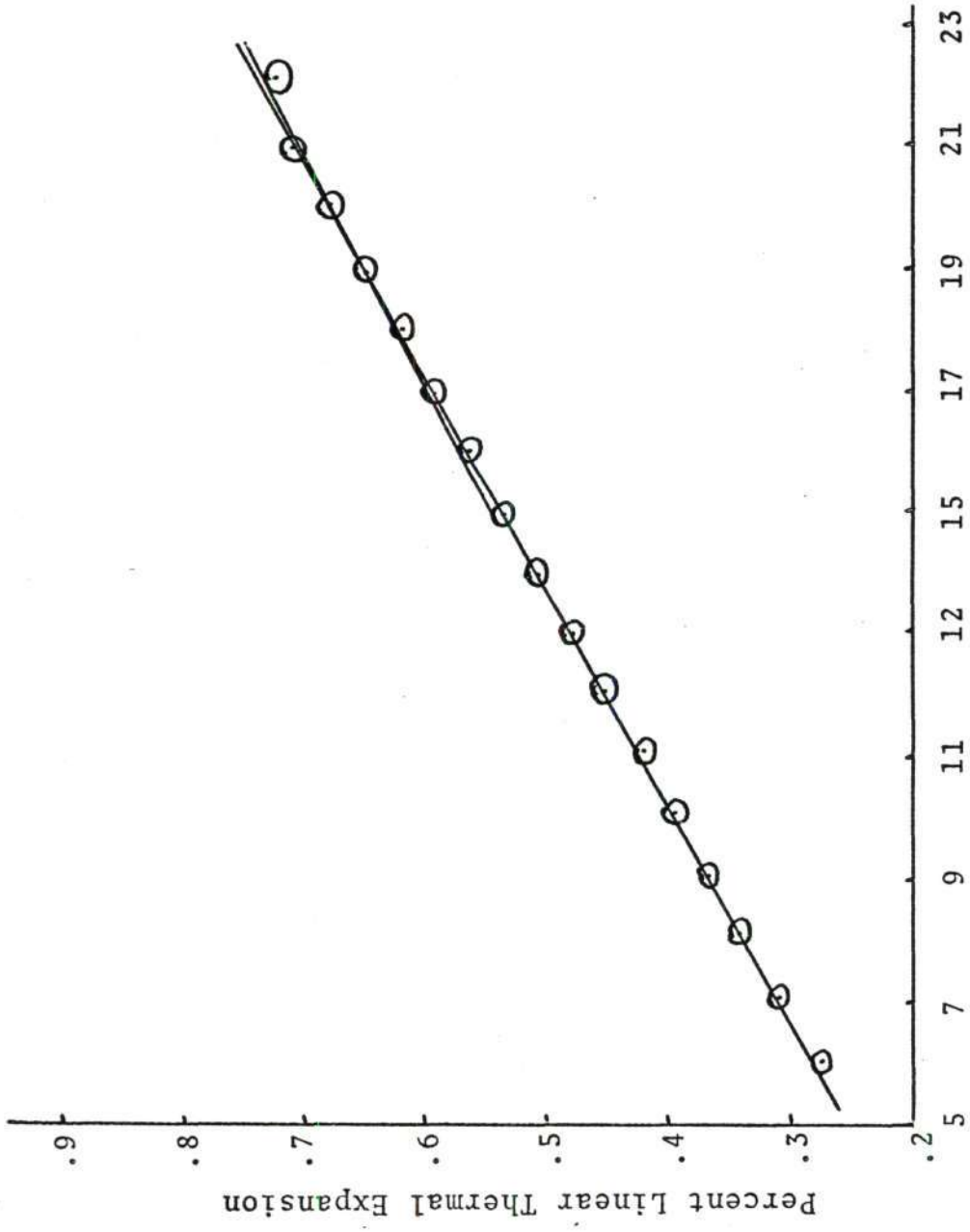

Figure 30. Linear Thermal Expansion Sample IV-2

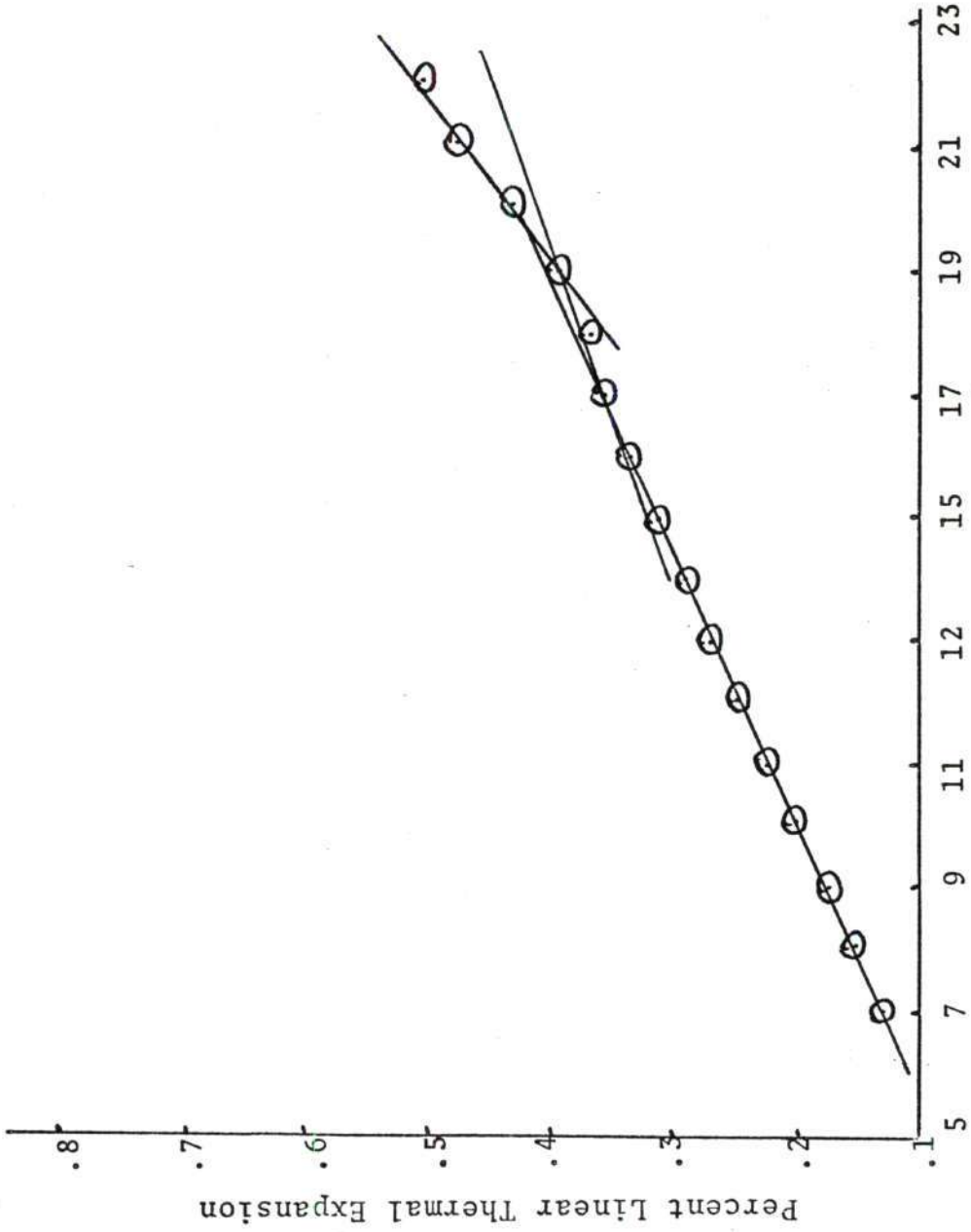

Figure 31. Linear Thermal Expansion Sample IV-37

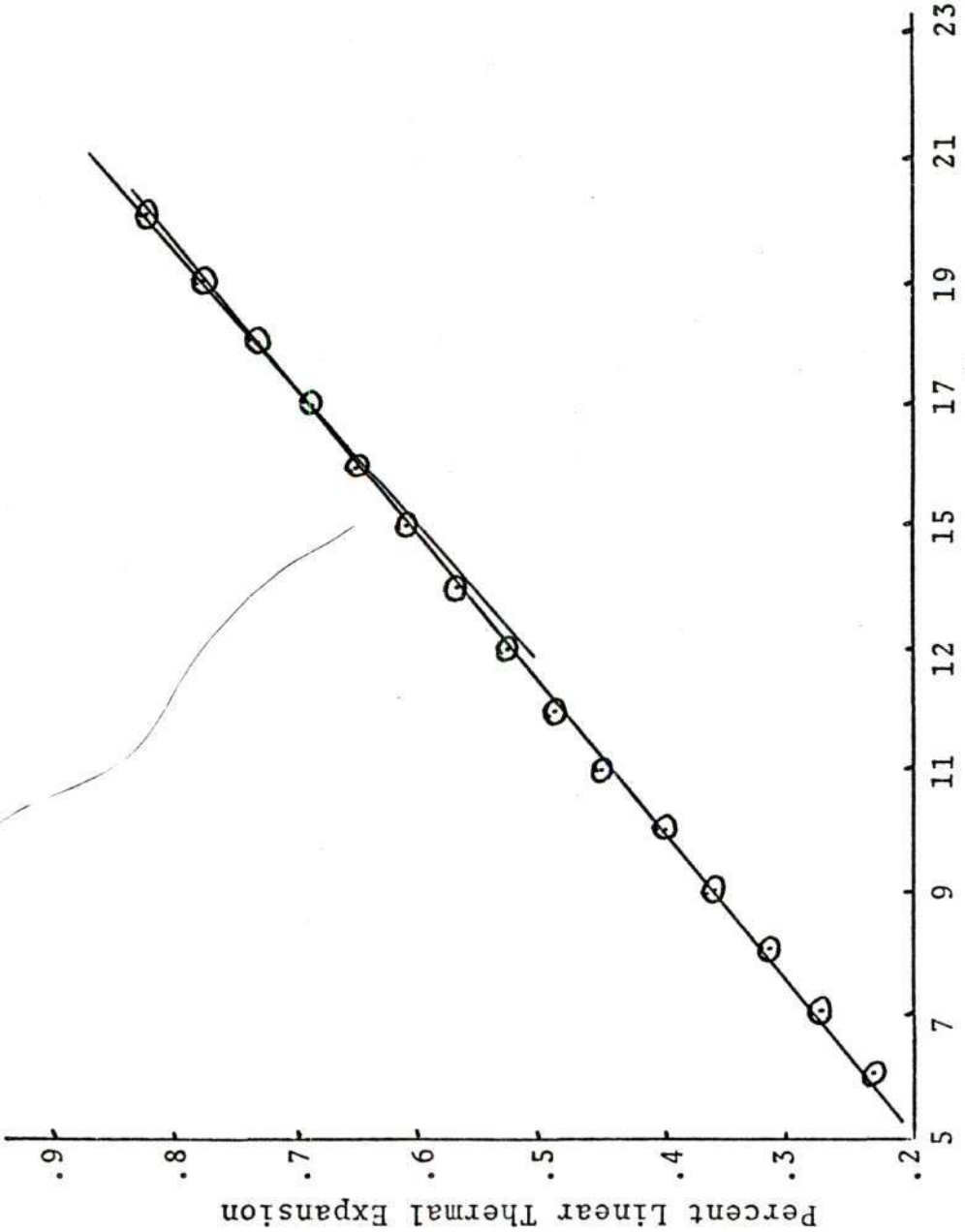

Figure 32. Linear Thermal Expansion Sample V-2

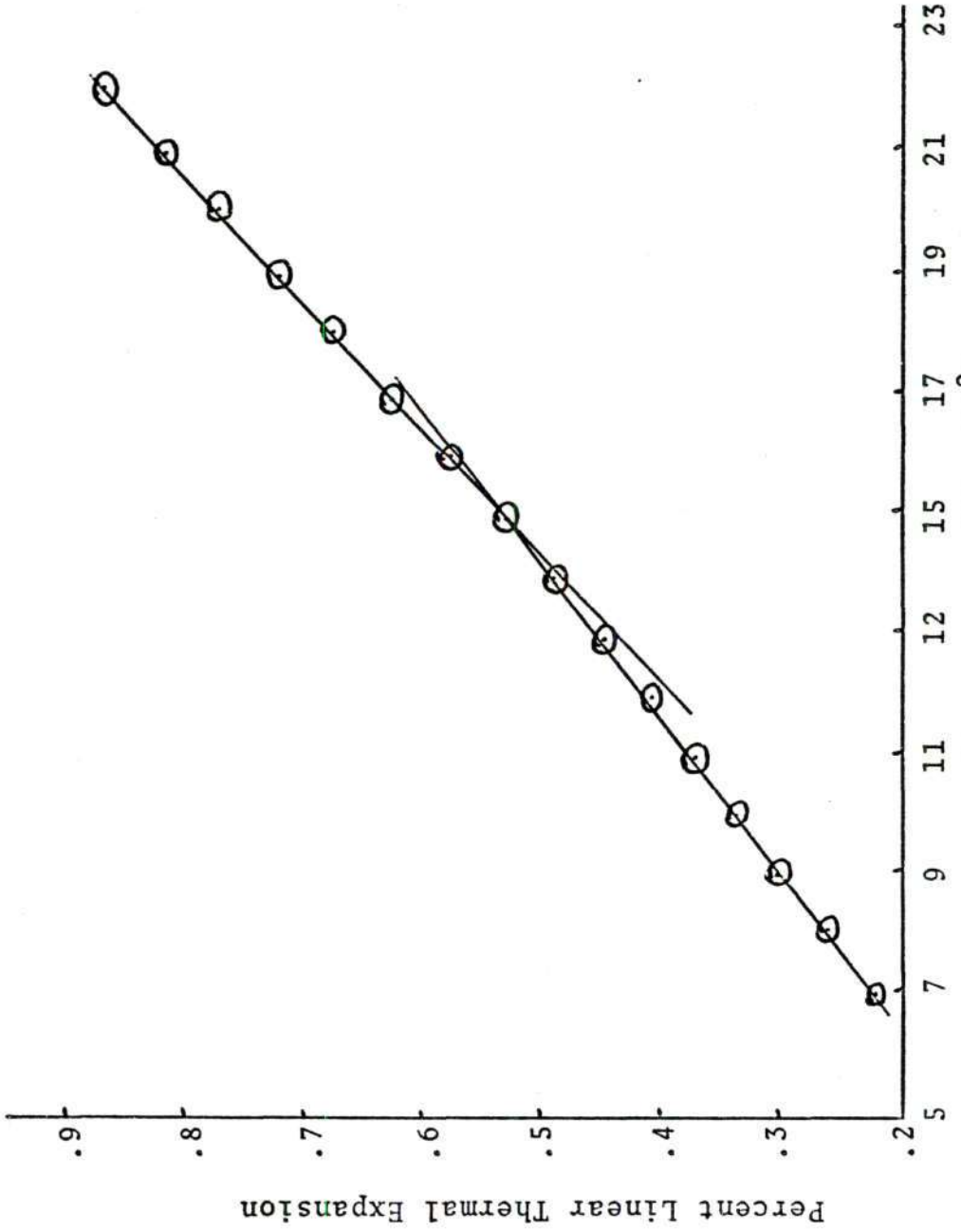

Figure 33. Linear Thermal Expansion Sample V-37

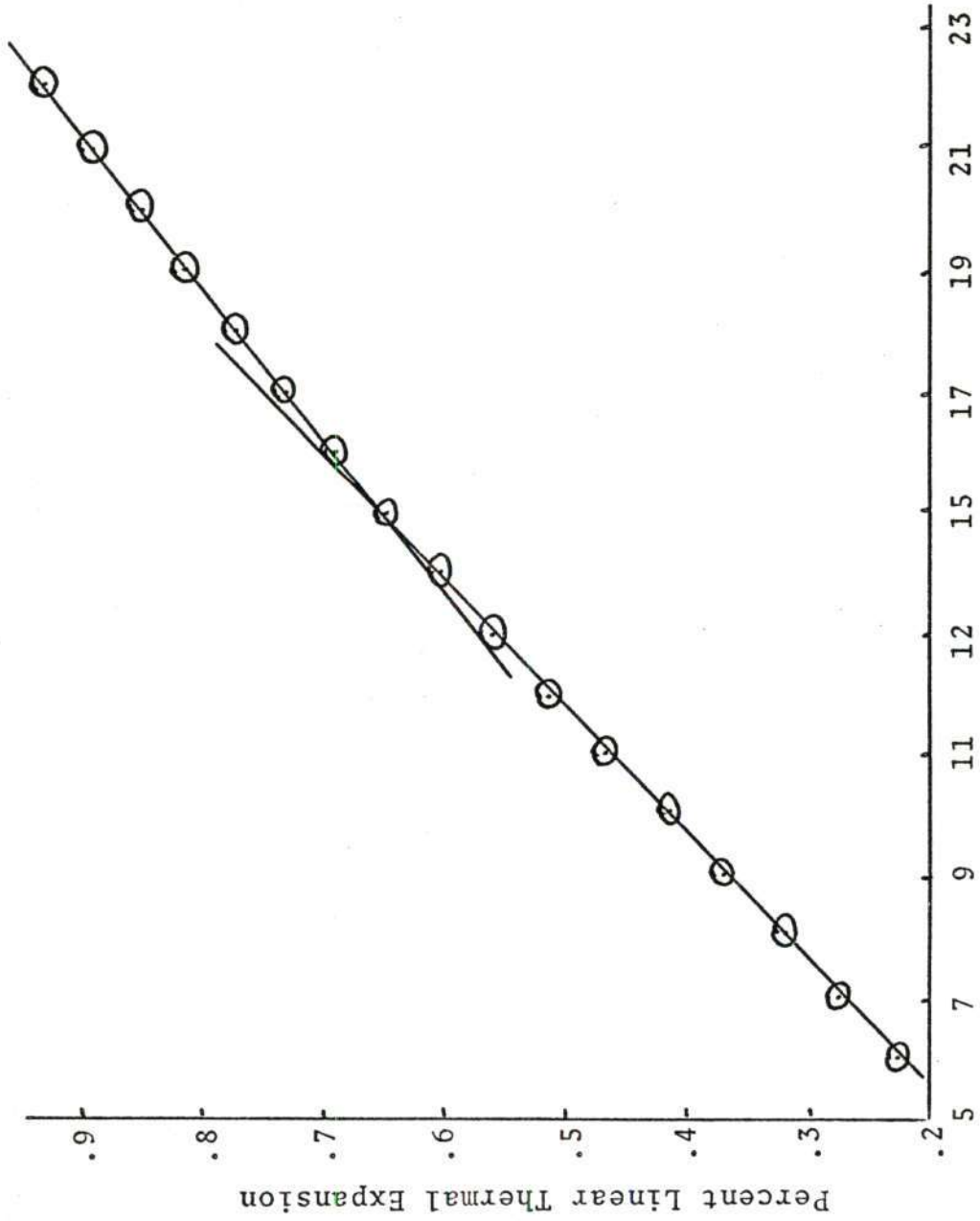

Figure 34. Linear Thermal Expansion Sample VI-3

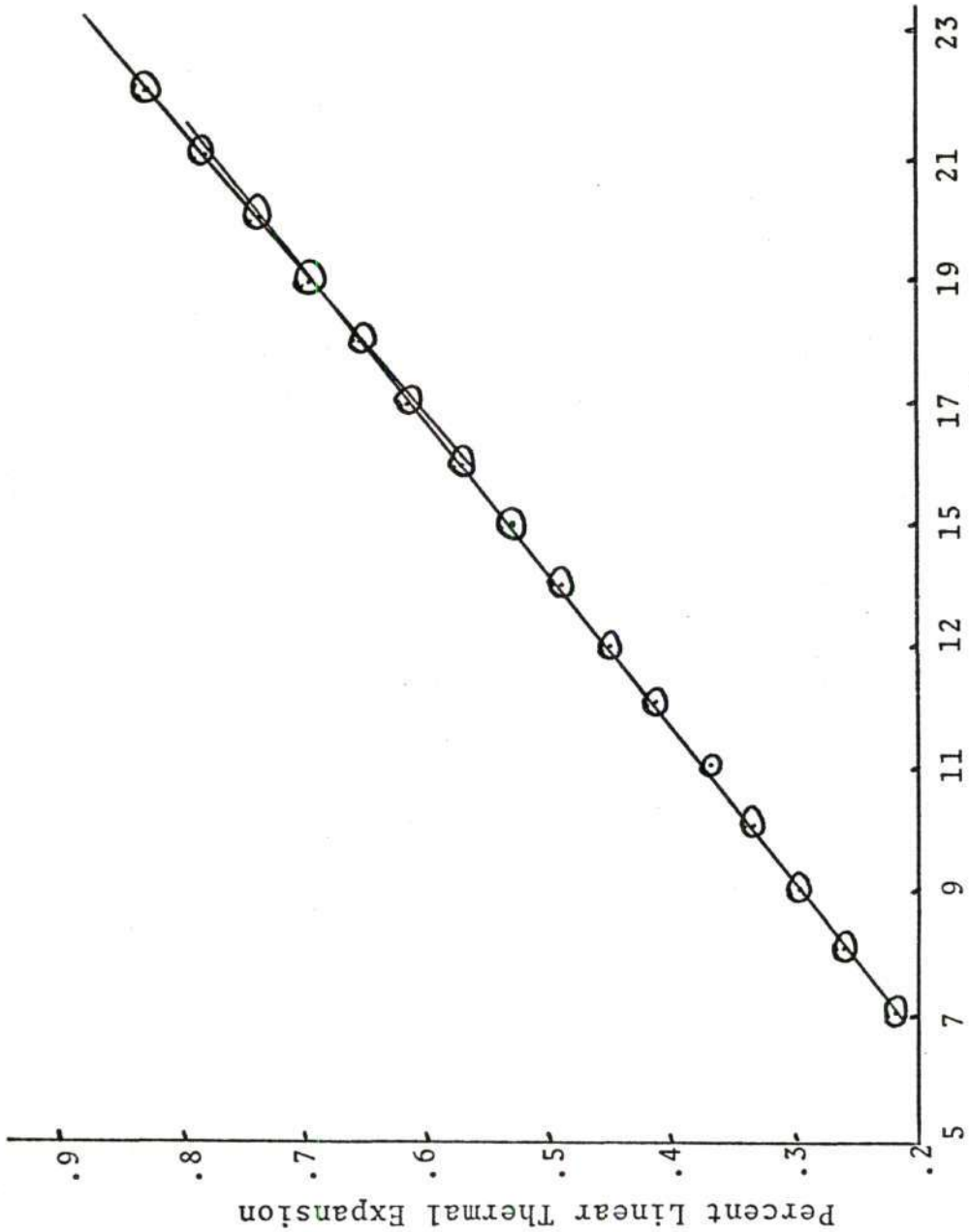

Figure 35. Linear Thermal Expansion Sample VI-38

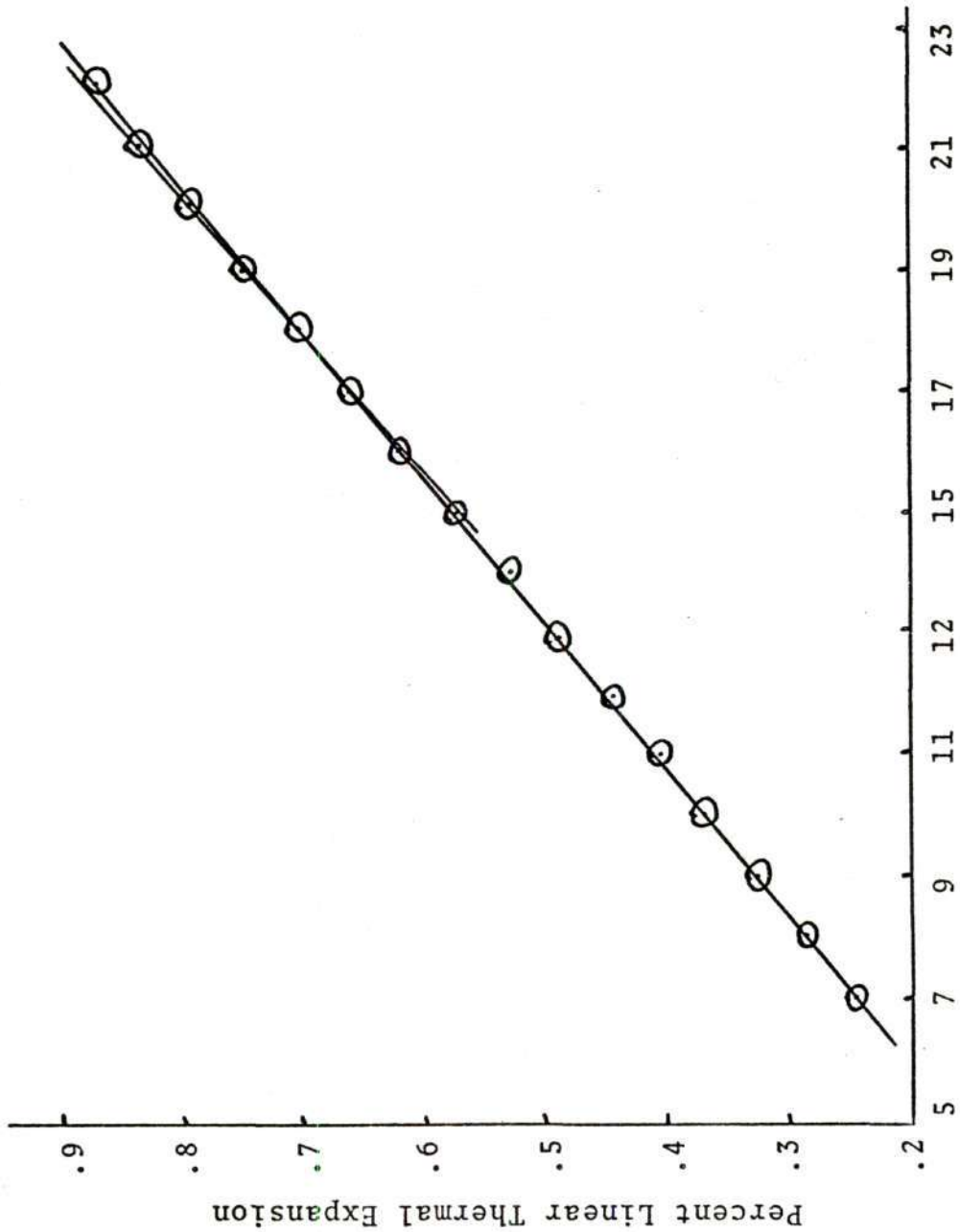

Figure 36. Linear Thermal Expansion Sample VII-3

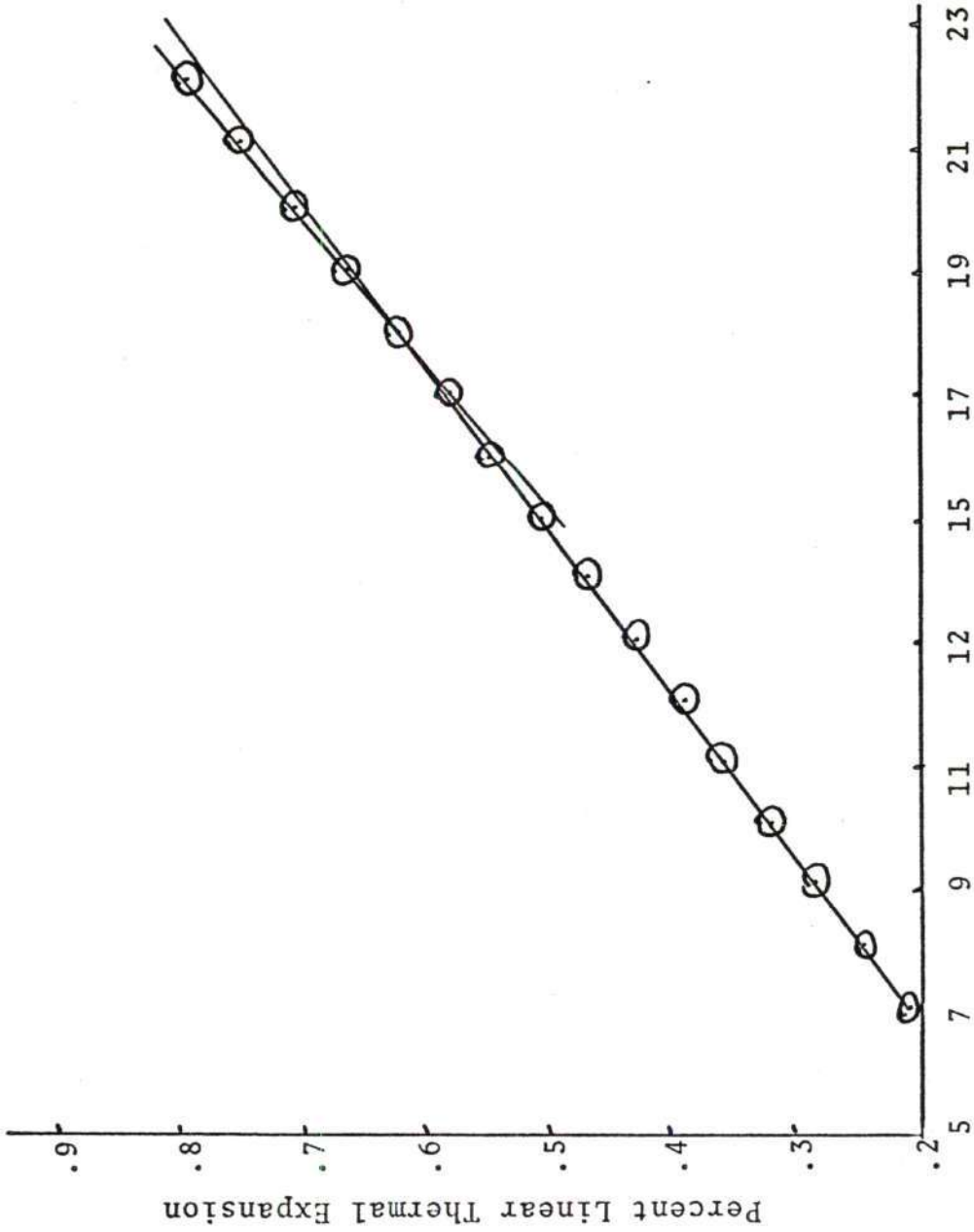

Figure 37. Linear Thermal Expansion Sample VII-37

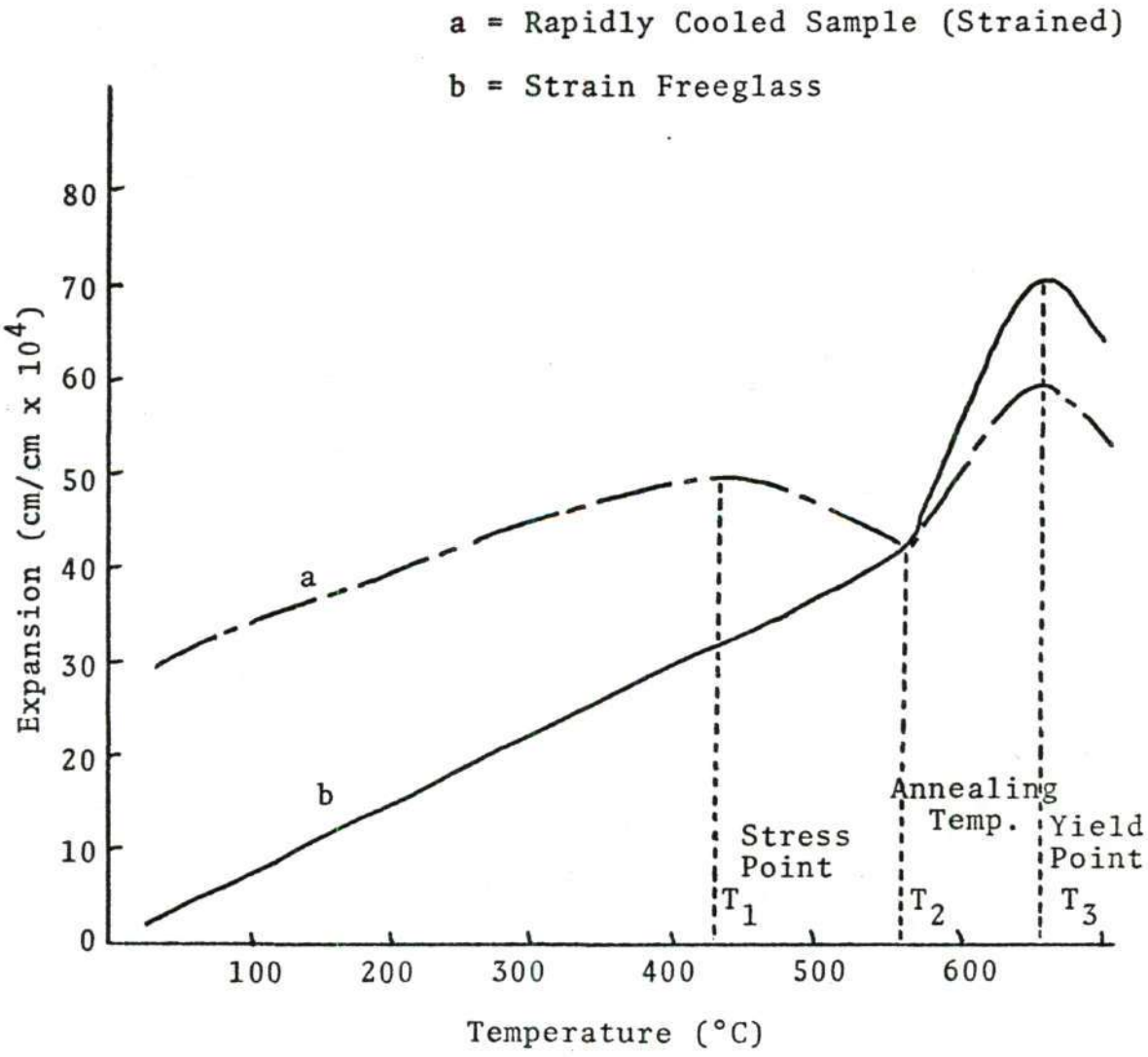

Figure 38. Thermal Expansion of a Glass

structure. At higher temperature T_3, the yield point of the glass is reached and flow occurs easily. Between the annealing temperature and yield point, the peak modulus of rupture values should occur. This temperature varies with the amount of pressure applied and would be where rapid decreases in strength would be expected. Comparison of Figure 38 with the refractory expansions curves (Figures 16-37) indicates that similar behavior has occurred.

Expansion curves for the crystalline phases present [36-37] in the refractory samples are given in Figure 39. The thermal expansion occurs in Figures 16-37 are the result of the combined expansion of these phases (quartz, cristobalite, mullite, and alumina) and the glass.

Two expansion curves are given for cristobalite: one is linear [36] during the recorded strength increased temperature range and the other curve changes slope [37] at 1500°F. Both curves have been reported as the expansion curves for cristobalite. Regardless of which curve is correct, no sudden deviations in expansion have been observed for cristobalite that would explain the non-linear behavior in expansion noted in Figures 16-37. The expansion curves of the other crystalline materials also do not explain the sudden change in slope that occurs between 1500°F and 2000°F. The change in slope is similar, as noted before, to that observed for glass.

Two types of expansion curves were observed for the

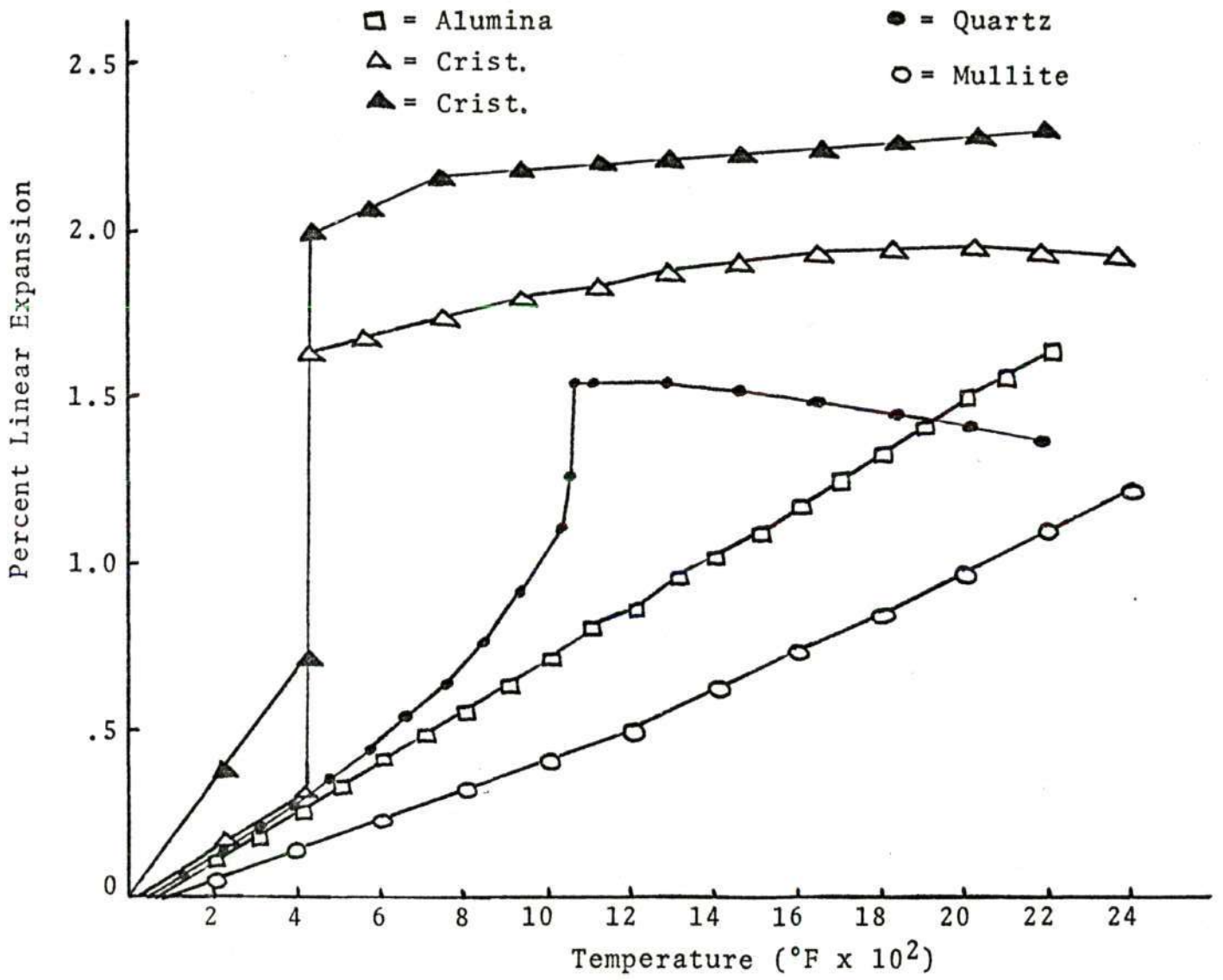

Figure 39. Linear Thermal Expansion of Phases Present

refractory samples: curves showing a quenched stress relief glassy behavior (see Figure 25) and curves with an absence of this quenched behavior (see Figure 18). Samples broken at 2800°F were air quenched and exhibited expansion characteristics similar to the quenched glass (a) in Figure 38. Stresses were set up in the glass from differential thermal expansion by rapid cooling which were not present under normal cooling conditions, and thus the cooling curve behavior is a reflection of where stress relief may begin to occur since the stresses present are greatly magnified above those that occur in normal cooling. Also, the samples have received some additional firing while being broken at 2800°F. Expansion samples that were broken at room temperature exhibited deviations similar to those in curve b of Figure 38. Some stresses must have been present in these specimens but were of low enough magnitude not to alter the thermal expansion curves.

Mixes I-V were all high-mullite compositions. Their room temperature expansion curves tend to follow curve b of Figure 38, and the 2800°F expansion curves appear to follow curve a. Table 11 gives the temperature of deflections and their direction. There is good agreement between the deflection behavior of glass and the refractory samples except for samples I-4 and II-3. Their deflection is opposite to that expected from glass behavior at high temperatures (greater than T_2). Particle size of the materials, the

Table 11. The Temperatures of Thermal Expansion Slope Changes

Graph No.	Sample No.	M.O.R. Conditions	Temp. of Slope Changes	Direction of Slope Change
13	I-2	Room Temp.	1860°F	Up
14	I-4	Room Temp	1740°F	Down
15	I-4	Room Temp	1620°F	Down
16	I-4	Room Temp.	1660°F	Down
17	I-4	Room Temp.	1560°F	Down
Avg.	Graphs 13-17		1748°F	Up and Down
18	I-38	2800°F	1480°F 1780°F	Down Up
19	II-3	Room Temp.	1410°F	Down
20	II-37	2800°F	1560°F 1810°F	Down Up
21	II-37	2800°F	1620°F 1860°F	Down Up
22	II-37	2800°F	1780°F 1820°F	Down Up
23	II-37	2800°F	1740°F 1860°F	Down Up
24	II-37	2800°F	1740°F 1870°F	Down Up
Avg.	Graphs 20-24		1680°F 1844°F	Down Up
25	III-3	Room Temp.	1680°F	Up
26	III-38	2800°F	1530°F 1800°F	Down Up
27	IV-2	Room Temp.	1910°F	Up
28	IV-37	2800°F	1640°F 1960°F	Down Up
29	V-2	Room Temp.	1760°F	Up
30	V-37	2800°F	1500°F	Up
31	VI-3	Room Temp.	1500°F	Down
32	VI-38	2800°F	1940°F	Up
33	VII-3	Room Temp.	1870°F	Up
34	VII-37	2800°F	1780°F	Up

amount of glass present, or strains present could have caused this behavior.

The large amount of alumina in mixes V, VI, and VII mask the effect of the small quantities of glass present. Slight positive deviations were noted in the thermal expansion curves for all samples except sample VI-3. Again, particle size, strain, or the amount of glass could cause this expected variation from Figure 38. Quenching of the high temperature modulus of rupture samples (2800°F) did not magnify stress relaxation enough to become detectable by thermal expansion.

The temperatures where slope changes occurred for mixes I-VII are given in Table 11. The mullite compositions (mixes I-IV) show the effect of stress relief in the glass due to sample quenching. For this reason, two temperatures are given for these samples as there are two temperatures where the slope distinctly changes. These two temperatures are where stress relief begins (strength begins to increase) and the temperature where annealing occurs (strength maximizes). Samples I-38, II-37, III-38, and IV-37 were broken at 2800°F and show these two distinct breaks in their curves. All other thermal expansion samples show only the second temperature change.

The change in slope for samples I-2 and I-4 (room temperature) occurs at 1748°F. Sample I-38 (2800°F) shows two breaks in the slope, occurring at 1480°F and 1780°F. The

first break in sample I-38 is due to stress relief, as mentioned earlier, and is the temperature where strength should begin to increase. The plot of hot modulus of rupture values in Figure 8 shows that strength has increased from 761 psi at room temperature to 964 psi at 1600°F. The annealing temperature for samples I-2 and I-4 (1748°F) and sample I-38 (1780°F) are where strength should maximize because of particle movement. Table 12 shows that for mix I strength reached a maximum value at 1800°F of 53 percent above room temperature values.

A good correlation between strength behavior predicted by thermal expansion data with the actual temperature where strength maximized as determined by hot modulus of rupture occurred for the other mullite compositions. The 2800°F samples for mixes II, III, and IV predicted that strength should begin to rise at the strain points of 1680°F, 1530°F, and 1640°F. Examining Figures 9, 10, and 11, strength was found to increase from 555 psi at room temperature to 664 psi at 1600°F for mix II, to increase from 1333 to 1653 psi for mix III, and to increase from 935 to 1038 psi for mix IV. The thermal expansion curves for mix II predict that strength should maximize at 1410°F and 1844°F for samples II-3 (room temperature) and II-37 (2800°F). Although the value of 1410°F was probably low, strength peaked at 1800°F, indicating a good correlation between values predicted by thermal expansion and those actually measured by hot

Table 12. Hot Modulus of Rupture Peak Temperature and Percent Strength Increase for Mixes I-VII

Mix	Strength Peak Temp. (±200°F)	Percent Strength Increase Above Room Temp.
I	1800°F	53
II	1800°F	61
III	1800°F	48
IV	2000°F	22
V	1800°F	47
VI	1800°F	55
VII	1800°F	38

$$\text{Percent Strength Increase} = \frac{\text{Room Temp. Strength-Peak Strength}}{\text{Peak Strength}} \times 100$$

modulus of rupture. Mix III showed that strength reached a maximum at 1680°F and 1800°F for samples III-3 (room temperature) and III-38 (1800°F). Modulus of rupture measurements indicated strength reached a maximum at 1800°F for mix III. The strength peak for mix IV was determined to be at 2000°F by modulus of rupture and was predicted to occur at 1910°F and 1960°F by thermal expansion samples IV-2 (room temperature) and IV-37 (2800°F). Glass relaxation in the high mullite bodies correlated well with strength changes. When glass relaxation allows stress relief, the strength begins to increase. When the glass reached the annealing temperature, the strength reached a maximum and then began to decrease as the glass allowed particle movement.

Changes in linearity were difficult to detect for samples of the high alumina compositions (mixes V, VI, and VII). The thermal expansion slope change for samples V-2 (room temperature) and V-37 (2800°F) predicted strength to maximize at 1760°F and 1500°F. Mix VI predicted strength to peak at 1500°F (sample VI-3) and 1940°F (sample VI-38) while mix VII predicted strength to peak at 1870°F (sample VII-3) and 1780°F (sample VII-37). Strength reached a maximum at 1800°F for all these mixes as measured by modulus of rupture. In spite of the difficulty in interpreting the data due to the small glass content, the thermal expansion curves for only two samples (V-37 and VI-3) predicted the temperatures of the strength maximums which were off by more than 150°F.

Thermal expansion behavior for mixes I-VII indicated that glass stress relief occurred in the same temperature range where maximum strength values occurred. The theory of strength increased by stress relief supported by Duncan in contrast to the crystal precipitation mechanism proposed by Smith appears to be the cause of the observed strength peaks.

CHAPTER V

CONCLUSIONS AND RECOMMENDATIONS

Conclusions

1. The hot modulus of rupture strengths of four mullite and three high-alumina refractory compositions reached a maximum value at 1800°F for six of the compositions and at 2000°F for one composition.

2. The weight percent of alumina, mullite, cristobalite, quartz, and glass (by difference) remained constant for all of the compositions from room temperature to about 2400°F. This is above the temperature range where hot modulus of rupture strength reached a maximum value, thus, changes in phase content were not related to the strength increase at high temperature.

3. Changes in the slope of thermal expansion curves were shown to be related to stress relief and crystalline particle movement in the glassy phase present.

4. A correlation between the temperature of slope changes in the thermal expansion curves and the temperature of hot modulus of rupture maximum strength indicated that stress relief of the glass and crystalline particle movement were the major factors causing the strength increases.

Recommendations

Additional studies investigating the effect of glass and cristobalite on hot modulus of rupture strength are needed. Such studies could indicate the influence of crystal precipitation on hot modulus of rupture values. These studies could be accomplished by firing a high-mullite body similar to the one investigated to a temperature where no free quartz or cristobalite exists (probably 2800°F). Measuring the hot modulus of rupture of these samples would give the effect of strength increases due to stress relief and crystal precipitation. Refiring a second group of the samples to the temperature range where cristobalite precipitated, then measuring the hot modulus of rupture of the samples would give the influence on strength of only stress relief, as the cristobalite would have already precipitated. Fired density of the samples would not have changed significantly, eliminating its role in strength behavior. Calculating the percentage increase in strength of both samples, differences in the percent strength increases would be due to cristobalite precipitation and thus indicate the influence of phase precipitation on strength. Although the present work concludes that cristobalite precipitation and glass decreases are not a cause of strength increases, their possible influence on the magnitude of strength increase is not eliminated.

APPENDICES

APPENDIX A

MODULUS OF RUPTURE DATA

Composition I

(Rate of Loading = 12.5 lb/min)

Sample No.	Breaking Temp.	Width (in)	Depth (in)	Breaking Wt. (lbs)	MOR (psi)
I-1	Room Temp	1.00	1.00	145.6	874
I-2	Room Temp	1.00	1.01	127.4	750
I-3	Room Temp	1.00	0.98	104	650
I-4	Room Temp	1.00	1.01	126.1	742
I-5	Room Temp	1.00	1.00	131.3	788
				Average	761
I-6	1600°F	1.01	1.01	136.2	787
I-7	1600°F	1.01	1.00	145.6	865
I-8	1600°F	1.00	0.99	176.8	1083
I-9	1600°F	1.00	1.00	153.4	920
I-10	1600°F	1.01	0.99	192.4	1166
				Average	964
I-11	1800°F	1.00	1.01	211.9	1247
I-12	1800°F	1.00	1.00	245.7	1474
I-13	1800°F	1.00	1.01	162.5	956
I-14	1800°F	1.00	1.02	214.5	1238
I-15	1800°F	1.01	1.02	161.2	920
				Average	1167
I-16	2000°F	1.00	1.04	193.7	1074
I-17	2000°F	1.00	1.00	182.0	1092
I-18	2000°F	1.00	0.99	149.5	915
I-19	2000°F	1.00	1.02	183.3	1085
I-20	2000°F	1.00	1.00	169.0	1014
				Average	1031

Sample No.	Breaking Temp.	Width (in)	Depth (in)	Breaking Wt. (lbs)	MOR (psi)
I-21	2200°F	1.00	1.02	100.1	578
I-22	2200°F	1.00	1.01	88.4	520
I-23	2200°F	1.00	1.00	101.4	608
I-24	2200°F	1.00	1.02	44.2	255
I-25	2200°F	1.00	0.99	94.9	581
				Average	508
I-26	2400°F	1.00	1.00	55.9	335
I-27	2400°F	1.00	1.01	68.9	405
I-28	2400°F	1.00	1.02	78.0	450
I-29	2400°F	1.00	1.02	79.3	458
I-30	2400°F	1.00	1.00	59.8	359
				Average	401
I-31	2600°F	1.00	1.01	52.0	306
I-32	2600°F	1.00	1.00	44.2	265
I-33	2600°F	1.00	1.01	49.4	291
I-34	2600°F	1.00	1.01	55.9	329
I-35	2600°F	1.00	1.00	54.6	328
				Average	304
I-36	2800°F	1.00	1.02	37.7	218
I-37	2800°F	1.00	1.00	35.1	211
I-38	2800°F	1.00	1.00	40.3	242
I-39	2800°F	1.00	1.01	33.8	199
I-40	2800°F	1.00	1.00	45.5	273
				Average	229

Composition II

Sample No.	Breaking Temp.	Width (in)	Depth (in)	Breaking Wt. (lbs)	MOR (psi)
II-1	Room Temp	1.00	0.99	92.6	589
II-2	Room Temp	1.00	1.03	109.2	617
II-3	Room Temp	1.00	1.01	84.5	497
II-4	Room Temp	1.00	1.01	85.8	505
II-5	Room Temp	1.00	1.01	96.2	566
				Average	555
II-6	1600°F	1.00	1.01	81.9	482
II-7	1600°F	1.01	1.02	114.4	653
II-8	1600°F	1.00	1.03	131.3	742
II-9	1600°F	1.00	1.04	130.0	721
II-10	1600°F	1.00	1.02	124.8	720
				Average	664
II-11	1800°F	1.00	1.02	166.4	960
II-12	1800°F	1.00	1.03	178.1	1007
II-13	1800°F	1.00	1.01	145.6	857
II-14	1800°F	1.00	1.02	145.6	840
II-15	1800°F	1.00	1.02	141.7	818
				Average	896
II-16	2000°F	1.00	1.04	145.6	808
II-17	2000°F	1.00	1.03	109.2	617
II-18	2000°F	1.00	1.03	126.5	772
II-19	2000°F	1.00	1.02	150.8	870
II-20	2000°F	1.00	1.03	132.6	750
				Average	763
II-21	2200°F	1.00	1.04	91.0	505
II-22	2200°F	1.00	1.02	115.7	668
II-23	2200°F	1.00	1.04	104.0	577
II-24	2200°F	1.00	1.02	94.9	548
II-25	2200°F	1.00	1.02	94.9	548
				Average	569
II-26	2400°F	1.00	1.04	53.3	296
II-27	2400°F	1.00	1.04	75.4	418
II-28	2400°F	1.00	1.03	67.6	382
II-29	2400°F	1.00	1.06	63.7	340
II-30	2400°F	1.00	1.02	53.3	308
				Average	349

Sample No.	Breaking Temp.	Width (in)	Depth (in)	Breaking Wt. (lbs)	MOR (psi)
II-31	2600°F	1.00	1.04	39.0	216
II-32	2600°F	1.00	1.04	39.0	216
II-33	2600°F	1.00	1.03	41.6	235
II-34	2600°F	1.00	1.05	42.9	233
II-35	2600°F	1.00	1.03	39.0	221
				Average	224
II-36	2800°F	1.00	1.03	27.3	154
II-37	2800°F	1.00	1.05	35.1	191
II-38	2800°F	1.00	1.05	39.0	212
II-39	2800°F	1.00	1.02	35.1	203
II-40	2800°F	1.00	1.03	35.1	211
				Average	194

Composition III

Sample No.	Breaking Temp.	Width (in)	Depth (in)	Breaking Wt. (lbs)	MOR (psi)
III-1	Room Temp	0.97	0.92	162.5	1188
III-2	Room Temp	0.96	0.92	180.7	1334
III-3	Room Temp	0.96	0.92	193.7	1430
III-4	Room Temp	0.96	0.90	158.6	1224
III-5	Room Temp	0.96	0.92	201.5	1488
				Average	1333
III-6	1600°F	0.96	0.92	189.8	1402
III-7	1600°F	0.96	0.92	193.7	1430
III-8	1600°F	0.96	0.89	267.8	2114
III-9	1600°F	0.96	0.91	211.9	1599
III-10	1600°F	0.96	0.92	232.7	1718
				Average	1653
III-11	1800°F	0.97	0.93	210.6	1507
III-12	1800°F	0.96	0.93	340.6	2460
III-13	1800°F	0.96	0.92	241.8	1786
III-14	1800°F	0.96	0.90	250.9	1936
III-15	1800°F	0.96	0.91	248.7	2148
				Average	1967
III-16	2000°F	0.96	0.97	214.5	1420
III-17	2000°F	0.96	0.95	247	1710
III-18	2000°F	0.96	0.94	269.1	1904
III-19	2000°F	0.96	0.95	275.6	1908
III-20	2000°F	0.96	0.95	288.6	1998
				Average	1789
III-21	2200°F	0.97	0.93	176.8	1265
III-22	2200°F	0.96	0.93	171.6	1239
III-23	2200°F	0.96	0.92	192.4	1421
III-24	2200°F	0.96	0.93	210.6	1521
III-25	2200°F	0.96	0.93	150.8	1089
				Average	1307
III-26	2400°F	0.97	0.92	113.1	827
III-27	2400°F	0.97	0.93	106.6	763
III-28	2400°F	0.96	0.93	102.7	742
III-29	2400°F	0.96	0.93	101.4	732
III-30	2400°F	0.96	0.93	109.2	789
				Average	771

Sample No.	Breaking Temp.	Width (in)	Depth (in)	Breaking Wt. (lbs)	MOR (psi)
III-31	2600°F	0.98	0.96	63.7	423
III-32	2600°F	0.96	0.92	53.3	394
III-33	2600°F	0.96	0.93	50.7	366
III-34	2600°F	0.97	0.92	50.7	371
III-35	2600°F	0.96	0.93	52.0	376
				Average	386
III-36	2800°F	0.96	0.93	36.4	263
III-37	2800°F	0.96	0.94	31.2	221
III-38	2800°F	0.96	0.93	29.9	216
III-39	2800°F	0.96	0.93	32.5	235
III-40	2800°F	0.96	0.93	35.1	254
				Average	238

Composition IV

Sample No.	Breaking Temp.	Width (in)	Depth (in)	Breaking Wt. (lbs)	MOR (psi)
IV-1	Room Temp	1.00	0.98	157.3	983
IV-2	Room Temp	1.00	0.98	130.0	812
IV-3	Room Temp	1.00	0.97	158.6	1011
IV-4	Room Temp	1.00	0.97	133.9	854
IV-5	Room Temp	1.00	0.96	156.0	1015
				Average	935
IV-6	1600°F	1.00	0.98	183.3	1145
IV-7	1600°F	1.00	0.99	157.3	963
IV-8	1600°F	1.00	0.98	157.3	983
IV-9	1600°F	1.00	0.99		
IV-10	1600°F	1.00	0.99	172.9	1059
				Average	1038
IV-11	1800°F	1.00	1.02	202.8	1170
IV-12	1800°F	1.00	1.01	175.5	1033
IV-13	1800°F	1.00	1.00	210.6	1264
IV-14	1800°F	1.00	1.00	130.0	780
IV-15	1800°F	1.00	0.99	191.1	1170
				Average	1083
IV-16	2000°F	1.00	0.98	208.0	1299
IV-17	2000°F	1.00	0.99	187.2	1146
IV-18	2000°F	1.00	0.96	153.4	998
IV-19	2000°F	1.00	0.96	163.8	1066
IV-20	2000°F	1.00	0.98	191.1	1194
				Average	1141
IV-21	2200°F	1.00	0.98	124.8	780
IV-22	2200°F	1.00	0.99	144.3	884
IV-23	2200°F	1.00	0.97	146.9	937
IV-24	2200°F	1.00	0.98	150.8	942
IV-25	2200°F	1.00	0.97	123.5	788
				Average	866
IV-26	2400°F	1.00	0.96	80.6	525
IV-27	2400°F	1.00	0.98	81.7	544
IV-28	2400°F	1.00	0.96	84.5	550
IV-29	2400°F	1.00	0.96	83.2	541
IV-30	2400°F	1.00	0.97	76.7	489
				Average	530

Sample No.	Breaking Temp.	Width (in)	Depth (in)	Breaking Wt. (lbs)	MOR (psi)
IV-31	2600°F	1.00	0.95	45.5	302
IV-32	2600°F	1.00	0.97	46.8	294
IV-33	2600°F	1.00	0.98	44.2	276
IV-34	2600°F	1.00	0.97	48.1	307
IV-35	2600°F	1.00	0.97	44.2	282
				Average	292
IV-36	2800°F	1.00	0.98	40.3	252
IV-37	2800°F	1.00	0.98	37.7	235
IV-38	2800°F	1.00	0.99	39.0	239
IV-39	2800°F	1.00	0.97	39.0	249
IV-40	2800°F	1.00	0.98		
				Average	244

Composition V

Sample No.	Breaking Temp.	Width (in)	Depth (in)	Breaking Wt. (lbs)	MOR (psi)
V-1	Room Temp	1.00	0.97	219.7	1401
V-2	Room Temp	1.00	0.97	213.2	1360
V-3	Room Temp	1.00	0.97	257.4	1641
V-4	Room Temp	1.00	0.96	256.1	1667
V-5	Room Temp	1.00	0.97	235.3	1500
				Average	1514
V-6	1600°F	1.00	0.97	284.7	1816
V-7	1600°F	1.00	0.96	361.4	2352
V-8	1600°F	1.00	0.96	253.5	1650
V-9	1600°F	1.00	0.92	280.8	1964
V-10	1600°F	1.00	0.96	297.7	1936
				Average	1944
V-11	1800°F	1.00	0.95	322.4	2143
V-12	1800°F	1.00	0.96	396.5	2580
V-13	1800°F	1.00	0.96	282.1	1836
V-14	1800°F	1.00	0.95	314.6	2091
V-15	1800°F	1.00	0.96	379.6	2470
				Average	2224
V-16	2000°F	1.00	0.96	247.0	1607
V-17	2000°F	1.00	0.97	214.5	1368
V-18	2000°F	1.00	0.95	330.2	2195
V-19	2000°F	1.00	0.96	218.4	1421
V-20	2000°F	1.00	0.96	167.7	1091
				Average	1536
V-21	2200°F	1.00	0.93	119.6	830
V-22	2200°F	1.00	0.95	84.5	562
V-23	2200°F	1.00	0.95	125.2	899
V-24	2200°F	1.00	0.95	175.5	1166
V-25	2200°F	1.00	0.97	75.4	481
				Average	788
V-26	2400°F	1.00	0.98	61.1	382
V-27	2400°F	1.00	0.98	196.3	1226
V-28	2400°F	1.00	0.98	167.7	1027
V-29	2400°F	1.00	0.98	161.2	1007
V-30	2400°F	1.00	0.98	107.9	674
				Average	863

Sample No.	Breaking Temp.	Width (in)	Depth (in)	Breaking Wt. (lbs)	MOR (psi)
V-31	2600°F	1.00	1.00	70.2	421
V-32	2600°F	1.00	0.98	79.3	495
V-33	2600°F	1.00	0.98	79.3	495
V-34	2600°F	1.00	0.98	62.4	390
V-35	2600°F	1.00	0.98	61.1	382
				Average	437
V-36	2800°F	1.00	0.99	88.4	561
V-37	2800°F	1.00	0.98	71.5	447
V-38	2800°F	1.00	0.97	71.5	456
V-39	2800°F	1.00	0.98	72.8	464
V-40	2800°F	1.00	0.99	65.0	398
				Average	461

Composition VI

Sample No.	Breaking Temp.	Width (in)	Depth (in)	Breaking Wt. (lbs)	MOR (psi)
VI-1	Room Temp	1.00	1.03	305.5	1727
VI-2	Room Temp	0.99	1.00	286.0	1698
VI-3	Room Temp	1.00	1.02	209.3	1208
VI-4	Room Temp	1.00	1.01	193.7	1140
VI-5	Room Temp	1.00	1.02	249.6	1400
				Average	1443
VI-6	1600°F	1.00	1.02	267.8	1545
VI-7	1600°F	1.00	1.01		
VI-8	1600°F	1.00	1.00	167.7	1006
VI-9	1600°F	1.00	1.00	230.1	1381
VI-10	1600°F	1.00	1.00	244.4	1466
				Average	1350
VI-11	1800°F	1.00	1.00	343.2	2059
VI-12	1800°F	1.00	1.02	280.9	2198
VI-13	1800°F	1.00	0.99	344.5	2109
VI-14	1800°F	1.00	1.00	449.8	2699
VI-15	1800°F	1.00	1.02	370.5	2138
				Average	2241
VI-16					
VI-17	2000°F	1.00	1.00	226.2	1357
VI-18	2000°F	1.00	0.98	222.3	1389
VI-19	2000°F	1.00	0.98	198.9	1242
VI-20	2000°F	1.00	0.99	205.4	1258
				Average	1312
VI-21	2200°F	1.00	0.97	118.3	754
VI-22	2200°F	1.00	0.99	132.6	812
VI-23	2200°F	1.00	0.98	117.0	731
VI-24	2200°F	1.00	1.00	132.6	796
VI-25	2200°F	1.00	0.98	130.0	812
				Average	781
VI-26	2400°F	1.00	1.00	67.6	406
VI-27	2400°F	1.00	1.00	139.1	835
VI-28	2400°F	1.00	0.99	85.8	525
VI-29	2400°F	1.00	0.99	79.3	486
VI-30	2400°F	1.00	1.00	71.5	429
				Average	536

Sample No.	Breaking Temp.	Width (in)	Depth (in)	Breaking Wt. (lbs)	MOR (psi)
VI-31	2600°F	1.00	0.99	42.9	236
VI-32	2600°F	1.00	0.98	41.6	260
VI-33	2600°F	1.00	1.00	45.5	273
VI-34	2600°F	1.00	1.02	52.0	300
VI-35	2600°F	1.00	1.00	46.8	281
				Average	275
VI-36	2800°F	1.00	1.00	156.0	936
VI-37	2800°F	1.00	0.98	150.8	942
VI-38	2800°F	1.00	0.99	133.9	820
VI-39	2800°F	1.00	0.98	137.8	861
VI-40	2800°F	1.00	0.98	189.8	1186
				Average	949

Composition VII

Sample No.	Breaking Temp.	Width (in)	Depth (in)	Breaking Wt. (lbs)	MOR (psi)
VII-1	Room Temp	1.00	1.03	213.2	1205
VII-2	Room Temp	1.00	0.99	222.3	1361
VII-3	Room Temp	1.00	1.03	215.8	1220
VII-4	Room Temp	1.00	1.01	232.7	1369
VII-5	Room Temp	1.00	0.97	232.7	1484
				Average	1328
VII-6					
VII-7	1600°F	1.00	1.01		
VII-8	1600°F	1.00	1.01	180.7	1063
VII-9	1600°F	1.00	1.02	39.0	225
VII-10	1600°F	1.00	1.02	267.8	1545
				Average	1304
VII-11	1800°F	1.00	1.02	305.5	1763
VII-12	1800°F	1.00	1.02	254.8	1470
VII-13	1800°F	1.00	1.01	353.6	2081
VII-14	1800°F	1.00	1.02	323.7	1868
VII-15	1800°F	1.00	0.99	318.5	1950
				Average	1826
VII-16	2000°F	1.00	1.03	227.5	1286
VII-17	2000°F	1.00	1.01	252.2	1484
VII-18	2000°F	1.00	1.01	275.6	1622
VII-19	2000°F	1.00	1.00	250.9	1505
VII-20	2000°F	1.00	1.01	270.4	1591
				Average	1498
VII-21	2200°F	1.00	1.02	169.0	975
VII-22	2200°F	1.00	1.02	184.6	1065
VII-23	2200°F	1.00	1.02	161.2	930
VII-24	2200°F	1.00	1.02	171.6	990
VII-25	2200°F	1.00	1.02	182.0	1050
				Average	1002
VII-26	2400°F	1.00	1.02	110.5	638
VII-27	2400°F	1.00	1.01	102.7	604
VII-28	2400°F	1.00	1.01	104.0	612
VII-29	2400°F	1.00	1.03	109.2	617
VII-30	2400°F	1.00	1.02	36.4	210
				Average	536

Sample No.	Breaking Temp.	Width (in)	Depth (in)	Breaking Wt. (lbs)	MOR (psi)
VII-31	2600°F	1.00	1.02	70.2	405
VII-32	2600°F	1.00	1.00	78.0	468
VII-33	2600°F	1.00	1.00	78.0	468
VII-34	2600°F	1.00	1.02	83.2	480
VII-35	2600°F	1.00	1.01	88.4	520
				Average	468
VII-36	2800°F	1.00	1.03	58.5	331
VII-37	2800°F	1.00	1.04	54.6	303
VII-38	2800°F	1.00	1.02	57.2	330
VII-39	2800°F	1.00	1.00	62.4	374
VII-40	2800°F	1.00	1.02	57.2	330
				Average	334

APPENDIX B

X-RAY PHASE ANALYSIS

(Wt. Percent Phase)

Sample		Rutile	Alumina	Crist	Quartz	Mullite
Std. 1	Counts	27146	18256	87970	None	17757
	Ratio		0.6725	3.2406		.6541
	Wt. %		25.01	24.02		43.45
Std. 1	Counts	26614	17494	89359	None	17551
	Ratio		0.6573	3.3576		0.6595
	Wt. %		24.57	24.87		43.29
Std. 1	Counts	26998	18268	88652	None	19052
	Ratio		0.6766	3.2837		0.7057
	Wt. %		25.12	24.34		46.22
Std. 2	Counts	25285	2870	34400	None	28044
	Ratio		0.1135	1.3605		1.1092
	Wt. %		8.92	10.35		71.79
Std. 2	Counts	26372	3402	35556	None	28511
	Ratio		0.1290	1.3482		1.0811
	Wt. %		9.37	10.26		70.01
Std. 2	Counts	25037	2527	35242	None	28544
	Ratio		0.1009	1.4076		1.1401
	Wt. %		8.56	10.69		73.75
Std. 3	Counts	29281	44018	35837	7230	10814
	Ratio		1.5033	1.2239	0.2469	0.3693
	Wt. %		48.91	9.35	9.92	24.90
Std. 3	Counts	28328	44251	35529	7169	10563
	Ratio		1.5621	1.2542	0.2531	0.3729
	Wt. %		50.61	9.57	10.13	25.13
Std. 3	Counts	28923	44784	36571	7612	10267
	Ratio		1.5484	1.2644	0.2634	0.3550
	Wt. %		50.21	9.65	10.50	24.00

Sample		Rutile	Alumina	Crist	Quartz	Mullite
Std. 3	Counts	25195	39965	32082	6719	9615
	Ratio		1.5862	1.2733	0.2667	0.3816
	Wt. %		51.30	9.71	10.61	25.68
Std. 3	Counts	26207	40136	32248	6153	9936
	Ratio		1.5315	1.2305	0.2348	0.3791
	Wt. %		49.72	9.40	9.49	25.52
Std. 4	Counts	26090	19155	84870	16313	8728
	Ratio		0.7342	3.2530	0.6253	0.3345
	Wt. %		26.78	24.11	23.29	22.70
Std. 4	Counts	25753	19265	85264	18056	9038
	Ratio		0.7481	3.3108	0.7011	0.3509
	Wt. %		27.18	24.53	25.97	23.74
Std. 4	Counts	27055	19019	86621	18453	8764
	Ratio		0.7030	3.2017	0.6821	0.3239
	Wt. %		25.88	23.74	25.30	22.02
Std. 5	Counts	29336	85033	None	3312	1545
	Ratio		2.8986		0.1129	0.0527
	Wt. %		89.07		5.18	4.84
Std. 5	Counts	28343	84303	None	2916	1768
	Ratio		2.9744		0.1029	0.0624
	Wt. %		91.25		4.82	5.45
Std. 5	Counts	27990	84546	None	3616	1858
	Ratio		3.0206		0.1292	0.0664
	Wt. %		92.58		5.75	5.71
Std. 6	Counts	28122	77719	17740	2947	1845
	Ratio		2.7636	0.6308	0.1048	0.0656
	Wt. %		85.18	5.04	4.89	5.66
Std. 6	Counts	29704	80261	18015	2663	2147
	Ratio		2.7020	0.6055	0.0897	0.0722
	Wt. %		83.41	4.86	4.36	6.07
Std. 6	Counts	29636	80176	17907	2513	1774
	Ratio		2.1976	0.6042	0.0848	0.0599
	Wt. %		68.89	4.85	4.18	5.29
Std. 7	Counts	30201	66372	18352	6015	5068
	Ratio		2.1976	0.6077	0.1992	0.1678
	Wt. %		68.89	4.87	8.23	12.13

Sample		Rutile	Alumina	Crist	Quartz	Mullite
Std. 7	Counts	28186	61993	17120	5275	5199
	Ratio		2.1994	0.6074	0.1871	0.1845
	Wt. %		68.95	4.87	7.80	13.19
Std. 7	Counts	28711	63967	17527	8255	5113
	Ratio		2.2280	0.6105	0.2875	0.1781
	Wt. %		69.77	4.89	11.35	12.79
Std. 8	Counts	24449	None	101215	None	23381
	Ratio			4.1398		0.9563
	Wt. %			30.56		62.10
Std. 8	Counts	25036	None	104848	None	24043
	Ratio			4.1879		0.9603
	Wt. %			30.91		62.35
Std. 8	Counts	24830	None	105146	None	24535
	Ratio			4.2346		0.9881
	Wt. %			31.25		64.11
Std. 9	Counts	24429	None	51399	9498	23814
	Ratio			2.1040	0.3888	0.9748
	Wt. %			15.76	14.93	63.27
Std. 9	Counts	23938	None	51134	10483	24492
	Ratio			2.1361	0.4379	1.0231
	Wt. %			15.99	16.67	66.39
Std. 9	Counts	25774	None	51268	9667	24846
	Ratio			1.9891	0.3751	0.9640
	Wt. %			14.92	14.45	62.59
Std. 10	Counts	29368	63976	35953	3190	5483
	Ratio	2.1784	2.1784	1.2242	0.1086	0.1867
	Wt. %	68.34	68.34	9.36	5.03	13.33
Std. 10	Counts	28828	65060	35884	3509	5467
	Ratio		2.2568	1.2448	0.1217	0.1896
	Wt. %		70.60	9.51	5.49	13.51
Std. 10	Counts	28587	64691	36160	3116	5662
	Ratio		2.2630	1.2649	0.1090	0.1981
	Wt. %		70.78	9.65	5.04	14.05
Std. 11	Counts	24932	3727	35313	7441	25078
	Ratio		0.1495	1.4164	0.2985	1.0059
	Wt. %		9.96	10.75	11.74	65.24

Sample		Rutile	Alumina	Crist	Quartz	Mullite
Std.11	Counts	25479	4043	35457	6479	24441
	Ratio		0.1587	1.3916	0.2543	0.9593
	Wt. %		10.22	10.57	10.18	62.29
Std.11	Counts	25141	3710	36076	6116	24675
	Ratio		0.1476	1.4349	0.2433	0.9815
	Wt. %		9.90	10.89	9.79	63.70
I-2	Counts	24252	13411	50428	None	14132
	Ratio		0.5530	2.0793		0.5827
	Wt. %		21.56	15.57		38.42
I-3	Counts	23410	15364	51991	None	13731
	Ratio		0.6563	2.2209		0.5865
	Wt. %		24.53	16.60		38.66
I-5	Counts	24074	15082	49156	None	13653
	Ratio		0.6265	2.0419		0.5671
	Wt. %		23.68	15.30		37.43
I-8	Counts	23581	20465	52310	None	14633
	Ratio		0.8679	2.2183		0.6205
	Wt. %		*30.62	16.58		40.81
I-9	Counts	23398	14057	52281	None	13709
	Ratio		0.6276	2.3342		0.6121
	Wt. %		23.71	17.42		40.28
I-10	Counts	23304	12454	58287	None	13767
	Ratio		0.5344	2.5012		0.5908
	Wt. %		21.03	18.64		38.93
I-11	Counts	22534	13089	47490	None	13512
	Ratio		0.5809	2.1075		0.5996
	Wt. %		22.36	15.78		39.49
I-14	Counts	23540	11905	55023	None	14429
	Ratio		0.5057	2.3374		0.6130
	Wt. %		20.20	17.45		40.34
I-15	Counts	24934	12080	64262	None	16580
	Ratio		0.4845	2.5773		0.6650
	Wt. %		19.59	19.19		43.63
I-18	Counts	24171	14192	60737	None	15206
	Ratio		0.5871	2.5128		0.6291
	Wt. %		22.54	18.72		41.36

Sample		Rutile	Alumina	Crist	Quartz	Mullite
I-19	Counts	25827	14329	54704	None	15098
	Ratio		0.5548	2.1181		0.5846
	Wt. %		21.61	15.85		38.54
I-20	Counts	23539	13969	56107	None	15316
	Ratio		0.5934	2.3836		0.6507
	Wt. %		22.72	17.78		42.73
I-23	Counts	21848	12384	52841	None	14273
	Ratio		0.5668	2.4186		0.6533
	Wt. %		21.96	18.04		42.89
I-24	Counts	25032	15683	44491	None	14173
	Ratio		0.6265	1.1774		0.5662
	Wt. %		24.53	*9.01		37.37
I-25	Counts	23265	29225	58655	None	15350
	Ratio		*1.2562	2.5212		0.6598
	Wt. %		*41.80	18.78		4331
I-28	Counts	24117	14577	49249	None	14272
	Ratio		0.6044	2.0421		0.5918
	Wt. %		23.04	15.30		39.00
I-29	Counts	22700	13188	48698	None	14237
	Ratio		0.5810	2.1453		0.6272
	Wt. %		22.37	16.05		41.24
I-30	Counts	22854	14590	51394	None	14396
	Ratio		0.6384	2.2488		0.6299
	Wt. %		24.02	16.80		41.41
I-33	Counts	25150	14236	43972	None	15833
	Ratio		0.5660	1.7484		0.6295
	Wt. %		21.94	13.16		41.39
I-34	Counts	23326	15879	38867	None	14009
	Ratio		0.6807	1.6663		0.6006
	Wt. %		25.24	12.57		39.55
I-34	Counts	25623	13050	41301	None	15388
	Ratio		0.5093	1.6119		0.6006
	Wt. %		20.30	12.17		39.55
I-35	Counts	24369	11413	37650	None	15390
	Ratio		0.4683	1.5450		0.6315
	Wt. %		19.12	11.68		41.51

Sample		Rutile	Alumina	Crist	Quartz	Mullite
I-36	Counts	23706	10713	1498	280	16362
	Ratio		0.4519	0.0632	0.0118	0.6902
	Wt. %		18.65	0.91	*1.60	45.23
I-37	Counts	21926	11085	4042	None	16904
	Ratio		0.5056	0.1843		0.7710
	Wt. %		20.20	1.79		50.35
I-40	Counts	22934	9053	1123	None	17322
	Ratio		0.3947	0.0490		0.7553
	Wt. %		17.01	0.80		49.36
II-3	Counts	21978	14119	42092	None	14085
	Ratio		0.6424	1.9152		0.6409
	Wt. %		24.13	14.38		42.11
II-4	Counts	21949	18229	50246	None	14075
	Ratio		0.8305	2.2892		0.6413
	Wt. %		29.55	17.10		42.13
II-5	Counts	23229	13761	51997	None	15187
	Ratio		0.5924	2.2385		0.6538
	Wt. %		22.70	16.73		42.92
II-6	Counts	23047	14238	50247	None	14707
	Ratio		0.6178	2.1802		0.6381
	Wt. %		23.43	16.30		41.93
II-7	Counts	24665	14487	54198	None	14861
	Ratio		0.5874	2.1974		0.6025
	Wt. %		22.55	16.43		39.67
II-10	Counts	23509	12378	45624	None	14269
	Ratio		0.5265	1.9407		0.6070
	Wt. %		20.80	14.56		39.96
II-13	Counts	22510	14201	50685	None	14539
	Ratio		0.6309	2.2517		0.6459
	Wt. %		23.80	16.82		42.42
II-14	Counts	24023	14762	52324	None	15584
	Ratio		0.6145	2.1781		0.6487
	Wt. %		23.33	16.29		42.60
II-15	Counts	24816	16118	57600	None	16584
	Ratio		0.6495	2.3211		0.6683
	Wt. %		24.34	17.33		43.84

Sample		Rutile	Alumina	Crist	Quartz	Mullite
II-18	Counts	24288	15155	49780	None	15739
	Ratio		0.6240	2.0496		0.6480
	Wt. %		23.61	15.35		42.56
II-19	Counts	24093	20262	46580	None	13816
	Ratio		0.8410	1.9333		0.5734
	Wt. %		*29.85	14.51		*37.83
II-20	Counts	24135	13867	52076	None	15863
	Ratio		0.5746	2.1577		0.6573
	Wt. %		22.18	16.14		43.15
II-23	Counts	23596	14204	41714	None	14383
	Ratio		0.6020	1.7678		0.6096
	Wt. %		22.97	13.31		40.12
II-24	Counts	23620	13225	43885	None	14401
	Ratio		0.5599	1.8580		0.6097
	Wt. %		21.76	13.96		40.13
II-25	Counts	24417	14486	50503	None	15881
	Ratio		0.5933	2.0684		0.6504
	Wt. %		22.72	15.49		42.71
II-27	Counts	23763	12281	40552	None	14932
	Ratio		0.5168	1.7065		0.6284
	Wt. %		20.52	12.86		41.32
II-28	Counts	24630	16119	46749	None	15775
	Ratio		0.6544	1.8981		0.6405
	Wt. %		24.48	14.25		42.08
II-30	Counts	22099	12434	42557	None	14425
	Ratio		0.5626	1.9257		0.6527
	Wt. %		21.84	14.45		42.86
II-33	Counts	23109	11609	37476	None	14006
	Ratio		0.5024	1.6217		0.6061
	Wt. %		20.11	12.24		*39.90
II-34	Counts	22918	13860	36953	None	15778
	Ratio		0.6048	1.6124		0.6885
	Wt. %		23.05	12.17		45.12
II-35	Counts	23828	12501	37248	None	16325
	Ratio		0.5246	1.5632		0.6851
	Wt. %		20.74	11.82		44.91

Sample		Rutile	Alumina	Crist	Quartz	Mullite
II-38	Counts	22173	11084	72	None	17511
	Ratio		0.4999	0.0032		0.7897
	Wt. %		20.03	0.47		51.54
II-39	Counts	20597	9685	443	160	16908
	Ratio		0.4702	0.0215	0.0078	0.8209
	Wt. %		19.18	0.60	*1.46	53.51
II-40	Counts	22013	9103	1188	287	17554
	Ratio		0.4135	0.0540	0.0130	0.7974
	Wt. %		17.55	0.84	*1.64	52.02
III-3	Counts	25532	19088	44476	None	13617
	Ratio		0.7476	1.7420		0.5333
	Wt. %		27.16	13.12		35.29
III-4	Counts	24239	12994	45959	None	14360
	Ratio		0.5361	1.8961		0.5924
	Wt. %		21.08	14.24		39.03
III-5	Counts	21427	14934	45151	None	13028
	Ratio		0.6970	2.1072		0.6080
	Wt. %		25.71	15.77		40.02
III-8	Counts	24435	13370	47081	None	14229
	Ratio		0.5472	1.9270		0.5823
	Wt. %		21.40	14.46		38.39
III-9	Counts	23926	13939	50643	None	13950
	Ratio		0.5827	2.1172		0.5832
	Wt. %		22.42	15.85		38.45
III-10	Counts	24570	15322	54193	None	14713
	Ratio		0.6236	2.2057		0.5988
	Wt. %		39.44	16.49		23.59
III-13	Counts	23042	15426	43222	None	13559
	Ratio		0.6695	1.8758		0.5884
	Wt. %		24.91	14.09		38.78
III-14	Counts	24209	16025	41680	None	13649
	Ratio		0.6619	1.7217		0.5638
	Wt. %		24.70	12.97		37.22
III-14	Counts	25581	13358	44149	None	13891
	Ratio		0.5222	1.7259		0.5430
	Wt. %		20.68	13.00		35.90

Sample		Rutile	Alumina	Crist	Quartz	Mullite
III-15	Counts	24764	17102	48422	None	14935
	Ratio		0.6906	1.9553		0.6031
	Wt. %		25.52	14.67		39.71
III-15	Counts	24237	14238	46567	None	14826
	Ratio		0.5874	1.9213		0.6117
	Wt. %		22.55	14.42		40.26
III-18	Counts	24265	18158	48261	None	14716
	Ratio		0.7483	1.9889		0.6065
	Wt. %		27.18	14.91		39.93
III-19	Counts	23480	16112	47493	None	13806
	Ratio		0.6862	2.0227		0.5880
	Wt. %		25.40	15.16		38.76
III-20	Counts	24044	14804	49282	None	14874
	Ratio		0.6157	2.0497		0.6186
	Wt. %		23.37	15.36		40.69
III-21	Counts	23556	14692	45327	None	14455
	Ratio		0.6237	1.9242		0.6136
	Wt. %		23.60	14.44		40.38
III-22	Counts	23949	13483	48131	None	15105
	Ratio		0.5630	2.0097		0.6307
	Wt. %		21.85	15.06		41.46
III-25	Counts	25758	13584	52675	None	15604
	Ratio		0.5274	2.0450		0.6058
	Wt. %		20.83	15.32		39.88
III-26	Counts	23287	13782	42440	None	14131
	Ratio		0.5918	1.8225		0.6068
	Wt. %		22.68	13.70		39.95
III-27	Counts	22435	11675	45909	None	13346
	Ratio		0.5204	2.0463		0.5949
	Wt. %		20.62	15.33		39.19
III-30	Counts	23215	22483	53152	None	16221
	Ratio		0.9685	2.2896		0.6987
	Wt. %		*33.52	*17.10		*45.77
III-33	Counts	24621	14502	41599	None	15673
	Ratio		0.5890	1.6896		0.6366
	Wt. %		22.60	12.74		41.84

Sample		Rutile	Alumina	Crist	Quartz	Mullite
III-34	Counts	23985	13241	42233	None	15253
	Ratio		0.5521	1.7608		0.6359
	Wt. %		21.54	13.25		41.79
III-35	Counts	23343	13161	38966	None	15129
	Ratio		0.5638	1.6693		0.6481
	Wt. %		21.87	12.59		42.56
III-36	Counts	24734	13437	2994	None	18678
	Ratio		0.5433	0.1210		0.7552
	Wt. %		21.28	1.33		49.35
III-37	Counts	21342	9377	1460	None	15323
	Ratio		0.4394	0.0684		0.7180
	Wt. %		18.29	0.95		46.99
III-40	Counts	23517	10500	None	None	17252
	Ratio		0.4465			0.7336
	Wt. %		18.50			47.98
IV-2	Counts	20676	10838	49350	None	13845
	Ratio		0.5242	2.3868		0.6696
	Wt. %		20.73	17.81		43.93
IV-3	Counts	21384	10842	48651	None	13910
	Ratio		0.5070	2.2751		0.6505
	Wt. %		20.24	16.99		42.72
IV-4	Counts	24705	13642	52263	None	15531
	Ratio		0.5522	2.1155		0.6287
	Wt. %		21.54	15.83		41.33
IV-6	Counts	24277	11109	51760	None	15625
	Ratio		0.4576	2.1321		0.6436
	Wt. %		18.82	15.95		42.28
IV-7	Counts	23376	12618	52543	None	15773
	Ratio		0.5398	2.2477		0.6748
	Wt. %		21.18	16.80		44.26
IV-10	Counts	22445	10109	49456	None	14656
	Ratio		0.4504	2.2034		0.6530
	Wt. %		18.61	16.47		42.87
IV-13	Counts	24948	10679	49671	None	15569
	Ratio		0.4281	1.9910		0.6241
	Wt. %		17.97	14.93		41.04

Sample		Rutile	Alumina	Crist	Quartz	Mullite
IV-14	Counts	23316	12409	51343	None	14801
	Ratio		0.5322	2.2021		0.6348
	Wt. %		20.96	16.46		41.72
IV-15	Counts	23493	12401	50968	None	14875
	Ratio		0.5279	2.1695		0.6332
	Wt. %		20.84	16.23		41.62
IV-18	Counts	23603	11919	48907	None	14589
	Ratio		0.5050	2.1102		0.6181
	Wt. %		20.18	15.80		40.66
IV-19	Counts	25682	14260	48849	None	15667
	Ratio		0.5553	1.9021		0.6100
	Wt. %		21.63	14.28		40.15
IV-20	Counts	26003	16049	59391	None	17088
	Ratio		0.6172	2.2840		0.6572
	Wt. %		23.41	17.06		43.14
IV-21	Counts	24484	12252	46776	None	14785
	Ratio		0.5004	1.9105		0.6039
	Wt. %		20.05	14.34		39.76
IV-22	Counts	25969	11594	49452	None	16012
	Ratio		0.4465	1.9043		0.6166
	Wt. %		18.50	14.30		40.57
IV-25	Counts	24476	13492	46918	None	15239
	Ratio		0.5512	1.9169		0.6226
	Wt. %		21.51	14.39		40.95
IV-28	Counts	24195	11912	47643	None	15763
	Ratio		0.4923	1.9691		0.6515
	Wt. %		19.82	14.77		42.78
IV-29	Counts	23845	11906	46159	None	15841
	Ratio		0.4993	1.9358		0.6643
	Wt. %		20.02	14.53		43.59
IV-30	Counts	19835	14384	51517	None	16372
	Ratio		0.7252	2.5973		0.8254
	Wt. %		*26.52	*19.34		*53.80
IV-33	Counts	22310	9730	40878	None	15353
	Ratio		0.4361	1.8323		0.6882
	Wt. %		18.20	13.77		45.10

Sample		Rutile	Alumina	Crist	Quartz	Mullite
IV-34	Counts	22545	13575	42658	None	15911
	Ratio		0.6021	1.8921		0.7057
	Wt. %		22.98	14.21		46.21
IV-35	Counts	22888	10899	41795	None	16627
	Ratio		0.4762	1.8261		0.7265
	Wt. %		19.35	13.73		47.53
IV-37	Counts	22354	8627	803	107	18377
	Ratio		0.3859	0.0359	0.0048	0.8221
	Wt. %		16.75	0.71	*1.35	53.59
IV-38	Counts	23249	6963	294	90	17870
	Ratio		0.2995	0.0126	0.0039	0.7686
	Wt. %		14.27	0.54	*1.32	50.20
IV-39	Counts	23650	7487	None	144	19861
	Ratio		0.3166		0.0061	0.8398
	Wt. %		14.76		*1.40	54.71
V-1	Counts	27062	72957	9242	596	4132
	Ratio		2.6959	0.3415	0.0220	0.1527
	Wt. %		83.23	2.93	1.96	11.17
V-2	Counts	24144	63616	6510	220	3275
	Ratio		2.6349	0.2696	0.0091	0.1356
	Wt. %		81.47	2.41	11.50	10.09
V-5	Counts	21417	74123	6820	1333	1109
	Ratio		3.4609	0.3184	0.0622	0.0518
	Wt. %		*105.24	*2.76	*3.38	*4.78
V-8	Counts	24348	74460	8014	1532	923
	Ratio		3.0582	13291	0.0629	0.0379
	Wt. %		93.65	2.84	3.41	3.90
V-9	Counts	24500	68881	86344	2099	1476
	Ratio		2.8115	0.3524	0.0857	0.0602
	Wt. %		86.55	3.01	4.21	5.31
V-10	Counts	24240	71376	7862	1236	1456
	Ratio		2.9446	0.3243	0.0510	0.0601
	Wt. %		90.38	2.81	2.99	5.30
V-11	Counts	24699	71483	8943	1925	898
	Ratio		2.8942	0.3621	0.0779	0.0364
	Wt. %		88.93	3.08	3.94	3.80

Sample		Rutile	Alumina	Crist	Quartz	Mullite
V-14	Counts	24556	81198	8435	1695	1284
	Ratio		3.3066	0.3435	0.0690	0.0523
	Wt. %		100.80	2.95	3.62	4.81
V-15	Counts	27380	85640	10579	1915	1078
	Ratio		3.1278	0.3864	0.0699	0.0394
	Wt. %		95.66	3.26	3.65	3.99
V-16	Counts	25494	68400	8246	1485	1861
	Ratio		2.6830	0.3234	0.0582	0.0730
	Wt. %		82.86	2.80	3.24	6.12
V-17	Counts	23746	65964	7880	1423	1486
	Ratio		2.7779	0.3318	0.0599	0.0626
	Wt. %		85.59	2.86	3.30	5.46
V-20	Counts	24260	68421	8862	1352	2165
	Ratio		2.8203	0.3653	0.0557	0.0892
	Wt. %		86.81	3.10	3.15	7.15
V-22	Counts	22444	68614	6916	1341	979
	Ratio		3.0571	0.3081	0.0597	0.0436
	Wt. %		93.62	2.69	3.29	4.26
V-24	Counts	23200	66509	9395	1784	1518
	Ratio		2.8668	0.4050	0.0769	0.0654
	Wt. %		88.15	3.39	3.90	5.64
V-25	Counts	22707	69362	7464	1393	1400
	Ratio		3.0547	0.3287	0.0613	0.0617
	Wt. %		93.55	2.84	3.35	5.40
V-28	Counts	22821	70653	7377	568	3675
	Ratio		3.0960	0.3233	0.0249	0.1610
	Wt. %		94.74	2.80	2.60	11.70
V-29	Counts	24639	65327	6351	1116	2909
	Ratio		2.6514	0.2578	0.0453	0.1181
	Wt. %		81.95	2.32	2.78	8.98
V-30	Counts	21238	62255	5712	855	2485
	Ratio		2.9313	0.2690	0.0403	0.1170
	Wt. %		90.00	2.40	2.61	8.91
V-31	Counts	25744	74815	5452	1486	3116
	Ratio		2.9061	0.2118	0.0577	0.1210
	Wt. %		89.28	1.99	3.22	9.16

Sample		Rutile	Alumina	Crist	Quartz	Mullite
V-32	Counts	24066	69378	3907	1278	2670
	Ratio		2.8828	0.1623	0.0531	0.1109
	Wt. %		88.61	1.63	3.06	8.52
V-35	Counts	26389	74324	5012	951	3268
	Ratio		2.8165	0.1899	0.0360	0.1238
	Wt. %		86.70	1.83	2.45	9.34
V-37	Counts	22169	66792	1658	None	3770
	Ratio		3.0129	0.0748		0.1701
	Wt. %		92.35	0.99		12.27
V-38	Counts	25013	57239	None	189	3567
	Ratio		2.2884		0.0076	0.1426
	Wt. %		71.50		1.45	10.53
V-40	Counts	20975	64786	342	181	3558
	Ratio		3.0887	0.0163	0.0086	0.1696
	Wt. %		94.53	0.57	1.49	12.24
VI-3	Counts	22769	69410	5356	1973	786
	Ratio		3.0484	0.2352	0.0867	0.0345
	Wt. %		93.37	2.16	4.25	3.68
VI-4	Counts	24642	75972	5928	2174	484
	Ratio		3.0830	0.2406	0.0882	0.0196
	Wt. %		94.37	2.20	4.30	2.74
VI-5	Counts	24388	77527	6549	2414	356
	Ratio		3.1789	0.2685	0.0990	0.0146
	Wt. %		97.13	2.40	4.68	2.42
VI-8	Counts	22645	67841	3425	1934	131
	Ratio		2.9958	0.1512	0.0854	0.0058
	Wt. %		91.86	1.55	4.20	1.86
VI-9	Counts	25597	75284	6793	2586	269
	Ratio		2.9411	0.2654	0.1010	0.0105
	Wt. %		90.28	2.38	4.75	2.16
VI-10	Counts	22023	76505	4654	1978	265
	Ratio		3.4739	0.2113	0.0898	0.0120
	Wt. %		*105.62	1.98	4.36	2.25
VI-11	Counts	23934	68864	4929	1933	503
	Ratio		2.8772	0.2059	0.0808	0.0210
	Wt. %		88.45	1.95	4.04	2.82

Sample		Rutile	Alumina	Crist	Quartz	Mullite
VI-12	Counts	28141	77634	3973	2166	540
	Ratio		2.7588	0.1412	0.0770	0.0192
	Wt. %		85.04	1.48	3.90	2.71
VI-15	Counts	22226	65707	6359	1498	874
	Ratio		2.9563	0.2861	0.0674	0.0393
	Wt. %		90.72	2.53	3.56	3.98
VI-17	Counts	28118	70707	5854	2215	662
	Ratio		2.5147	0.2082	0.0788	0.0235
	Wt. %		78.01	1.96	3.97	2.98
VI-19	Counts	23193	79991	5731	1641	937
	Ratio		3.4489	0.2471	0.0708	0.0404
	Wt. %		104.90	2.25	3.69	4.05
VI-20	Counts	22511	71089	4748	1545	578
	Ratio		3.1580	0.2109	0.0686	0.0257
	Wt. %		96.53	1.98	3.61	3.12
VI-23	Counts	25830	74876	6498	1688	799
	Ratio		2.8988	0.2516	0.0654	0.0309
	Wt. %		89.07	2.28	3.49	3.45
VI-24	Counts	26477	77892	5312	1534	834
	Ratio		2.9419	0.2006	0.0579	0.0315
	Wt. %		90.31	1.91	3.23	3.49
VI-25	Counts	22662	69568	6046	1924	630
	Ratio		3.0698	0.2668	0.0849	0.0278
	Wt. %		93.99	2.39	4.18	3.26
VI-26	Counts	22581	74461	4945	1690	534
	Ratio		3.2975	0.2190	0.0748	0.0236
	Wt. %		100.54	2.04	3.83	2.99
VI-27	Counts	24631	62892	6034	980	2334
	Ratio		2.5534	0.2450	0.0398	0.0948
	Wt. %		79.13	2.23	2.59	7.50
VI-30	Counts	22860	68960	6625	3421	713
	Ratio		3.0166	0.2898	0.1497	0.0311
	Wt. %		92.46	2.56	*6.47	3.59
VI-33	Counts	25793	71439	3856	1580	1915
	Ratio		2.7697	0.1495	0.0613	0.0742
	Wt. %		85.35	1.54	3.35	6.20

Sample		Rutile	Alumina	Crist	Quartz	Mullite
VI-34	Counts	27091	72325	4784	1454	1596
	Ratio		2.6697	0.1766	0.0537	0.0589
	Wt. %		82.47	1.73	3.08	5.23
VI-35	Counts	22468	74473	5791	None	3779
	Ratio		3.3146	0.2577		0.1682
	Wt. %		101.03	2.32		12.15
VI-38	Counts	24574	59668	1034	79	4885
	Ratio		2.4281	0.0421	0.0032	0.1988
	Wt. %		75.52	0.75	*1.30	14.09
VI-39	Counts	25822	62349	1127	28	4759
	Ratio		2.4146	0.0436	0.0011	0.1843
	Wt. %		75.13	0.77	*1.22	13.17
VI-40	Counts	24727	64384	1137	38	4822
	Ratio		2.0038	0.0460	0.0015	0.1950
	Wt. %		80.58	0.78	*1.24	13.85
VII-3	Counts	21769	61925	6888	None	3986
	Ratio		2.8446	0.3164		0.1831
	Wt. %		87.51	2.75		13.10
VII-4	Counts	25685	64515	8490	None	4940
	Ratio		2.5118	0.3305		0.1923
	Wt. %		77.93	2.85		13.68
VII-5	Counts	24751	64384	8770	None	4601
	Ratio		2.6013	0.3543		0.1859
	Wt. %		80.51	3.02		13.27
VII-8	Counts	22915	72206	2848	1338	1780
	Ratio		3.1510	*0.1243	*0.0584	*0.0777
	Wt. %		*96.32	*1.35	*3.25	*6.42
VII-9	Counts	26664	62506	8151	None	4749
	Ratio		2.3442	0.3057		0.1781
	Wt. %		73.11	2.67		12.78
VII-10	Counts	26155	64501	6844	None	4851
	Ratio		2.4661	0.2617		0.1855
	Wt. %		76.62	2.35		13.25
VII-11	Counts	23981	59718	6516	None	4270
	Ratio		2.4902	0.2717		0.1781
	Wt. %		77.31	2.42		12.78

Sample		Rutile	Alumina	Crist	Quartz	Mullite
VII-12	Counts	21172	59361	5616	None	4430
	Ratio		2.8038	0.2653		0.2092
	Wt. %		86.33	2.38		14.75
VII-15	Counts	26431	66344	4649	None	5669
	Ratio		2.5101	0.1759		0.2145
	Wt. %		77.88	1.73		15.09
VII-16	Counts	24141	59957	5371	None	4898
	Ratio		2.4836	0.2225		0.2029
	Wt. %		77.12	2.07		14.35
VII-17	Counts	25005	57873	5328	None	4745
	Ratio		2.3145	0.2131		0.1898
	Wt. %		72.25	2.00		13.52
VII-20	Counts	28203	80142	7927	None	5632
	Ratio		2.8416	0.2811		0.1997
	Wt. %		87.42	2.49		14.15
VII-23	Counts	26300	71335	3812	None	5454
	Ratio		2.7124	0.1449		0.2074
	Wt. %		83.70	1.50		14.64
VII-24	Counts	24970	68154	4097	None	4628
	Ratio		2.7294	0.1641		0.1853
	Wt. %		84.19	1.64		13.24
VII-25	Counts	27894	59007	2986	8	5302
	Ratio		2.1154	0.1070	0.0003	0.1901
	Wt. %		66.52	1.23	*1.19	13.54
VII-25	Counts	28624	65611	2723	None	6102
	Ratio		2.2922	0.0951		0.2132
	Wt. %		71.61	1.14		15.00
VII-26	Counts	24168	56757	1517	None	5256
	Ratio		2.3484	0.0628		0.2175
	Wt. %		73.23	0.90		15.28
VII-27	Counts	24291	66240	940	5	5315
	Ratio		2.7269	0.0287	0.0002	0.2188
	Wt. %		84.12	0.73	*1.19	15.36
VII-30	Counts	25631	64500	2701	None	6046
	Ratio		2.5165	0.1054		0.2359
	Wt. %		78.07	1.21		16.44

Sample		Rutile	Alumina	Crist	Quartz	Mullite
VII-33	Counts	22552	54887	56	52	6072
	Ratio		2.4338	0.0025	0.0023	0.2692
	Wt. %		75.69	0.47	*1.26	18.55
VII-34	Counts	23876	62750	413	16	6347
	Ratio		2.6282	0.0173	0.0007	0.2658
	Wt. %		81.28	0.57	*1.21	18.34
VII-35	Counts	23912	56326	None	None	6289
	Ratio		2.3556			0.2630
	Wt. %		73.44			18.16
VII-36	Counts	25467	60190	660	143	8679
	Ratio		2.3635	0.0259	0.0056	0.3408
	Wt. %		73.66	0.64	*1.38	23.09
VII-37	Counts	21575	53553	191	153	8830
	Ratio		2.4822	0.0089	0.0071	0.4093
	Wt. %		77.08	0.51	*1.43	27.43
VII-40	Counts	26250	58848	400	None	9920
	Ratio		2.2418	0.0152		0.3779
	Wt. %		70.16	0.56		25.44
1600°F (air)	Counts	24877	11825	60064	None	13412
	Ratio		0.4753	2.4144		0.5391
	Wt. %		19.33	18.01		35.66
1600°F (air)	Counts	24481	12620	60840	None	13363
	Ratio		0.5155	2.4851		0.5458
	Wt. %		20.47	18.51		36.08
1600°F (water)	Counts	22308	14051	61794	None	14345
	Ratio		0.6299	2.7700		0.6430
	Wt. %		23.78	20.60		42.24
1600°F (water)	Counts	22069	13781	60602	None	14213
	Ratio		0.6244	2.7460		0.6440
	Wt. %		23.60	20.42		42.30
1800°F (air)	Counts	20995	13534	64858	None	14433
	Ratio		0.6446	3.0892		0.6874
	Wt. %		24.20	22.92		45.06
1800°F (air)	Counts	21364	14693	63886	None	14260
	Ratio		0.6877	2.9903		0.6674
	Wt. %		25.44	22.20		43.78

Sample		Rutile	Alumina	Crist	Quartz	Mullite
1800°f (water)	Counts	21366	14799	63149	None	13454
	Ratio		0.6926	2.9556		0.6297
	Wt. %		25.58	21.94		41.40
1800°F (water)	Counts	21073	12307	64966	None	13976
	Ratio		0.5840	3.0829		0.6632
	Wt. %		22.46	22.88		43.52
2000°F (air)	Counts	22311	17046	64985	None	15004
	Ratio		0.7640	2.9127		0.6725
	Wt. %		27.64	21.64		44.11
2000°F (air)	Counts	21856	13902	63379	None	13803
	Ratio		0.6360	2.898		0.6315
	Wt. %		23.94	21.52		41.51
2000°F (water)	Counts	21522	15868	64039	None	14424
	Ratio		0.7373	2.9755		0.6702
	Wt. %		26.87	22.09		43.97
2000°F (water)	Counts	20860	17181	61905	None	13977
	Ratio		0.8236	2.9676		0.6700
	Wt. %		29.35	22.03		43.95
2200°F (air)	Counts	21893	12437	62483	None	14376
	Ratio		0.5680	2.8540		0.6566
	Wt. %		22.00	20.21		43.11
2200°F (air)	Counts	21993	10717	62017	None	14364
	Ratio		0.4872	2.8198		0.6531
	Wt. %		19.66	21.95		42.87
2200°F (water)	Counts	21072	12739	59532	None	14157
	Ratio		0.6045	2.8251		0.6718
	Wt. %		23.05	21.00		44.07
2200°F (water)	Counts	20882	13382	59210	None	14117
	Ratio		0.6408	2.8354		0.6760
	Wt. %		24.07	21.06		44.33
2400°F (air)	Counts	21532	17836	55302	None	14474
	Ratio		0.8283	2.5684		0.6722
	Wt. %		29.49	19.13		44.10
2400°F (air)	Counts	21062	12915	54441	None	13854
	Ratio		0.6131	2.5847		0.6577
	Wt. %		23.29	19.25		43.16

Sample		Rutile	Alumina	Crist	Quartz	Mullite
2400°F (water)	Counts	20983	12534	56098	None	14900
	Ratio		0.5973	2.6735		0.7101
	Wt. %		22.84	19.90		46.50
2400°F (water)	Counts	20905	12158	54166	None	14872
	Ratio		0.5815	2.5910		0.7114
	Wt. %		23.38	19.28		46.56
I-9	Counts	22890	13877	8616	None	14014
	Ratio		0.6062	2.5607		0.6122
	Wt. %		23.10	19.08		40.29
I-9	Counts	19736	15234	51714	None	12148
	Ratio		0.7718	2.6205		0.6155
	Wt. %		27.86	19.51		40.50
I-19	Counts	20980	13713	55015	None	13265
	Ratio		0.6536	2.6222		0.6322
	Wt. %		24.46	19.52		41.56
I-19	Counts	21993	12297	60159	None	14763
	Ratio		0.5591	2.7353		0.6712
	Wt. %		21.74	20.35		44.03
I-28	Counts	22098	12635	55977	None	14715
	Ratio		0.5718	2.5331		0.6658
	Wt. %		22.11	18.88		43.69
I-28	Counts	20721	12038	48773	None	13251
	Ratio		0.5809	2.3537		0.6443
	Wt. %		22.37	17.57		42.33

*Sample Reading not used.

APPENDIX C

X-RAY PHASE ANALYSIS RESULTS

Phase Analysis of Mix I at Each Modulus Temperature

Temperature	Percent Alumina	Percent Crist	Percent Quartz	Percent Mullite	Total
Room Temp	22.3	15.8	None	38.2	76.3
1600°F	22.4	17.6	None	40.0	80.0
1800°F	20.7	17.5	None	41.2	79.4
2000°F	22.3	17.5	None	40.9	80.7
2200°F	22.3	18.4	None	41.2	82.9
2400°F	23.1	16.1	None	40.6	79.8
2600°F	21.7	12.4	None	40.5	74.6
2800°F	18.6	1.2	None	48.3	68.1

Phase Analysis of Mix II at Each Modulus Temperature

Temperature	Percent Alumina	Percent Crist	Percent Quartz	Percent Mullite	Total
Room Temp	25.5	16.1	None	42.4	84.0
1600°F	22.3	15.8	None	40.5	78.6
1800°F	23.8	16.8	None	43.0	83.6
2000°F	22.9	15.3	None	42.9	81.1
2200°F	22.5	14.3	None	41.0	78.8
2400°F	22.3	13.9	None	42.1	78.3
2600°F	21.3	12.1	None	45.0	78.4
2800°F	18.9	0.6	None	52.4	71.9

Phase Analysis of Mix III at Each Modulus Temperature

Temperature	Percent Alumina	Percent Crist	Percent Quartz	Percent Mullite	Total
Room Temp	24.7	14.4	None	38.1	77.2
1600°F	22.5	15.6	None	38.8	76.9
1800°F	23.7	13.9	None	38.4	75.9
2000°F	22.0	15.1	None	39.8	76.9
2200°F	22.1	14.9	None	40.6	77.6
2400°F	21.7	14.5	None	39.6	75.8
2600°F	22.0	12.9	None	42.0	76.9
2800°F	19.4	0.8	None	48.1	68.3

Phase Analysis of Mix IV at Each Modulus Temperature

Temperature	Percent Alumina	Percent Crist	Percent Quartz	Percent Mullite	Total
Room Temp	20.8	16.9	None	42.7	80.4
1600°F	19.5	16.4	None	43.1	79.0
1800°F	19.9	15.9	None	41.5	77.3
2000°F	21.7	15.7	None	41.3	78.7
2200°F	20.0	14.3	None	40.4	74.7
2400°F	19.9	14.7	None	43.2	77.8
2600°F	20.2	13.9	None	46.3	80.4
2800°F	15.3	0.4	None	52.8	68.5

Phase Analysis of Mix V at Each Modulus Temperature

Temperature	Percent Alumina	Percent Crist	Percent Quartz	Percent Mullite	Total
Room Temp	82.4	2.7	1.7	10.6	97.4
1600°F	90.2	2.9	3.5	4.8	101.4
1800°F	95.1	3.1	3.7	4.2	106.1
2000°F	85.1	2.9	3.2	6.2	97.4
2200°F	91.8	3.1	3.5	5.1	103.5
2400°F	88.9	2.5	2.7	9.9	104.0
2600°F	88.2	1.8	2.9	9.0	101.9
2800°F	86.1	0.5	1.5	11.7	99.8

Phase Analysis of Mix VI at Each Modulus Temperature

Temperature	Percent Alumina	Percent Crist	Percent Quartz	Percent Mullite	Total
Room Temp	95.0	2.3	4.4	2.9	104.6
1600°F	91.1	2.0	4.4	2.1	99.6
1800°F	88.1	2.0	3.8	3.2	97.1
2000°F	93.1	2.1	3.8	3.4	102.4
2200°F	91.1	2.2	3.6	3.4	100.3
2400°F	90.7	2.3	3.2	4.7	100.9
2600°F	89.6	1.9	2.1	7.9	101.5
2800°F	77.1	0.8	None	13.7	91.6

Phase Analysis of Mix VII at Each Modulus Temperature

Temperature	Percent Alumina	Percent Crist	Percent Quartz	Percent Mullite	Total
Room Temp	82.0	2.9	None	13.4	98.3
1600°F	74.9	2.5	None	13.0	90.4
1800°F	80.5	2.2	None	14.2	96.9
2000°F	78.9	2.2	None	14.0	95.1
2200°F	76.5	1.4	None	14.1	92.0
2400°F	78.5	0.9	None	15.7	95.1
2600°F	76.8	0.3	None	18.4	95.5
2800°F	73.6	0.6	None	25.3	99.5

BIBLIOGRAPHY

1. Smith, Russell G., "Compositional Changes Occurring in Alumino-Silicate Refractories Exhibiting Increased Strength at Elevated Temperatures," M.S. Thesis, Georgia Institute of Technology, (1968).

2. Duncan, Frank D., "Thermo-Mechanical Behavior of Bauxite-Based Alumino-Silicate Refractories," Ph.D. Thesis, Ohio State University, (1970).

3. Bodin, V., "Resistance Tests on Refractory Products Under Load at Different Temperatures," Transactions of the British Ceramic Society, 21, 56-65, (1922).

4. Heindl, R. A. and Pendergast, W. L., "III Progress Report on Investigation of Sagger Clays: Their Elasticity and Transverse Strength at Several Temperatures," Journal of the American Ceramic Society, 10 [7], 524-534, (1927).

5. Hirsch, Hans, "Strength of Refractory Materials at Elevated Temperatures," Berichte der Deutscher Keramischer Gesellschaft, 9 [11], 577-596, (1928). --Abstracted in Ceramic Abstracts, 8, (1929).

6. Roberts, A. L. and Cobb, J. W., "IV. The Behavior of Refractory Materials Under Torsion at Different Temperatures," Transactions of the British Ceramic Society, 32, 22-44, (1933).

7. Hunt, E. B. and Bradley, R. S., "Description of Hot Modulus of Rupture and Hot Crushing Strength Tests and Discussions of Results," Bulletin of the American Ceramic Society, 20 [8], 267-269, (1941).

8. Wiechula, B. A. and Roberts, A. L., "The Elastic and Viscous Properties of Alumino-Silicate Refractories," Transactions of the British Ceramic Society, 51, 173-197, (1952).

9. Padgett, G. C., "The Effect of Viscous Constituents on the High-Temperature Mechanical Behavior of Refractories," Proceedings of the Sixth International Conference on Science of Ceramics, published by the European Ceramic Association at Baden-Baden, 14-18, (November, 1971).

10. Padgett, G. C., Cox, J. A., and Clements, J. F., "Stress/Strain Behavior of Refractory Materials at High Temperatures," Transactions of the British Ceramic Society, 68, 63-72, (1969).

11. Folk, H. F. and Bohling, W. C., "High Temperature Strength of High Alumina Refractories," Bulletin of the American Ceramic Society, 47 [6], 580-583, (1968).

12. Rigby, G. R., "The Origin of Mechanical Strength in Ceramic Materials," Transactions of the British Ceramic Society, 50, 75-86, (1951).

13. Houseman, D. H., "The Development of Bond Strength During Firing," The Refractories Journal, 33 [4], 146-158, (1957).

14. Allison, E. B., Brock, P.,,and White, J., "The Rheology of Aggregates Containing a Liquid Phase with Special Reference to the Mechanical Properties of Refractories at High Temperatures," Transactions of the British Ceramic Society, 58, 495-531, (1959).

15. Houseman, D. H. and White, J., "Development of Bond Strength During Firing--A New Approach and its Technical Implications," Transactions of the British Ceramic Society, 40 [9], 299-306, (1957).

16. Mattyasovszky-Zsolnay, L., "Mechanical Strength of Porcelain," Journal of the American Ceramic Society, 40 [9], 299-306, (1957).

17. Fulrath, R. M., "Internal Stresses in Model Ceramic Systems," Journal of the American Ceramic Society, 42 [9], 423-429, (1959).

18. Bressman, J. R., "Method for Determining Tensile Properties of Refractory Materials at Elevated Temperatures," Journal of the American Ceramic Society, 30 [5], 145-152, (1947).

19. Das, S. S. and Roberts, A. L., "A Study of Silica Refractories by Torsion Methods," Transactions of the British Ceramic Society, 48, 215-234, (1949).

20. Davis, W. R. and Rigby, G. R., "The Measurement of Young's Modulus of Alumina-Silica Refractories," The Gas Council, 47th Report of the Joint Refractories Committee, 40, (1955-1956).

21. Chaklader, A. C. D. and Roberts, A. L., "Relationships Between Constitution and Properties of Silica Refractories--III Effect of Heat Treatment on the Mechanical Properties," Transactions of the British Ceramic Society, 57, 126-147, (1958).

22. Palfreyman, M., "Hot Strength of High-Alumina Refractories," Bulletin of the American Ceramic Society, 49 [7], 638-642, (1970).

23. Davis, W. R. and Rigby, G. R., "Basic Refractories: Variation with Temperature of Modulus of Elasticity," Transactions of the British Ceramic Society, 56, 259-276, (1957).

24. Anonymous, "Study of the Mechanical Properties of Refractories at Working Temperatures," The Gas Council, 59th Report of the Joint Refractories Research Committee and British Ceramic Research Association, (1967-1968).

25. Miller, E. D. and Davis, B., "Modulus of Rupture of Alumina-Silica Refractories at Elevated Temperatures," Bulletin of the American Ceramic Society, 45 [8], 710-713, (1966).

26. Padgett, G. C. and Clements, J. F., "Deformation Behavior of Heterogeneous Ceramic Materials at High Temperatures," Proceedings of the Fifth International Conference on Science of Ceramics, published by the European Ceramic Association at Ronneby Brunn, Sweden, 20-23, (April 1969).

27. Crouch, A. G. and Jolliffe, K. H., "The Effect of Stress Rate on the Rupture Strength of Alumina and Mullite Refractories," Proceedings of the British Ceramic Society, 15 [1], 37-46, (1970).

28. Alexanderson, W. H., "High Alumina Refractories--Relationship of Density, Thermal Shock Resistance and Hot Modulus of Rupture," 74th Annual Meeting of the American Ceramic Society, (May 9, 1972).

29. Tripp, Jeffrey A., "Hot Modulus of Rupture Behavior of Aluminous Refractories," M. S. Thesis, Ohio State University, (1966).

30. Roberts, A. L., "Elasticity-Temperature Relationships in Refractories," Transactions of the British Ceramic Society, 53, 724-730, (1954).

31. Rigby, G. R., "The Mechanical Properties of High-Alumina Refractories Utilizing Various Bonding Agents," Transactions of the British Ceramic Society, 70, 199-208, (1971).

32. Studt, P. L. and Fulrath, R. M., "Mechanical Properties and Chemical Reactivity in Mullite-Glass Systems," Journal of the American Ceramic Society, 45 [4], 182-188, (1962).

33. Chaklader, A. C. D. and Roberts, A. L., "Relationships Between Constitution and Properties of Silica Refractories; I, Effects of the Devitrification of Silica Glass," Transactions of the British Ceramic Society, 56, 331-334, (1957).

34. Klug, H. P. and Alexander, L. E., X-Ray Diffraction Procedures for Polycrystalline and Amorphous Materials, (New York: John Wiley and Sons, 1974).

35. Kingery, W. A., Introduction to Ceramics, (New York: John Wiley and Sons, 1960).

36. Lynch, J. F., Ruderer, C. G., and Duckworth, W. H., Engineering Properties of Ceramics, compiled by Battelle Memorial Institute, Columbus, Ohio.

37. Ricke, R., "Rontgenagraphische Ausdehnugsmessunger Kristalliner Masson I," Berichte Der Detschen Keramischer Gesellaschaft, 16, 381-392, (1935).